

**Bovine and Porcine Adipogenesis, Myogenesis, and Tissue Engineering Strategies
to Improve Flavor and Pigmentation of Cell-Based Meat**

A dissertation submitted
to Kent State University in partial
fulfillment of the requirement of the
degree of Doctor of Philosophy

by

Jess Krieger

December 2020

© Copyright

All rights reserved

Except for previously published material

Dissertation written by

Jessica Krieger

B.A., Kent State University, 2013

B.S., Kent State University, 2013

Ph.D., Kent State University, 2020

Approved by

Min-ho Kim, PhD, Chair, Doctoral Dissertation Committee

Dr. Min-ho Kim

Oleg Lavrentovich, PhD, Members, Doctoral Dissertation Committee

Dr. Oleg Lavrentovich

Kristy Welshhans, PhD

Dr. Kristy Welshhans

Feng Dong, PhD

Dr. Feng Dong

Songping Huang, PhD

Dr. Songping Huang

Accepted by

Ernest Freeman, PhD, Chair, Department of Biomedical Sciences

Dr. Ernest Freeman

Mandy Munro-Stasiuk, PhD, Interim Dean, College of Arts and Sciences

Dr. Mandy Munro-Stasiuk

TABLE OF CONTENTS

TABLE OF CONTENTS	III
LIST OF FIGURES	VII
LIST OF TABLES.....	IX
LIST OF ABBREVIATIONS	X
DEDICATION.....	XIII
ACKNOWLEDGMENTS	XIV
Chapter 1	1
Chapter 2	4
BACKGROUND AND SPECIFIC AIMS	4
2.1. Meat, Pandemics, and Public Health.....	5
2.1.1. Zoonotic disease transmission.....	6
2.1.2. Viruses.....	6
2.1.3. Antibiotic resistant bacteria.....	7
2.1.4. The future of animal agriculture and zoonotic disease transmission.....	7
2.2 Environmental destabilization.....	8
2.2.1 Greenhouse gases.....	8
2.3 Transforming the animal agriculture industry to a cell-based meat model.....	10
2.4. Basic overview of cell-based meat technology.....	11
2.4.1 Cell Line Development.....	14
2.4.2 Cell Production.....	20
2.4.3 Product structuring.....	21
2.4.4 Industry Challenges.....	23
2.5. Specific Aims.....	24
Chapter 3	26
CHARACTERIZING PORCINE AND BOVINE MYOGENESIS AND ADIPOGENESIS	26
3.1. Introduction.....	26
3.2. Materials and Methods.....	27
3.2.1. Cell isolation protocol for bovine and porcine myoblasts and fibroblasts.....	27
3.2.2. Cell culture protocols.....	27
3.2.3. Myogenesis protocol	28
3.2.4. Adipogenesis protocol	28
3.2.5. Immunostaining	28
3.2.6. Oil Red O staining	29
3.2.7. Digital holographic microscopy.....	29
3.2.8. qPCR.....	29
3.2.9. Live imaging	30

3.2.10. Oil Red O quantification	31
3.2.11. Statistics	31
3.3. Results.....	31
3.3.1. Isolated bovine and porcine skeletal muscle progenitor cells undergo myogenesis with similar gene myogenic transcription factor gene expression patterns	31
3.3.2. Bovine and porcine myocytes undergo different magnitudes of hypertrophy.....	31
3.3.3. Isolated intramuscular fibroblasts from pigs have more robust adipogenic potential than bovine intramuscular fibroblasts but a rarely in population frequency.....	32
3.4. Discussion	32
Chapter 4	44
DRIVING FLAVOR AND PIGMENT PROFILES THROUGH PORCINE AND BOVINE MYOGENESIS	44
4.1. Introduction.....	44
4.2. Materials and Methods.	45
4.2.1. Cell culture protocols.....	45
4.2.2. Tissue synthesis and conditioned media culture.....	45
4.2.3. Beef and pork tissue sourcing	46
4.2.4. Myogenesis protocol	46
4.2.5. Preparation of culture vessels for electrical stimulation	46
4.2.6. Electrical stimulation of myocytes	46
4.2.7. Total myoglobin concentration with absorption spectroscopy	47
4.2.8. Colorimetry analysis	47
4.2.9. Fusion index assay for differentiating myoblasts.....	48
4.2.10. Macrophage polarization and conditioned media collection.....	48
4.2.11. Myogenesis assay with macrophage conditioned media	49
4.2.12. Proliferation assay for porcine myoblasts in macrophage conditioned media.....	49
4.2.13. Immunostaining	49
4.2.14. qPCR.....	50
4.2.15. Statistics	51
4.3. Results.....	51
4.3.1. In diffuse reflectance spectroscopy, C2C12s lack major wavelength peaks, while beef and pork have major wavelength peaks in the red wavelength spectrum.....	51
4.3.2. Differentiated bovine myoblasts express more myoglobin protein than undifferentiated myoblasts, but have lower myoglobin levels than skeletal muscle tissue from a cow.....	52
4.3.3. Electrical stimulation with positive waveform increases myogenin gene expression and myoglobin protein expression in bovine cells	52
4.3.4. M1 polarization increases gene expression of inflammatory cytokines and M2 polarization increases expression of tissue maturation factors	53
4.3.5. In porcine skeletal muscle cells, M0 and M2 conditioned media promote myogenesis and proliferation.....	56
4.4. Discussion	59
Chapter 5	65

EVALUATION OF TISSUE ENGINEERING METHODS FOR CULTIVATED MEAT	65
5.1. Introduction	65
5.2. Materials and Methods	66
5.2.1. Cell and tissue culture for comparing 2D cultures to 3D self-assembled tissues	66
5.2.2. Gene expression analysis	69
5.2.3. Immunostaining	70
5.2.4. Slack tests	71
5.2.5. Tissue elastic moduli assessments	71
5.2.6. Celery scaffold preparation and decellularization.....	72
5.2.7. Schiff staining of cellulose scaffolds.....	73
5.2.8. Cell seeding and culture in cellulose scaffolds.....	73
5.2.9. Porcine myogenesis on fibroblast and myofibroblast feeder layers	73
5.2.10. Fusion index assay for differentiating myoblasts.....	74
5.2.11. Statistics	74
5.3. Results.....	74
5.3.1. Fibroblast to myofibroblast differentiation is observed in 2D cultures treated with TGF- β 1, regardless of myoblast presence	74
5.3.2. Myogenesis is suppressed in 2D cultures with TGF- β 1 supplementation and in the presence of fibroblasts and myofibroblasts, yet fibroblasts increase myotube alignment.....	76
5.3.3. In comparison to fibroblasts grown on plastic, self-assembled tissues containing only fibroblasts have a suppressed ability to assume a myofibroblast phenotype.....	76
5.3.4. TGF- β 1 supplementation improves myoblast differentiation and alignment in myoblast-only self-assembled tissues	78
5.3.5. In self-assembled co-cultures, fibroblasts and myofibroblasts homogenize tissue surfaces, myofibroblasts improve myotube formation, and TGF- β 1 enhances myogenesis	81
5.3.6. Zero-force velocity is greatest in co-culture with TGF- β 1 supplementation in slack tests.....	84
5.3.7. Tissue elastic moduli increase in co-cultures and with TGF- β 1 exposure	85
5.3.8. Supplementation with TGF- β 1 and addition of myofibroblasts enhances myogenesis in collagen 1-based hydrogels	85
5.3.9. Porcine tissues undergo myogenesis, but are unstable in long term tissue culture.....	86
5.3.10. Freezing celery prior to decellularization creates a more flexible scaffold	87
5.3.11. Cellulose surface properties result in poor cell adhesion and promote cell aggregation of 3T3s and C2C12 cells on scaffold surfaces	88
5.3.12. Freezing scaffolds prior to cell seeding and treatment with TGF- β 1 improve myogenesis of C2C12s	89
5.3.13. Porcine myofibroblast feeder layers improve adhesion and myogenic differentiation of myoblasts	90
5.4. Discussion	93
Chapter 6	99
SUMMARY AND FUTURE STUDY	99
6.1. Summary	99
6.2 Future study.....	102

REFERENCES 107

LIST OF FIGURES

Figure 2.1. Cell-based meat bioprocess workflows, product development strategies, product compositions, and regulatory oversight.....	12
Figure 2.2. Mitotic capacity of cells.....	14
Figure 2.3. Various cell types used for cell-based meat and their differentiation.....	17
Figure 2.4. Polarized microscopy image of porcine skeletal muscle tissue structure.....	22
Figure 3.1. Bovine muscle tissue biopsy and cell morphology of bovine and porcine myoblasts and fibroblasts.....	33
Figure 3.2. Immunocytochemistry of fibroblasts and differentiated muscle cells and myogenic gene expression.....	34
Figure 3.3. Digital holographic and phase microscopy live imaging of myogenesis.....	35
Figure 3.4. Adipogenesis of bovine and porcine intramuscular fibroblasts.....	36
Figure 4.1. Colorimetry myoglobin protein concentration of cell cultures and meat samples.....	54
Figure 4.2. Gene and protein expression of bovine myoblasts under electrical stimulation regime.....	55
Figure 4.3. Gene expression analysis of M0, M1, and M2 polarized macrophages.....	57
Figure 4.4. Macrophage conditioned media in 2D and 3D myogenesis and proliferation assays.....	58
Figure 5.1. Technical protocol for 2D/3D culture systems and experimental conditions design.....	68
Figure 5.2. Immunostaining and morphological characterization of 2D cultures.....	75
Figure 5.3. Gene expression of fibroblast collagen 1 and α -SMA and myoblast myogenin in 2D cell cultures and 3D self-assembled tissue conditions.....	77
Figure 5.4. Zero force shortening of self-assembled tissues and their surface characteristics.....	79
Figure 5.5. Biomechanical and elastic properties of 3D tissue constructs.....	80
Figure 5.6. Histology of self-assembled myoblast monocultures.....	82

Figure 5.7. Histology of self-assembled co-cultures.....	83
Figure 5.8. Histology of mono- and co-cultures in collagen 1-based hydrogels.....	86
Figure 5.9. Histology and integrity of self-assembled and hydrogel-based porcine tissue.....	87
Figure 5.10. Frozen and unfrozen celery scaffold structures.....	88
Figure 5.11. 3T3 and C2C12 seeding into unfrozen and frozen cellulose scaffolds.....	89
Figure 5.12. Cross sectional view of C2C12 myogenesis with and without TGF β treatment in unfrozen scaffolds.....	91
Figure 5.13. Porcine fibroblast and myofibroblast feeder layer cultures with porcine skeletal muscle cells.....	92
Figure 6.1. Japanese Meat Grading Association and USDA meat quality standards.....	104

LIST OF TABLES

Table 1.1 Material selection considerations for cell-based meat bioprocesses.....	3
Table 3.1 Sequences of primers used for PCR in this study.....	30
Table 3.2. Average intramuscular fat % and muscle fiber type in the <i>biceps femoris</i> and <i>longissimus thoracis</i> in various cattle breeds.....	38
Table 3.3. Intramuscular fatty acid compositions in the <i>longissimus</i> muscle in cattle fed high calorie diets.....	40
Table 4.1. Sequences of primers used for PCR in this study.....	51
Table 5.1. Sequences of primers used for PCR in this study.....	69
Table 6.1. Japanese and US beef quality scoring metrics.....	103
Table 6.2. Japanese and US beef quality grades determined by intramuscular fat %.....	103

LIST OF ABBREVIATIONS

GHGs - greenhouse gases

CO₂ - carbon dioxide

CH₄ - methane

N₂O - nitric oxide

CO₂ eq - carbon dioxide equivalent

EPA - Environmental Protection Agency

U.S. - United States

ECM - extracellular matrix

MC - mitotic capacity

MI - mitotic index

IMC - innate mitotic capacity

EMC - enhanced mitotic capacity

UMC - unlimited mitotic capacity

ES - electrical stimulation

U - undifferentiated myoblasts

D - differentiated myocytes

D-A - differentiated myocytes with alternating electrical pulses

D-P - differentiated myocytes with positive electrical pulses

PC - positive control

SF - serum free

FBS - fetal bovine serum

FGM - fibroblast growth media

MGM - myoblast growth media

MDM - myoblast differentiation medium

PAMs - porcine alveolar macrophages

hDFs - human neonatal dermal fibroblasts

C2C12s - mouse myoblast cell line

ORO - Oil Red O

DHM - digital holographic microscopy

CM - conditioned media

DMEM - Dulbecco's Modified Eagle's Medium

DMEM/F12 - Mixture of Dulbecco's Modified Eagle's Medium and Ham's F-12 medium

aP2 - adipocyte protein 2

GLUT 4 - glucose receptor 4

IBMX - 3-isobutyl-1-methylxanthine

C/EBP β - CCAATT enhancer binding proteins β

C/EBP δ - CCAATT enhancer binding proteins δ

PPAR γ - peroxisome proliferator-activated receptor γ

C/EBP α - CCAATT enhancer binding proteins α

TZD - thiazolidinedione

Wnt - wiggless and Int

Mb - myoglobin

OMb - oxymyoglobin

DMb - deoxymyoglobin

MMb - metmyoglobin

HGF - hepatocyte growth factor

FGF-2 - fibroblast growth factor 2

VEGF - vascular endothelial growth factor

IGF-1 - insulin-like growth factor 1

LIF - Leukemia inhibitory factor

TGF- β 1 - transforming growth factor β -1

EGF - epithelial growth factor

TNF α - tumor necrosis factor α

INF γ - interferon γ

ANG - angiopoietin

IL-6 - interleukin 6

FFAs - free fatty acids

MHC - myosin heavy chain

MYH2 - myosin heavy chain type 2

MYH4 - myosin heavy chain type 4

IMF - intramuscular fat

JMGA - Japanese Meat Grading Association

USDA - United States Department of Agriculture

FibMyo - porcine fibroblast feeder layer and bovine myoblast seeding

MyoMyo - porcine myofibroblast feeder layer and bovine myoblast seeding

2D FibCon - 2D cultures of hDFs without TGFB treatment

2D MyoCon - 2D cultures of C2C12s without TGFB treatment

2D FibTGFB - 2D cultures of hDFs with TGFB treatment

2D MyoTGFB - 2D cultures of C2C12s with TGFB treatment

2D CoCon - 2D co-cultures of hDFs and C2C12s without TGFB treatment

2D CoTGFB - 2D co-cultures of hDFs and C2C12s with TGFB treatment

3D FibCon - 3D cultures of hDFs without TGFB treatment

3D MyoCon - 3D cultures of C2C12s without TGFB treatment

3D FibTGFB - 3D cultures of hDFs with TGFB treatment

3D MyoTGFB - 3D cultures of C2C12s with TGFB treatment

3D CoCon - 3D co-cultures of hDFs and C2C12s without TGFB treatment

3D CoTGFB - 3D co-cultures of hDFs and C2C12s with TGFB treatment

RGD - Arg-Gly-Asp

IKVAV - Ile-Lys-Val-ala-Val

DEDICATION

I'd like to dedicate this dissertation to everyone who inspired, supported, and believed in me during this journey:

This is for my family, Dave, Brett, Laura, Susan, Al, and Sue;

my grandparents, who gifted me with their strength;

my chosen family, Shane, who understands me like no other;

my good friends Diane, Taras, Greta, and Erin;

my colleagues Isha, Kate, Natalie, Andrew, Scott, and Jim;

Bruce Friedrich, whose work opened my eyes to the reality of animal agriculture;

my advisor Dr. Min-Ho Kim, who helped me spread my wings and fly;

Dallas, the light of my life, who has been with me for 11 years, who is a son to me;

the strangers who have cheered me on;

and all the lives, both animal and human, who I hope I can help with my work.

ACKNOWLEDGMENTS

I would like to acknowledge first and foremost my advisor Dr. Min-Ho Kim, who I met during my undergraduate work at Kent State when I took one of his classes. Dr. Kim has consistently been a supportive person at all stages of my career. I feel very lucky that he believed in me and in the potential of cultured meat research to help improve the world. He created an opportunity to continue this research when it seemed impossible to pursue my passions. This work wouldn't have happened without being a graduate student in his lab. I'm forever grateful for this opportunity to learn from and work with him professionally and personally. I will take these lessons and experiences with me through the rest of my life.

I'd like to thank Isha Datar, Dr. Kate Krueger, and Erin Kim for their financial and emotional support during my time as a New Harvest fellow. The fellowship was a launchpad for which I was able to move forward with my research and dreams of building a better world.

I'd also like to thank my committee, Dr. Kristy Welshhans, Dr. Feng Dong, Dr. Songping Huang, and Dr. Oleg Lavrentovich for supporting me through my PhD. All of my committee members have been gracious, patient, and understanding through the many challenges that come with graduate school. Dr. Dong and Dr. Huang have inspired me at difficult moments and encouraged me to keep moving forward. I would especially like to thank Dr. Welshhans who I've learned a great deal from as a role model for a woman scientist in a leadership role, and collaborated with on new inventions. That collaboration added great value to my work. Thank you to Dr. Lavrentovich for letting me use his lab and equipment for cultured meat research, for the delicious coffee hours, and the good conversations.

Lastly, I would like to acknowledge Dr. Taras Turiv, who is one of my most valued collaborators. Taras assisted with many aspects of my dissertation research, including performing experiments, developing technical assays, and stimulating my imagination with cool science. My PhD would not have been the same without his professional collaboration and personal friendship. We have both learned a lot from each other and I'm grateful for those experiences.

Chapter 1

INTRODUCTION

Cell-based meat is meat grown from isolated animal cells, instead of using the entire animal to produce meat products. The isolated cells are grown in cell culture and are used to develop cell lines that can be grown in bioreactors to produce animal free meat products¹. Cell-based meat has been called many things, such as cultured meat, cultivated meat, lab-grown meat, and *in vitro* meat. The term “cultivated” is becoming increasingly adopted in public discourse because it is more appealing to consumers and for its scientific accuracy². Meat culture uses similar technology to yeast fermentation for producing bread or beer, although mammalian cells have more complex growth requirements than microbes. The pioneers and proponents of cell-based meat are greatly concerned about the impact of animal agriculture on public health, the environment, global food security, and animal welfare, and view cell-based meat as a way to produce the products that people desire without the destructive effects of breeding and slaughtering billions of animals annually to produce meat.

Cell-based meat research is a new sub-discipline of science that combines traditional meat and food science with bioengineering and biomanufacturing. Producing meat without the animal requires advances in cell line development, cell cultivation, bioprocess scale up, and product development. Biomedical technology is used for meat cultivation³, but has cost and material restrictions. Culture conditions for cell-based therapies have ample margins to be expensive, but cultivated meat products must reach price parity with animal meat to be commercially viable. All inputs into the cultivation system have to be cheap and food grade, including media components, microcarriers, and tissue or product structuring components. Cell-based meat research is guided by the material selection requirements for the bioprocess with respect to food, sourcing, and performance considerations (Table 1.1).

Consequently, new research methodologies, goals, and guidelines should be developed in contrast to techniques commonly used in biomedical research.

The goal of this dissertation is to define a basic foundation for areas of cell-based meat research, along with guiding parameters for how the approach to this field of study differs from biomedical research. An investigation of myogenesis, adipogenesis, and tissue engineering strategies for cell-based meat product development follows, with respect to these outlined research guidelines.

Table 1.1. Material selection considerations for cell-based meat bioprocesses.

Material Selection Considerations		Examples
Food Considerations	Food Safety	<i>The material should be edible or removable before the final product is prepared</i> Inedible and unremovable materials may impact the quality of the product, have negative effects on human health, or be unable to receive regulatory approval for use in food. <i>Edible:</i> cells and plant scaffolds <i>Inedible:</i> cell culture media and reagents
	Consumer Acceptance	<i>Consumers should be comfortable with the material and the way it's prepared</i> A negative consumer reaction can hurt an individual product and company, as well as general perception of the industry overall. Differences in cell line engineering methods may be opaque and incomprehensible to consumers.
	Food Regulation	<i>Simple or nonexistent regulatory oversight will expedite scale up</i> The FDA may require safety data for a novel material or an existing material used in a novel way. A critical material may be worth the effort, but not every material in the bioprocess. A recombinant collagen is useful for the bioprocess but would require GRAS notification.
Sourcing Considerations	Low Cost	<i>The material should be negligible in cost</i> Generally, animal meats are subsidized commodity items, making them extremely low cost. Cell-based meat must drive down costs to be affordable to consumers and to reach price parity with meat from animal. <i>Low Cost:</i> Chemical composition of cell culture media <i>High Cost:</i> Laminin
	Animal Free	<i>The material should not be animal derived</i> Animal products will potentially increase the cost of production, and cell-based meat cannot become a sustainable method of food production by still requiring animal derived products. <i>Animal Derived:</i> FBS, fish oil <i>Animal Free:</i> Plant based scaffolds
	Scalable Sourcing	<i>The production yield or availability of the material should be enough to supply food to a human population</i> A material that cannot be currently produced in an animal free way, or is difficult to source or manufacture will increase product cost and production timeline. A protein can be sourced in enough quantity for a scaled production level bioprocess.
Performance Considerations	High Efficacy	<i>The material should substantially improve cell activity or bioprocess productivity</i> A highly effective material should compensate for its cost by optimizing cellular proliferation, differentiation, flavor, or harvest yield. An ECM protein enhances cell adhesion rate on substrates, improving biomass yield.
	Upstream Bioprocess Compatibility	<i>Incorporation and functional activity of the material must be supported by the bioprocess</i> A material's usefulness to the bioprocess decreases if the inclusion of the material into the bioprocess isn't technically feasible with current equipment. The material should also function effectively within the bioprocess conditions. Developing a scalable method for cell encapsulation in hydrogels. Cell encapsulated hydrogels must maintain integrity under shear forces.
	Downstream Product Effects	<i>Incorporation of a material during an upstream process should not have unwanted downstream effects</i> A material's usefulness is also limited if the material causes unwanted effects in subsequent stages of upstream processing, downstream processing, and product preparation. An enzyme used upstream remains active into downstream processing, killing cells or decreasing effectiveness of food binders.

Chapter 2

BACKGROUND AND SPECIFIC AIMS

“When one tugs at a single thing in nature, he finds it attached to the rest of the world.”

John Muir, The Yosemite

The concept of growing meat without the animal was first envisioned by futurists, who presented a vision of how food production would change with the advancement of technology. In 1931, Winston Churchill predicted in his essay '50 Years Hence' that, "... we shall escape the absurdity of growing a whole chicken in order to eat the breast or wing by growing these parts separately under a suitable medium." This concept became a common theme in science-fiction, where meat is derived from advanced technology. In 1997, the first patent application for cultivated meat products was filed by a Dutch physician named Dr. Willem Van Eelen of the Netherlands, one of the field's earliest pioneers, who realized cells could be grown as a food⁴. Van Eelen's idea came after suffering from starvation in a Japanese prisoner-of-war camp and being exposed to cell culture technology in medical school after the war ended. His expired patent⁵ used tools from biomedical research to design systems where meat could be grown from cell culture. However, the early technology stage of bioengineering and biomanufacturing at the time could not feasibly bring cultivated meats to commercialization. The first research paper on cultured meat was published in *Acta Astronautica* by Benjaminson, Gilchrist, and Lorenz⁶, who did a feasibility study to evaluate the growth of muscle cells *in vitro* as a food source for space travelers. The study design included harvesting goldfish muscle explants and incubating the tissue under various culture conditions. The researchers found that culturing the muscle explants in FBS increased growth of the explants by 13.7%, demonstrating the first proof of concept for edible muscle tissue biomass growth in culture.

In 2004, Dr. Jason Matheny founded a non-profit called New Harvest, an organization that grew to support and fund cultivated meat research. He published the first scientific article on cultivated meat in 2005, "Such "cultured meat" could enjoy some health and environmental advantages over conventional meat, and the techniques required to produce it are not beyond imagination"⁷. Then, in 2008, the People for the Ethical Treatment of Animals (PETA) next offered a \$1 million prize for inventors who could develop a cultivated chicken nugget⁸. PETA was concerned with both the mistreatment of animals and the environmental effects of the animal agriculture industry and wanted to find a solution for producing meat products where no animal would be hurt. That effort was not successful but excited further examination of the possibility of cultivating meat to inventors, entrepreneurs, and thought leaders worldwide. Finally, on August 5th in 2013, Dr. Mark Post of the Netherlands introduced the world to the first cultivated beef burger. The burger was grown from skeletal muscle cells from a cow. The cells were synthesized into small tissues which were then mixed into a patty containing breadcrumbs, salt, and pepper. During the burger's public taste testing, a panel of tasters describe it as having the taste and texture of meat. One commentator mentioned that the burger was quite lean and lacked fat content, and could be improved with the addition of fat⁹. Furthermore, the burger highly resembled raw and cooked beef burgers from an animal.

Within a few years the first handful of cultivated meat companies and a nonprofit called the Good Food Institute were founded, and the dawn of a new industry began. By the year 2020, a handful of cultivated meat companies increased to over 60, and the rationale for transitioning the animal agriculture industry to growing meat without the animal became increasingly apparent. Destructive climate events caused by climate change are increasing in severity and the animal-originated novel coronavirus pandemic is spreading across the world.

2.1. Meat, Pandemics, and Public Health.

The livestock industry does not exist within a vacuum; it is a globalized industry with worldwide consequences that affected the past, impact earth in the present, and will continue to worsen in the future. The most destructive impacts of animal agriculture are the ways that it damages public health and the environment, causes climate change, and continuously enforces the normalization of speciesism, a

nearly invisible and invincible belief system that humans have absolute superiority and precedence over all other forms of life¹⁰. Speciesism has led to the psychological decoupling of humans from nature, leading to devastation in nonhuman lifeforms at the risk of threatening the sustainable ecological balance of our biosphere. This belief greatly influences cultural norms and institutionalized decision making in public policy, government, and private enterprise. A summary follows of the effects of speciesism on public health disruption and environment destruction.

2.1.1. Zoonotic disease transmission.

Zoonoses occurs when harmful pathogens such as viruses, bacteria, parasites, or fungi are communicable to a human host, and can happen from the interactions of humans with livestock, wild animals, and domesticated pets. The biggest threats to public health are viruses and antibiotic resistant bacteria. 75% of all emerging infectious diseases come from animals¹¹. For decades, medical professionals, public health scientists, and the Center for Disease Control has warned that breeding and housing animals to produce animal products results in zoonotic disease transmission from animals to humans.

2.1.2. Viruses.

Harmful viral infections are difficult to treat due to the need to develop an effective vaccine, which can take years, while the suffering and mortality rate of people infected with the virus continues to accelerate. The first vaccine was developed to treat smallpox in 1796 by Dr. Edward Jenner. Smallpox has existed since 10,000 BC and has claimed millions of lives over the course of human history¹². In some cases, such as the 1918 flu that killed 50-100 million people worldwide, a preventative vaccine cannot be developed in time to prevent an immense cost of human life¹³.

Influenzas, coronaviruses, and other viral species commonly originate from the interactions between humans with livestock or wild animals. The 1918 flu likely originated from a pig farm in Kansas¹³, the H5N1 bird flu from a chicken farm in China, and the H1N1 swine flu from a pig farm in North Carolina. Vaccines were developed for the latter two influenzas^{14, 15}. Many respiratory coronaviruses have animal origins as well, such as MERS-CoV, which was transmitted from camels, and SARS-CoV and SARS-

CoV-2, both hypothesized to originate from bats^{16,17}. SARS-CoV-2 may have had an intermediate pangolin species reservoir¹⁸, and has become a worldwide pandemic, restructuring societies in previously impossible ways.

2.1.3. Antibiotic resistant bacteria.

The industrialized livestock sector increases profit by reducing the amount cubic space required to support animal breeding and maturation. This translates to living conditions where animals are kept in close proximity, which facilitates rapid spread of pathogens through herds. To keep the animals healthy from bacterial infections, and thus reducing threats to the meat supply chain, the industry has dealt with this issue through prophylactic administration of antibiotics to animals¹⁹. The Center for Disease Control stated, "It is difficult to directly compare the amount of drugs used in food animals with the amount used in humans, but there is evidence that more antibiotics are used in food production"²⁰. The continuous and unmitigated use of antibiotics increases the development of antibiotic resistant bacteria, which has dire implications for human health. Antibiotic resistant bacteria can be spread to workers in meatpacking facilities and through animal meat. These untreatable infections will increase the incidence of sickness and death, and result in infections from unrelated treatments at contaminated hospitals or medical facilities²¹. Public health experts have warned that antibiotic resistant bacteria evolving at the factory farms is a looming public health crisis, and the Food and Drug Administration has advised the animal agriculture industry to phase out its prophylactic use of antibiotics²².

2.1.4. The future of animal agriculture and zoonotic disease transmission.

The most devastating viruses have come from food systems that provide humans with animal meat, such as the farm that spawned the 1918 flu and the wet market in Wuhan, China, that gave rise to SARS-CoV-2. Vaccines and antibiotics are measures used to treat symptoms of the problem, but do not mediate the likelihood of emergent zoonotic disease transmission to humans. The only way to reduce the incidence of zoonosis from factory farming and the consumption of wildlife and still have meat available is to shift from a model using animals to cultivating meat products.

2.2 Environmental destabilization.

2.2.1 Greenhouse gases.

Rising anthropogenic greenhouse gas emissions will warm the planet between 1.5°C - 4.8°C by 2100. The warmer the planet becomes, the more devastating the effects on the biosphere, which includes extreme heat waves, sea level rises, declining global food stocks, water scarcity, and mass migration events. These risks will destabilize the support systems humans need to survive and increase the likelihood of the collapse of human civilization and possible extinction²³. Scientists have advised that a global temperature must be held under 2°C to avoid the worst effects of climate change, but our current trajectory is on track for 4°C²⁴.

The livestock sector has been increasingly recognized as a major contributor to climate change through greenhouse gas emissions and environmental destruction. In a 2013 report by the Food and Agriculture Organization of the United Nations called *Tackling Climate Change through Livestock: A Global Assessment of Emissions and Mitigation Opportunities*, a complete life cycle analysis of the environmental impact of factory farming showed that the industry is responsible for 14.5% of global greenhouse emissions, which are majorly composed of CO₂, CH₄, and N₂O²⁵. Methane and nitric oxide are extremely potent greenhouse gases. CH₄ has 25 times the global warming potential of CO₂, and N₂O has 298 times the warming potential²⁶. The bigger our global herd of livestock, the more greenhouse gases are emitted and the worse the consequences for the environment. By far, most of those emissions come from beef and dairy, which produce 41% and 20% of emissions, respectively.

14.5% of greenhouse gases are produced by animal agriculture though both direct and indirect emissions, about 7.1 gigatons of CO₂.eq (carbon equivalent). CO₂.eq is a metric used to compare the emissions from various greenhouse gases on the basis of their global-warming potential, by converting amounts of gases to the equivalent amount of carbon dioxide with the same global warming effect. Demand for meat will double by 2050, and are likely to increase emissions to ~14.2 gigatons of CO₂.eq. This will be devastating for the planet, since humans are currently producing over 49 gigatons of CO₂.eq globally from all human activities²⁵. If we want to minimize global warming to 1.5°C (likely our best case

scenario) but keep animal agriculture on track as projected, animal agriculture would compose 49% of the total global emissions budget in 2030²⁷.

Direct emissions.

Direct emissions from the livestock sector are produced by animals themselves, such as gases released during normal homeostasis of cattle. CH₄ and N₂O are produced from cattle in high quantities due to enteric fermentation and manure management. According to a 2018 report by the Environmental Protection Agency examining GHG emissions in the U.S., CH₄ emissions account for 10.1% and N₂O for 4.9% of total GHGs in the United States in 2016. The leading sources of CH₄ are produced by enteric fermentation (25.9%) and manure management (10.3%) of livestock, which is 36.2% of total CH₄ emissions, and 4.9% of N₂O emissions come from manure management. The EPA estimated that 3.9% of total GHGs are produced by direct emissions from the animal agriculture industry, approximately 255.9 million metric tons of CO₂ eq.²⁶. However, these U.S. values don't include emissions from infrastructure supporting animal agriculture, such as transportation of animals, animal products, or feed for animals; energy used by the industry; or animal feed production. A complete life cycle analysis is required to understand the full scope of the global impact of animal agriculture, as well as an examination of the GHGs produced by individual livestock and poultry species.

Indirect emissions.

Indirect emissions do not come from the animals themselves but are instead produced from the raw material inputs into animal agriculture, such as feed production, the energy required to power animal and meat processing facilities, and transporting billions of pounds of animal meat across countries, continents, and oceans. According to the 2013 FAO study, the animal agriculture industry is globally responsible for 7.1 gigatons of CO₂ eq per annum. Of total GHG emissions from the sector, 39% results from enteric fermentation and feed production, processing for animal's accounts for 36%, manure storage is 10%, 9% comes from expansion of pastures and feed crops into forests, and 6% comes from processing and transportation of animal products. 51% of emissions are produced indirectly by supporting

the industry, and 20% of emissions result from the burning of fossil fuels to supply energy to all levels of the supply chain.

Industry actions that reduce the availability of carbon sinks.

Carbon sinks remove carbon from the atmosphere and keep greenhouse gas emissions in check. Natural vegetation, such as forests, are important carbon sinks that convert CO₂ into O₂ during photosynthesis. Focusing on natural forest restoration while stopping global deforestation will remove CO₂ from the atmosphere and limit the degree of global warming to 1.5°C if implemented immediately²⁸. The Bonn Challenge, launched by the German government and the international Union for conservation of Nature, has led to an agreement between 43 countries across the tropics and subtropics to commit 350 million hectares of degraded land to forest restoration by 2030²⁹. However, 67% of global deforestation from agriculture, including the world's rainforests, is due to producing feed crops for livestock and poultry, with the greatest land changes necessary for beef and dairy cows³⁰.

2.3 Transforming the animal agriculture industry to a cell-based meat model.

The animal agriculture industry is a threat to human civilization due to a role in the development pandemics the destruction of the environment and its role in accelerating climate change. By 2050 we will have accelerated beyond the carbon equivalent threshold of warming the planet above 2.5°C, the worst case scenario for the climate crisis according to planetary scientists²³. Consequently, the expansion of the livestock industry cannot continue along its current path if humans want to have a future. Additionally, the current model of the animal agriculture in its industrialized capacity greatly increases the likelihood viral pandemic much more deadly than SARS-CoV-2.

As a civilization we cannot defeat demand for animal products but we can produce them in a new way due to advances in food science, biomanufacturing, and synthetic biology. Plant-based meat alternatives to meat from animals have improved in the last decade with companies like Beyond Meat and Impossible Foods entering a mainstream consumer diet. This new generation meet alternatives uses advanced food science methods to re-create the taste and texture of animal meat, and the plant-based meat industry has continuously increased its market share in the last decade. Consumer demand for

plant-based meat has not yet reached a point of significant competition with animal products because they are currently not similar enough to the animal meat to provide a suitable alternative. Cell-based meat adds similar flavor and juiciness to plant-based products that remarkably improve similarity to animal meat. Consequently, cell-based meat will provide an adequate solution to re-creating animal meat products without the animal, which provides a path towards revolutionizing an industry that will otherwise completely destabilize human civilization.

2.4. Basic overview of cell-based meat technology.

Cell culture technology has created new ways to produce cells *in vitro* to substitute cellular material from animals. Cell cultured meat research has thus created a new discipline of cultured meat science. The objective is to ultimately blend traditional meat science, biomedical engineering, and biomanufacturing to create foods from edible cell lines. Cells are isolated from a tissue biopsy from animals such as cattle, pigs, sheep, poultry, or aquatic species to develop cell lines that have specific functional or quality characteristics, such as enhanced cell division ability and specific flavor or nutrition³¹. A growth or cultivation *bioprocess* is developed to produce food from the cell lines, where animal cells are used as building blocks for a final food product³². This differs from traditional meat production, which reduces an animal carcass into specific products.

The flavor, texture, nutrition, and color of animal meat is produced at the cellular level. Cells express flavoring proteins and fats that yield distinct flavor profiles associated with different kinds of meats, species, and muscle organs³³. Consequently, cell lines used to cultivate meat must have similar proteins and lipid profiles to provide a similar sensory experience to animal meat. The way cell cultured products are structured is also dependent on which kind of meat product is being simulated. For example, the connective tissue in beef and pork is structured differently: marbling and intramuscular fat is highly visible in beef, whereas in most pork the intramuscular fat is not as anatomically visible and separated³⁴.

Currently, there are no cell cultured meat products available for consumer purchase because the technology is still in the developmental stages. As the technology matures, the basic culture process of cell cultured meat products will include *cell line development* and *cell production* where edible cell lines are grown in bioreactors with high fluid volumes. The cells can be used to formulate *unstructured*

products that simulate ground meat or *structured* products like steak or pork chops during a subsequent *structuring* step (Figure 2.1). Unstructured and structured cell-based meats will require unique equipment and processing steps. The cells used for unstructured products can be mixed as a raw food material into ground meat, such as chicken nuggets and hamburger; sauces such as fish sauce; or gourmet items like

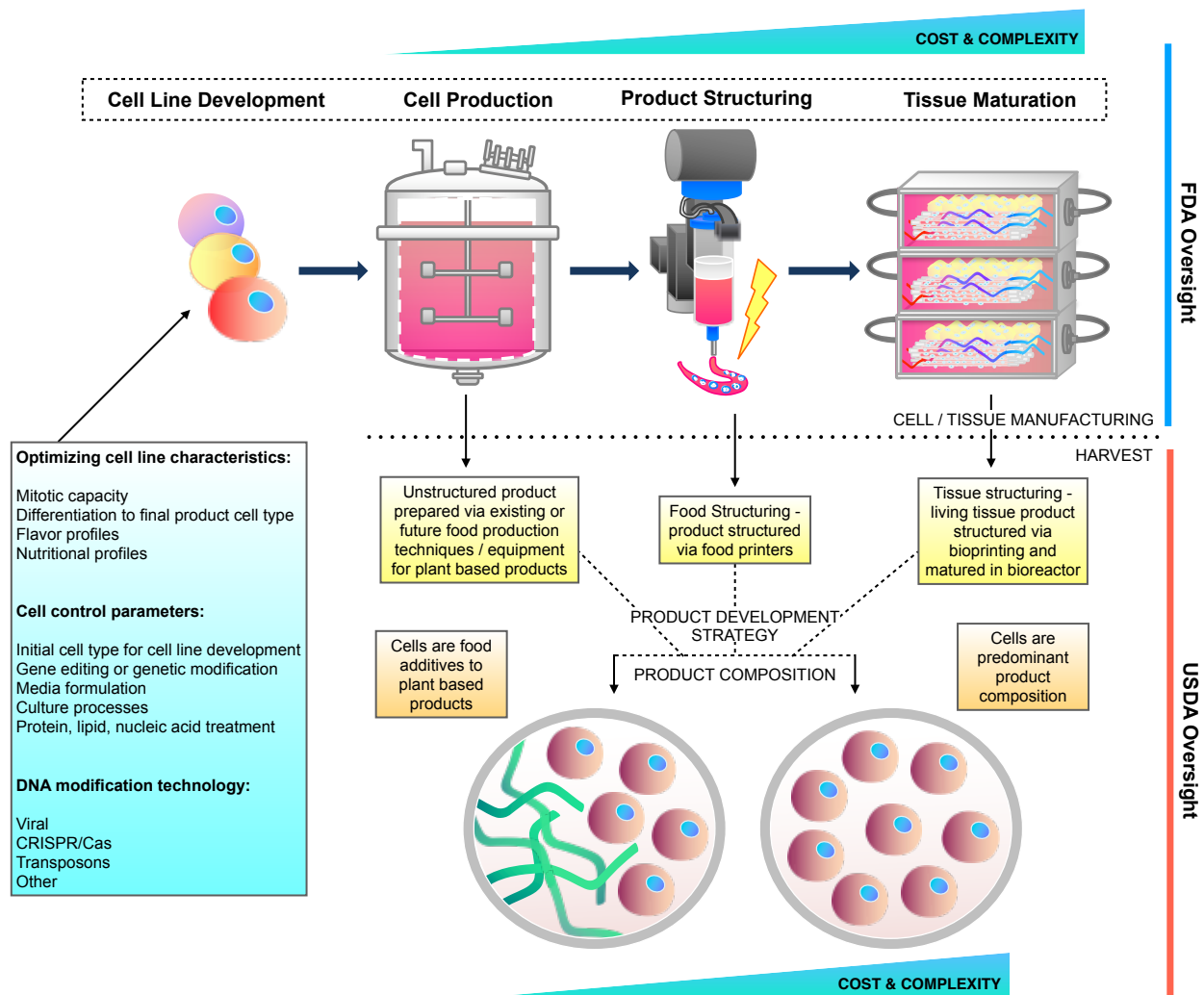


Figure 2.1. Cell-based meat bioprocess workflows, product development strategies, product compositions, and regulatory oversight. Cell line development requires optimizing cell line characteristics. Production costs increase with the complexity of the biomanufacturing workflow; the need for additional equipment; reagents; and cellular biomass. Consequently, costs stem from product development strategy and product composition.

pâté or croquettes. Unstructured products do not require the additional technology involved for structuring, but will still require special food processing steps or food manufacturing equipment to create texture and prepare the final product.

The structuring step can result in a finished food product during *food structuring*, or a living tissue product during *tissue structuring*. Tissue structuring, also called tissue engineering or tissue synthesis, embeds living cells within a 3D scaffold, which simulates connective tissue. A scaffold is a matrix composed of edible material that provides a 3D structure to the tissue. It can be composed of a protein matrix, such as collagen³⁵, a polysaccharide matrix, like cellulose from plants, or a blend of both. Protein and polysaccharide scaffolds can be produced from animal, plant, or microbial sources³⁶. The living tissue can then be matured in a tissue cultivation bioreactor. Tissue structured products produced by tissue engineering may also require extra cell types in order to recreate tissue patterns that include marbling and blood vessel networks, such as fibroblasts or endothelial cells, which form blood vessels during a process called vasculogenesis³⁷. Alternatively, cultivated cells may be incorporated into a product that simulates whole meat cuts during food structuring, but lacks hallmark tissue components such as living cells embedded into an extracellular matrix (ECM). These products undergo a food printing step to structure a final product instead of bioprinting step, which would result in a living tissue matured in a bioreactor. Cell-based foods structured from food printers would not result in a living product and could be served as-is. Additionally, 3D printing technology may not be used in all structuring applications. Other methods of structuring may be developed in the future.

Product development strategy creates different product types that will result from overcoming technical hurdles at each phase of the cultivation process (Figure 2.1). The first cell cultured meats will add small quantities of cells from animal or aquatic species to plant-based meat analogues. The animal cells will essentially serve as food additives that enhance the palatability or nutritional characteristics of edible plant protein, such as adding a small percentage of skeletal muscle cells grown from a chicken to a plant-based chicken nugget. Foods from subsequent product phases may be composed almost entirely of animal cells with very minimal or no plant-based protein extender.

2.4.1 Cell Line Development.

Cell line development, or cell line engineering, begins with extracting individual cells from a tissue biopsy of an animal. The cells obtained from an animal possess inherent limitations that make them unsuitable for a large-scale and indefinite manufacturing process. Aging occurs at the cellular level, and the harvested cells isolated from an animal will also age during culture³⁸. The aging process depletes the proliferative capacity of the cells by shortening telomeres through each cell division. Once the telomeres have shortened to their final length, they are no longer able to divide, and the cells undergo senescence. The limited number of cell divisions due to telomere shortening is called the Hayflick limit³⁹. The Hayflick limit is a threshold that limits the biomass that can be obtained from *primary animal cells* (Figure 2.2A).

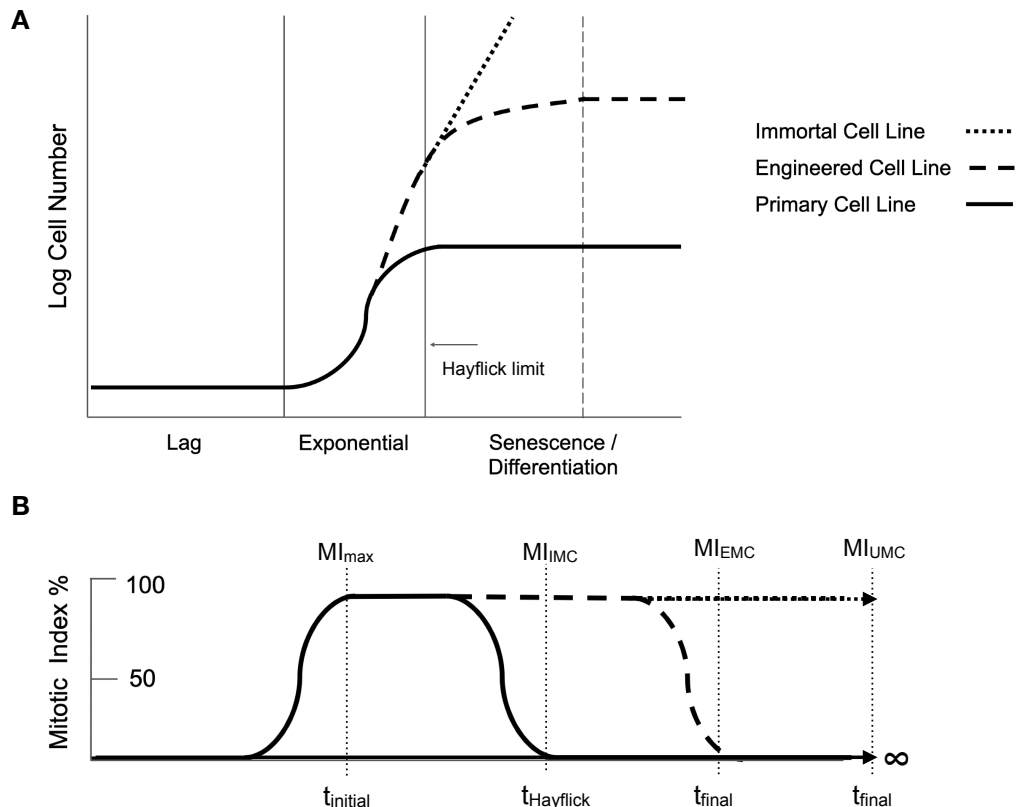


Figure 2.2. Mitotic capacity of cells. (A) The log cell number of immortal, engineered, and primary cell lines over time. (B) The mitotic index of immortal, engineered, and primary cells lines over time.

Increasing the time that cells are in an increasing or steady state of cell proliferation is enhanced mitotic capacity.

Culturing meat necessitates extending the ability of edible cells to undergo cycles of mitosis by extending or removing a limit to the total number of cell divisions. *Engineered cell lines* can extend the Hayflick limit and allow more cell divisions while still being subject to the limit. *Immortalized* cell lines completely bypass cellular aging to allow infinite expansion, like HeLa cells and C2C12s.

For a given cell population, the *mitotic capacity* (MC, formula 1) is the potential for the cell to undergo mitosis: the ratio of the change in *mitotic index* (MI, formula 2) over change in time (Figure 2.2B).

$$1) \quad \text{Mitotic Capacity (MC)} = \frac{MI_{\max} - MI_{\text{final}}}{t_{\text{initial}} - t_{\text{final}}} = \frac{\Delta MI}{\Delta t}$$

$$2) \quad \text{Mitotic Index (MI) \%} = \frac{\text{Number of proliferating cells}}{\text{Total cells in population}} * 100$$

$MI_{\max} = y_{\max}$ is used to determine the pattern of mitotic replications after the MI has reached its peak state.

Innate mitotic capacity (IMC) is the natural capacity of primary cells to undergo mitosis until they reach the Hayflick limit, where $MI_{\text{final}} = MI_{\text{IMC}} = 0$; since the cells reach $MI = 0\%$ and undergo senescence, and $t_{\text{final}} = t_{\text{Hayflick}}$. *Enhanced Mitotic Capacity* (EMC) extends the Hayflick limit past its innate number of cell divisions, although the cells are still eventually subject to limited rounds of mitosis, where $MI_{\text{final}} = MI_{\text{EMC}} = 0$; while $t_{\text{final}} > t_{\text{Hayflick}}$. *Unlimited mitotic capacity* (UMC) is an immortal cell line that can undergo cell replication indefinitely without being subject to the Hayflick limit, where $MI_{\max} = MI_{\text{final}} = MI_{\text{UMC}} > 0$ as the cells reach a steady state of cell proliferation and $t_{\text{final}} = \infty$. IMC and EMC are negative values, while $UMC = 0$ during steady state expansion. Therefore: $IMC < EMC < UMC = 0$.

A cell population *A* with a high MI_{\max} is a good candidate for developing a cell line, especially if it has a long t_{Hayflick} , meaning it can undergo high rate of proliferation without hitting the Hayflick limit too early in culture. However, a cell population *B* with a long t_{Hayflick} but a low MI_{\max} is a slowly dividing population that may have the same Hayflick limit of cell population *A* but would take a much longer time to develop a cell line from, since these cells will take longer to undergo a population doubling. You can increase the value

of MI_{max} or t_{final} to improve the performance of the cell line. However, increasing the value of MI_{max} without a concurrent strategy to extend t_{final} will result in a lower t_{final} value, since the cells will undergo proliferation more quickly and reach the Hayflick limit faster. Robust immortal cell lines should be optimized to have high $MI_{max} > 80\%$ that won't decrease over time. In this way, cell lines can scale indefinitely and rapidly produce biomass for human consumption.

Immortal cell lines can be created through genetically engineering cells^{40, 41}; by selecting a cell type for expansion with naturally enhanced or indefinite proliferation potential, such as stem cells⁴²; or depending on spontaneous immortalization of cells through natural genetic mutations that occur during serial cell culture⁴³. Cell lines are stored in a *master cell bank*, where they are cryopreserved in a state of suspended activity until they are needed. Cryopreserved cells can be thawed and re-animated in expanded in bioreactors.

Cells used for cell cultured meat can be derived from various kinds of stem or precursor cells found in animal embryos, bone marrow, or muscle tissue. Induced pluripotent stem cells (iPSCs) can also be used, which, along with embryonic stem cells, can be differentiated into any cell type in the body, such as skeletal muscle cells⁴⁴ (Figure 2.3A). Regardless of the initial cell population, the manufacturing process must result in the production of cells (e.g., muscle and fat) found in animal meat. The three dominant cell types that influence meat flavor, juiciness, and texture are skeletal muscle cells, intramuscular fat cells, and connective tissue cells called fibroblasts. Cell lines must be able to undergo *myogenesis* (the formation of multinucleated, contractile skeletal muscle cells⁴⁵ and *adipogenesis* (the development of fat cells containing intracellular lipid droplets^{46, 47} (Figure 2.3B, C). The capacity of a cell line to undergo myogenesis and adipogenesis determines meat quality. Cell lines that produce connective tissue cells like fibroblasts may also be used, since the texture of meat is greatly impacted by the connective tissue scaffold that holds cells together⁴⁸.

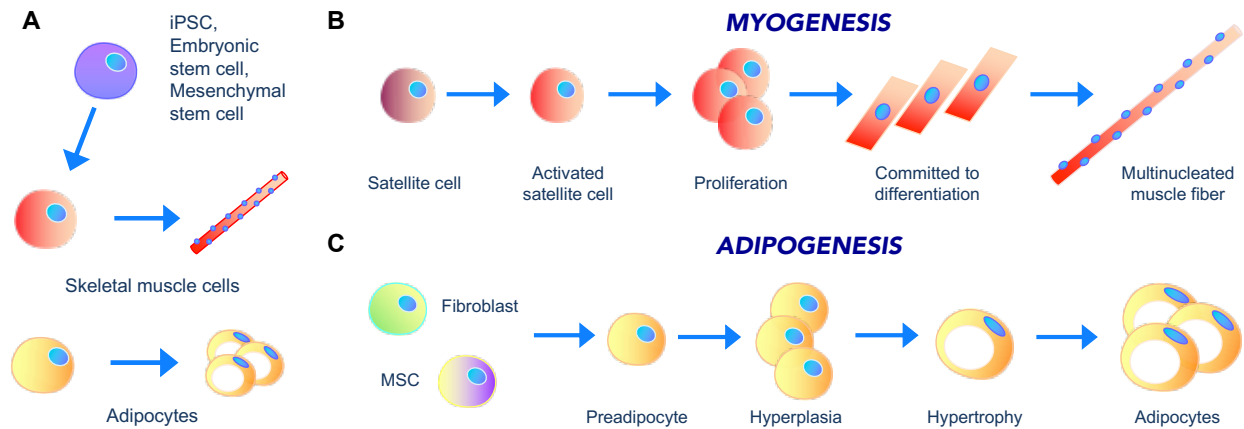


Figure 2.3. Various cell types used for cell-based meat and their differentiation. (A) Stem cell sources such as iPSCs, embryonic stem cells, and mesenchymal stem cells can be differentiated into cell types relevant for meat products. (B) Myogenesis begins with the activation of a muscle stem cell called a satellite cell and ends with a multinucleated muscle fiber. (C) Adipogenesis occurs when cells mature into adipocytes that contain flavorful lipid droplets.

Myogenesis and Adipogenesis.

Skeletal muscle cells are the main source of the umami flavor in meat that contains muscle-specific proteins which contribute to meat flavor and pigment⁴⁹. Myogenesis begins during embryogenesis and is characterized by mononuclear muscle progenitor cells fusing into multinucleated muscle fibers⁵⁰. This results in the production of high-density skeletal muscle cytoskeletal proteins, myosin heavy chain, and myoglobin, which serves as an oxygen reservoir for cells. Myoglobin is red in hue and its pigmentation arises from various redox forms and concentration within skeletal muscle cells⁵¹. Myogenesis is controlled by sequential expression of myogenic transcription factors and begins with the activation of quiescent Pax7⁺ expressing satellite cells, a muscle stem cell. In their activated form, Pax7⁺MyoD⁺Myf5⁺ satellite cells undergo asymmetric division to produce self-renewing satellite cells and *myoblasts* committed to undergo myogenesis. Pax7⁺MyoD⁺Myf5⁺ myoblasts undergo symmetric division to expand in numbers, then commit to terminal differentiation as Pax7⁺MyoD⁺Myf5⁺ MyoD⁺Myogenin⁺ mononuclear *myocytes* committed to exit the cell cycle and terminally differentiate⁵⁰. These mononuclear

cells begin to fuse into multinucleated muscle fibers, or myotubes, and develop sarcomeres, which are the contractile unit of the cell. Sarcomeres are composed of myosin heavy chain and actin filaments that consume ATP to slide against one another to shorten the length of the sarcomere and consequently the length of the muscle fiber. The unity of sarcomeres and muscle fibers contracting together creates the contractile force of muscle organs⁵².

Myogenesis is under the control of paracrine, biomechanical, and electrochemical signaling. Proliferation is controlled by hepatocyte growth factor (HGF) release in the early stages of muscle regeneration which activates quiescent satellite cells to enter the cell cycle. HGF⁵³, fibroblast growth factor 2 (FGF-2)⁵⁴, and vascular endothelial growth factor (VEGF) signaling stimulate proliferation but not differentiation of muscle progenitor cells⁵⁵. In early stages of myogenesis, insulin-like growth factor 1 (IGF-1) signaling promotes survival and proliferation of satellite cells. In later stages, IGF-1 drives differentiation into myotubes and also increases hypertrophy of muscle fibers through increased protein synthesis⁵⁶. Leukemia inhibitory factor (LIF) increases the rate of muscle regeneration by enhancing myoblast proliferation and hypertrophy of muscle fibers⁵⁷. LIF expression is ubiquitous during muscle repair and expressed by both macrophages and muscle cells⁵⁸. Although transforming growth factor beta-1 (TGF- β 1) has been found to be a potent inhibitor of myogenesis in 2D *in vitro* systems, we've previously found it to be an accelerator of myogenesis in 3D tissue-engineered systems at low concentration⁴⁸. Differentiation can be enhanced through reductions of mitotic growth factors and increasing expression of differentiation factors, cell-cell contact mediated through m-cadherin, and electrical pulses that cause membrane depolarization⁵⁹.

Fibroblasts support and stabilize muscle fiber architecture and biomechanics through basement membrane synthesis during embryogenesis and facilitate muscle regeneration with extracellular matrix (ECM) deposition and remodeling^{60, 61, 62}. The interaction between myoblasts and fibroblasts, two predominant cell types involved in skeletal muscle regeneration, with surrounding ECM and trophic factors determine healing outcomes. Transforming growth factor beta 1 (TGF- β 1), produced by multiple cell types during wound healing, is a primary mediator of the mechanical, biochemical, and cellular behaviors observed in response of muscle to injury⁶³. TGF- β 1 signaling differentiates fibroblasts into myofibroblasts, which are significant producers of collagen I (COL I), the main protein component of scar

tissue, and α -smooth muscle actin (α -SMA), a highly contractile form of actin⁶⁴. Normally these proteins are transiently expressed during muscle regeneration and contribute to tissue remodeling by temporarily providing physical substrates and biochemical cues for muscle fiber regeneration.

Adipogenesis regulates energy metabolism in the body by collecting free fatty acids (FFAs) bound to albumin from the blood into adipose cells for future energy use and releasing them back into the blood when glucose levels are low⁶⁵. When energy is plentiful, preadipocytes undergo differentiation into adipocytes during adipogenesis. Adipocytes accumulate intracellular lipid droplets that provide juiciness and additional flavor to meat through lipogenesis⁶⁶. Adipogenesis initiates in intramuscular preadipocytes with growth arrest and morphological changes that shifts the cells from a fibroblastic spindle shape to a rounded morphology. Preadipocytes start producing CCAATT enhancer binding proteins β (C/EBP β) and CCAATT enhancer binding proteins δ (C/EBP δ) transcription factors, which activate gene transcription of peroxisome proliferator-activated receptor γ (PPAR γ) and CCAATT enhancer binding proteins α (C/EBP α) transcription factors. PPAR γ is a master regulator of adipogenesis and a ligand-activated nuclear membrane receptor protein that can translocate into the nucleus to activate gene expression. PPAR γ and C/EBP α begin transcribing genes that promote insulin sensitization, glucose utilization, and adipocyte maturation, such as insulin receptor; fatty acid synthase; adipocyte protein 2 (aP2), also known as fatty acid binding protein 4 (FABP4); and glucose transporter type 4 (GLUT 4)⁶⁷. These proteins facilitate transportation of FFAs and glucose into the preadipocyte cytosol and promote intracellular lipogenesis.

Lipogenesis encompasses *de novo* fatty acid synthesis, the production of FFAs⁶⁸, and triglyceride synthesis, which esterifies three FFAs to glycerol to produce triglycerides that incorporate into lipid droplets⁶⁹. Lipolysis occurs when energy levels enter a fasting state. FFAs are enzymatically cleaved from intracellular triglycerides and transported to the blood. Cells in need of energy uptake the FFAs for β oxidation in the mitochondria to produce ATP. Fasting activates transcription of peroxisome proliferator-activated receptor alpha (PPAR α) in the liver, a transcription factor that activates a set of genes involved in fatty acid oxidation⁷⁰. The activation of PPAR- β/δ enhances fatty acid oxidation in skeletal muscle and adipose tissue. PPAR- β/δ ligands include several 14- to 18-carbon saturated fatty acids as well as 16- to 20-carbon polyunsaturated fatty acids⁷¹.

Adipogenesis can be initiated *in vitro* by media components that produce metabolic changes in preadipocytes. Adipogenic induction and differentiation medias containing FBS, high glucose, insulin, dexamethasone, IBMX (3-isobutyl-1-methylxanthine), thiazolidinediones (TZDs), and FFAs are commonly used to induce adipogenesis in preadipocytes^{65, 72, 73}. Dexamethasone is an anti-inflammatory corticosteroid used in many medical applications and IBMX is a small chemical compound which together activate expression of C/EBP β and C/EBP δ . TZDs like ciglitizone are ligands that activate PPAR γ to initiate downstream adipogenic gene transcription. Insulin, glucose, and free fatty acids contribute to intracellular lipogenesis by mediating cellular metabolism. Insulin binds to insulin receptors that activate intracellular signaling pathways to recruit the GLUT 4 transport protein to the plasma membrane, allowing glucose to enter into the cell. Glucose converts to Acetyl-CoA via the glycolytic pathway, which is used to produce fatty acids during *de novo* lipogenesis⁷⁴. Alternatively, FFAs such as erucic acid, elaidic acid, oleic acid, palmitoleic acid, myristoleic acid, phytanic acid, and pristanic acid can be transported through the cell membrane and solubilized into the cytosol via aP2⁴⁷. PPAR γ is also activated via FFA binding⁷⁵.

2.4.2 Cell Production.

The goal of *cell production* is to yield a large biomass of edible cells upwards of thousands of kilograms. The bioprocess must be scalable, meaning it can begin in very small culture volumes, such as a cell culture flask, and be expanded into larger and larger culture volumes, such as a 20,000 liter bioreactor⁷⁶. The growth process typically consists of an extended growth phase to yield a high biomass of cells which can then be differentiated into cell types found in animal meat. The culture media components used for cell cultivation stimulate the cells to undergo proliferation and differentiation. Different cell types need unique growth factor combinations, such as skeletal muscle cells requiring a different media composition than fat cells⁷². Cell cultured meat facilities may require hundreds of thousands of liters of cell culture media or more that will be supplied by a separate *media manufacturing* process or industry supplier.

There are many types of bioreactors that can be used for cell cultivation, the most common being stirred-tank bioreactors. These systems are already used to biomanufacture proteins used by the dairy industry to make cheese, such as fermentation-produced chymosin from microbes⁷⁷. The cells in stirred-tank bioreactors cells are grown in a fluid suspension as a single cell suspension, in cell aggregates, in

encapsulated form, or on microcarriers. Cells can be encapsulated into gel-like materials that lower shear forces on the cells while allowing their growth and differentiation⁷⁸. The gel material is usually an extracellular matrix protein or plant material component. Microcarriers are spherical units smaller than a millimeter in diameter which serve as an adhesive substrate for cells⁷⁹. Microcarriers can be made from edible material that can be incorporated into a food product, such as plant derived protein or cellulose, or an inedible material like plastic. Inedible microcarriers must be separated from the cells before the cells are mixed into a food product. Cells can be harvested at this point to prepare unstructured products, food structuring, or downstream tissue structuring applications.

2.4.3 Product structuring.

The architecture of skeletal muscle in livestock consists of aligned, contractile skeletal muscle fibers and intramuscular fat deposits (Figure 2.4). Product structuring attempts to recreate this architecture. *Food structuring* can be used to deliver different cell and ingredient mixtures into precision locations to mimic a cut of meat. For example, a steak could be developed by 3D printing technology. Fat cells can be printed in a pattern that simulates an interconnected web of marbling within a larger matrix of skeletal muscle material. First, a model is developed in a software program and mixtures made of protein, cells, and other components are formulated for extrusion by a food printer, then the cells are printed according to the model. Alternatively, localization of food and cell ingredients can be accomplished with other forms of deposition, such as depositing alternating sheet layers of fat and muscle mixtures. Ingredients can be converted from a liquid or paste into a solid, texturized form using food binders such as methyl cellulose or enzymes such as transglutaminase, otherwise known as meat glue.

During *tissue structuring*, cells are aggregated together into a defined pattern modeled after skeletal muscle tissue through tissue engineering systems such as bioprinters. Extracellular matrix, which functions as a polysaccharide or protein-based “glue”, embeds the cells into a 3-dimensional form⁸⁰. Bioprinting is a similar process to food printing but requires sterility and gentle handling to keep the cells alive. The cost of bio printers is much higher than food printers, and the process is more complex and costly. After printing, the cell cultured meat is then matured in a tissue bioreactor⁸¹. Bioprinting allows the use of multiple cell types to stabilize tissue architecture. Using co-culture systems allows bi-directional

signaling between fibroblasts and myoblasts that attenuates and stabilizes myogenesis. The inclusion of fibroblasts and myofibroblasts can be used to model skeletal muscle. Myofibroblasts are primarily known for their role in tissue regeneration, as they are hypersecretors of extracellular matrix and paracrine factors associated with wound healing⁴⁸.

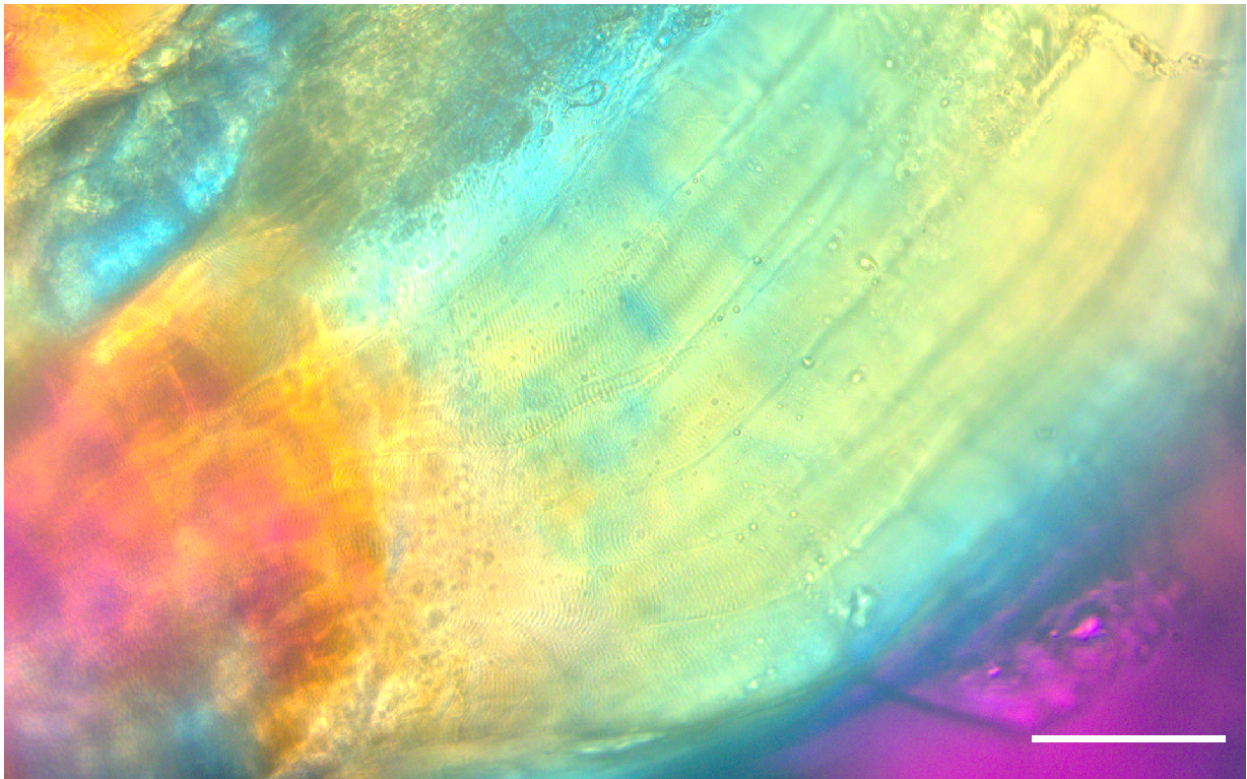


Figure 2.4. Polarized microscopy image of porcine skeletal muscle tissue structure. Image of thin longitudinal section of skeletal muscle. Muscle fascicles are visible as tubes in parallel orientation, and striations are visible within fascicles. Interference colors within tissue slice indicates internal cellular structures aligned in the same orientation. Scale bar = 300um Image courtesy of Dr. Taras Turiv at Kent State University.

The composition of culture media for tissue cultivation is different than in cell cultivation because of the need to differentiate or mature a combination of cell types within a tissue⁸². For example, media for adipocyte and myocyte co-culture may be different than their respective individual growth and differentiation medias, and growth factors can become useful in tissue engineered products that are not

useful for 2D culture or scale up. Signaling of profibrotic factors such as TGF- β 1 can deregulate the regenerative capacity of muscle and drive fibrosis when in excess^{83, 84} but regularly contribute to muscle regeneration at moderate levels. The use of TGF- β 1 may therefore be a means to organize tissue-engineered skeletal muscle development *in vitro*.

Maturing skeletal muscle tissue in cell culture scenarios requires additional design considerations for a new class of tissue maturation bioreactors. A tissue maturation bioreactor that can perfuse media through structured meat, induce an exercise regime, and support the survival of larger scale tissue volumes does not yet exist. However, upon development these bioreactors will have features similar to organ transplant care systems. These will be modeled after the systems used to keep donor hearts and lungs alive for recipients, which can connect the vasculature of the organ to a perfusion system that pumps oxygenated blood into the organ⁸⁵. In the body, muscle is exercised to increase contractile strength, which increases muscle volume and impacts meat texture. Similarly, bioreactors can stimulate synthesized muscle with electrical stimulation to promote maturation⁸⁶.

2.4.4 Industry Challenges.

Scaling up of cell cultivation is among current efforts of the cell cultured meat industry, which has several technology hurdles. These hurdles include lowering the cost of media, developing cell lines that can be expanded indefinitely and possess specific palatable and nutritional characteristics; establishing scalable bioprocesses, and reducing the operational costs of large-scale biomanufacturing facilities. Three major challenges with tissue manufacturing are the complexity of recreating tissue structure with bioprinters, an early technology level of tissue maturation bioreactors, and the associated costs of using tissue structuring and cultivation equipment. Tissue is complexly patterned in the body on the scale of micrometers, which current bioprinting systems have difficulty replicating⁸⁷. A delivery system for oxygen and nutrients to cells deep within the tissue is necessary by design, because passive diffusion of molecules becomes ineffective beyond 100 μ m of cell layers. The circulatory system accomplishes this in the body, and a vascular network, or equivalent perfusable system for fluid flow, is necessary to perfuse cell culture media through the tissues⁸⁸. Structuring cell mixtures with food printers can provide a lower cost alternative for tissue structuring.

2.5. Specific Aims.

Cultivated meat science is a nascent field with limited research published in the last few years^{89,90,79,31,91}. The objective of this work is to develop a new framework of foundational research principles, which includes cell line development, culture strategies to improve sensory properties, assessing low cost tissue engineering strategies and edible scaffolding materials, and a proposed protocol to develop a cultivated meat prototype. This research can create a blueprint for distinguishing cultivated meat science from biomedical research and lead to methodological success in the field, as well as reducing production costs for commercial products.

Specific Aim I: Development and characterization of cell isolation, culture, and differentiation protocols for bovine and porcine cell line development. In this aim, we tested the hypothesis that 1) a single cell isolation protocol can be used to develop bovine and porcine myoblasts and fibroblasts that can undergo myogenesis and adipogenesis, respectively, and that there would be species specific outcomes, 2) bovine myoblasts will undergo greater hypertrophy than porcine myoblasts during myogenesis, and 3) during adipogenesis, porcine adipocytes have a greater degree of adipogenesis than bovine adipocytes, although bovine cells have a greater population of differentiating adipocytes.

Specific Aim 2: Development cell culture processes and media formulations that improve sensory properties of meat cells. Different growth factors and cytokines in media can affect the outcome of myogenesis and can be influenced by optimizing growth factor and cytokine profiles in media, which can be investigated by conditioning media via macrophage cell culture. Cells grown in culture do not possess the same magnitude of gene and protein expression than cells *in vivo*, which can cause dissimilar flavor and texture profiles in cultured meat than meat from an animal. In this aim we tested the hypotheses that 1) increasing myoglobin expression is critical to enhancing pigment of meat cells in culture, 2) myogenesis and electrical stimulation would improve myoglobin expression in porcine and bovine myoblasts, 3) using conditioned media from polarized macrophages can

impact proliferation and differentiation of porcine cells, providing insight into growth factor and cytokine combinations to improve media development for culture meat.

Specific Aim 3: Evaluation of low-cost tissue engineering strategies and edible scaffolding

materials to improve texture and taste of cultivated meat. The cheapest tissue engineering strategies are self-assembly models or cell seeding techniques into plant-based scaffolds, which have the additional benefit of being edible. Tissue engineering can form microcarrier platforms for cell expansion or to create tissue engineered products, like bacon or steak. However, the formation of 3D muscle tissue may require co-culture with connective tissue cells such as fibroblasts. In this aim, we tested the hypotheses that 1) fibroblasts differentiated into myofibroblasts can enhance myogenesis in C2C12 self-assembled tissues 2) self-assembly models are more difficult to achieve in primary porcine myoblasts than C2C12s due to increased tensional forces exerted by porcine muscle cells, and 3) that edible, plant based scaffolds require additional RGD or ECM coating or a cell feeder layer to enhance rapid cell seeding, migration, and differentiation of cultivated meat.

Chapter 3

CHARACTERIZING PORCINE AND BOVINE MYOGENESIS AND ADIPOGENESIS

3.1. Introduction

Beef and pork are two of the most popular types of meat in western diets. *Bos Taurus* and *Sus Scrofa* have unique physiologies that yield specific sensory properties of their meat. These sensory properties arise in part from genetic differences between species⁹², breeds⁹³, and the nutritional profile of food for the animals⁹⁴. Animal meat contains skeletal muscle tissue with intramuscular fat that are created from myogenesis and adipogenesis. Myogenic and adipogenic mechanisms produce optimized sensory experiences in animal meat, but cell-based meat is produced in an artificial environment. *In vitro* treatments do not always result in the same outcome as *in vivo* mechanisms. Consequently, research is needed to explore differences between animal meat and cell-based meat between species and breeds to recreate the experience of eating animal meat.

The research approach for developing cell-based meat products is unique to regenerative medicine due to a requirement for low cost and food-grade material inputs and strategies. The objectives of this study involve first developing a protocol for isolating skeletal muscle and fat cells. This study tested the efficacy of a novel co-isolation strategy for these cell types. Baseline characterization of myogenesis and adipogenesis of pork and beef in cell cultures must be compared to meat from cattle and swine to identify and reduce disparities between cell-based and animal meat.

3.2. Materials and Methods.

3.2.1. Cell isolation protocol for bovine and porcine myoblasts and fibroblasts

Muscle tissue of 3-4 cm² (4-6 g) in size was harvested from the thigh muscle of a pig (1 month old) or a 2-month-old cow's hind leg (*biceps femoris*) from a local farm. To isolate bovine and porcine myoblasts, muscle tissue is cut into small pieces after removing blood vessels and fascia/connective tissue, suspended in a tissue digestion buffer containing DMEM, 1% penicillin/streptomycin and 0.5% collagenase IV (Worthington Bio), and incubated at 37°C for 60-90 minutes. Every 15 minutes the cell and tissue mixture was pipetted to improve tissue disintegration. The cell mixture is further filtered using a 40 µm cell strainer, neutralized by adding fetal bovine serum, and the suspended cells were collected by a 5-minute centrifuge at 1,200 rpm at room temperature. After a few washing steps with PBS with centrifugation, the heterogeneous cell mixture is resuspended in Advanced DMEM/F12, 20% FBS, and 1x P/S and undergo a pre-plating technique. The cells are seeded in standard tissue culture plates to allow fibroblasts attachment overnight at 37°C in 5% CO₂. The next day the unattached cells were collected, centrifuged, washed with PBS, resuspended in myoblast growth media (MGM, DMEM/F-12 with 20% FBS, 1% Glutamax, 1% Penicillin/Streptomycin and 2ng/mL FGF-2), and seeded in laminin-coated culture plates. The fibroblast plates were washed with PBS and fibroblast growth media was added (FGM, DMEM/F-12 with 10% FBS, 1% Glutamax, and 1% Penicillin/Streptomycin). After a 2-3 day incubation at 37°C and 5% CO₂, suspended (unwanted) cells and tissue debris will be removed by aspirating the culture medium followed by a few washes, and adherent myoblasts can be obtained.

3.2.2. Cell culture protocols

Primary bovine and porcine myoblasts are grown in MGM and passaged upon reaching 50-60% confluency, while fibroblasts are grown in FGM and passaged after reaching 70-80% confluency. All cells used for experiments were between passage 1-4.

3.2.3. Myogenesis protocol

Bovine and porcine myoblasts were cultured in MGM until reaching 80% confluency. Media was then switched to myoblast differentiation media (MDM, Advanced DMEM/F12, 2% horse serum, 1% glutamate, 1% P/S) and cultured for 72 hours.

3.2.4. Adipogenesis protocol

Bovine or porcine intramuscular fibroblasts were cultured in FGM until the adipogenesis assays. Fibroblasts were then switched to Promocell medias. First, the fibroblasts were adapted to preadipocyte growth medium (cat. C-27410) for 1 week, then switched to preadipocyte differentiation medium (Cat. C-27436) for 72 hours. After differentiation, cells were switched to adipocyte nutrition medium (cat. C-27438) for two weeks.

3.2.5. Immunostaining

Myogenic and fibroblastic cells were assessed qualitatively with immunostaining. 2D and 3D cultures were fixed with 4% formaldehyde for 20 min. 3D self-assembled tissues were then submerged in OCT media, frozen for cryosectioning, sectioned at 30 μ m thick, and applied to glass slides. After fixing, samples were permeabilized with 0.1% Triton X-100 in PBS for 20 min, and then incubated with a blocking solution consisting of 5% FBS in PBS for 20 min. Following blocking, samples were stained with myosin heavy chain (MF-20, 1:50; Developmental Studies Hybridoma Bank, Iowa City, IA, USA) or α -SMA (A 2547, 1:1,000; Sigma-Aldrich, St. Louis, MO, USA) primary antibodies. Primary antibody staining was followed by incubation with Alexa-Fluor 488 (1:250; Life Technologies, Carlsbad, CA, USA) and DAPI (1:50,000; Invitrogen, Carlsbad, CA, USA). Imaging of 2D samples was completed with an Olympus IX81 microscope (Olympus corporation of the Americas, Center Valley, PA, USA) and 3D self-assembled tissues were imaged with an Olympus Fluoview FV1000 Confocal Microscope. All images were processed with ImageJ (Version 1.48; National Institute of Health, Bethesda, MD, USA).

3.2.6. Oil Red O staining

The lipid droplets inside mature adipocytes were visualized by Oil Red O staining. ORO was prepared by dissolving Oil Red O in 20 ml of 100% isopropanol, mixing well and incubated at room temperature for 20 min. Oil Red O Working Solution was prepared by adding 3 parts of Oil Red O Stock Solution to 2 parts of dH₂O, mixing well, and incubated at room temp for 10 min. The solution was filtered with 0.2 µm syringe filter. The adipocyte cultures were then washed with PBS and fixed with formalin for 30 minutes. After fixation, cultures were washed twice with dH₂O. Isopropanol (60%) was prepared by adding 3 parts Isopropanol (100%) to 2 parts of water. Isopropanol (60%) was added to each well and incubated for 5 min. Isopropanol was removed and Oil Red O working solution added to the cultures. Samples were incubated for 20 min. Oil Red O solution was removed and samples were washed 2-5x with dH₂O.

3.2.7. Digital holographic microscopy

Bovine and porcine myoblasts were cultured until reaching 70-80% confluency and then differentiated for 72 hours. The height profile of the adherent cell is performed using transmission digital holographic microscopy (Lyncée Tec T-1000) equipped with an environmental control chamber for cell incubation. Images are processed in open-source software package Fiji/ImageJ2, further analysis is performed with the custom-written code in MATLAB (MathWorks) and/or Python.

3.2.8. qPCR

Total RNA is isolated using MicroElute Total RNA Kit (OMEGA, R6831) according to the manufacturer's protocol. Briefly, after harvesting the cells were centrifuged and the tube with pallet is quickly immersed into the liquid nitrogen and stored at -80°C. Using 350µL TRK Lysis Buffer (with 20µL of 2-mercaptoethanol per 1 mL) to resuspend the cell pallet and extract RNA lysate. After a sequence of vortex, centrifugation, and washes the RNA concentration is determined using NanoDrop 2000 nucleic acid and protein quantification spectrometer. Synthesis of cDNA is carried out using qScript cDNA SuperMix (Quantabio) and PCR-grade water. The temperature profile of the cDNA synthesis protocol was as follows: 1) 25°C, 5 min; 2) 42°C, 30 min; 3) 85°C, 5 min. The samples were stored at 4°C until use for quantitative PCR (QPCR). We choose reference genes to be glyceraldehyde-3-phosphate

dehydrogenase (GAPDH). Primer sets for porcine GAPDH, myogenin, myoglobin, and Pax7 are synthesized by Integrated DNA Technologies and sequence for forward and reverse primers is given below. The QPCR reaction (RealPlex 4, Eppendorf) was performed using SYBR Green Supermix (Bimake), primers (0.5 mM), PCR-grade water and cDNA in 20µL volume samples. The temperature profile was as follows: 3 min at 95°C, 40× (20 s at 95°C, 20 s at 60°C, 30 s at 72°C), 1 min at 95°C, 1 min at 65°C, followed by a melt curve analysis. Target gene expression is evaluated using the $\Delta\Delta CT$ method with results being normalized to GAPDH housekeeping gene and compared to corresponding control cultures. List of forward/reverse primers used (Table 3.1):

Table 3.1. Sequences of primers used for PCR in this study

Species	Name	Sequence
<i>Sus Scrofa</i>	GAPDH	F: TGGTGAAGGTCGGAGTGAAC
		R: CAGGTGCCCCAGCTACATTA
	MYOG	F: GCTATCCGGTTCCAAAGCCT
		R: CCCGGTATCATCAGCACAGG
	Pax7	F: TCCAAGATCCTCTGCCGCTA
		R: TCGAACTCACTAAACCTGAGGG
MB	F: ACCTGAAGAAGCACGGCAAC	
	R: ACCAAAGTCCCCAGGATGCTTG	
<i>Bos Taurus</i>	GAPDH	F: TCCCAACGTGTCTGTTGTGGATCT
		R: TGTTGAAGTCGCAGGAGACAACCT
	MB	F: TCTGCATGGTACCTGGCCTC
		R: CAAGTGGAGAGCCTAGCGTG
	MYOG	F: AGCCTCCAAATCCACTCCCTGAAA
		R: AGCCACTGGCATAGGAAGAGATGA

3.2.9. Live imaging

Bovine and porcine myoblasts were cultured until reaching 70-80% confluency and differentiated for 72 hours in DM. Once the media was switched, cell cultures were placed in an environmental chamber (Chamlide TC-W, ver. 1.0.0, Live Cell Instrument) with 5% CO₂ and 95% humidity at 37C and underwent live imaging via an inverted phase-contrast microscopes AmScope AE2000 equipped with AmScope MU-2003-BI-CK camera. Images are processed in open-source software package Fiji/ImageJ2, further analysis is performed with the custom-written code in MATLAB (MathWorks) and/or Python.

3.2.10. Oil Red O quantification

Representative images were taken of porcine and bovine adipocytes after 2 weeks of differentiation. The area of ORO stain was calculated for each image at the same magnification level in Image J. The areas of ORO stain were averaged for porcine and bovine cells and compared statistically.

3.2.11. Statistics

All data are presented as means and their standard error bars. One-tailed, unpaired Student's t-tests or one-way ANOVAs were used to compare gene expression levels. Differences were considered significant at $p < 0.05$. A simple linear regression was used to establish fit in DHM cellular volume data.

3.3. Results

3.3.1. Isolated bovine and porcine skeletal muscle progenitor cells undergo myogenesis with similar gene myogenic transcription factor gene expression patterns

Bovine and porcine myoblasts and fibroblasts were successfully isolated from the *biceps femoris* muscle of a calf and piglet, and myoblasts could undergo myogenesis (Figure 3.1A-H). Both porcine and bovine muscle fibers expressed myosin heavy protein (Figure 3.2A, B) and expressed typical gene expression patterns for myogenesis, with myogenin transcription factor upregulation and Pax7 downregulation (Figure 3.2E, F). For both species, myoglobin gene expression was unregulated during differentiation. All groups were significant different from their respective undifferentiated myoblast controls. Porcine and bovine fibroblasts also expressed α -SMA protein (Figure 3.2C, D).

3.3.2. Bovine and porcine myocytes undergo different magnitudes of hypertrophy

Because *sus scrofa* and *bos taurus* have different physiological characteristics, it is important to identify how this translates to *in vitro* cell line characteristics to guide cell line and bioprocess development for pork and beef products. DHM imaging analysis showed increases in the average cell height of differentiating bovine and porcine myocytes over 55 hours (Figure 3.3A, B), and accompanying phase contrast images (Figure 3.3C, D). Cell volume % changes are displayed in Figure 3.3E. Bovine myocyte hypertrophy reached a 242% maximum increase and porcine hypertrophy reached a 202% maximum

increase before muscle fibers would detach from plates. While porcine cells had a higher peak volume increase, there was a greater degree of variability in the dataset. The porcine cells average increase in cell volume per hour was 1.3%, and the bovine cells increased by 2.2% volume per hour. These results suggest that myogenic beef and pork cell lines may have different characteristics in their innate ability to produce biomass.

3.3.3. Isolated intramuscular fibroblasts from pigs have more robust adipogenic potential than bovine intramuscular fibroblasts but a rarely in population frequency

Differences were observed in myogenesis between cell populations, so adipogenesis was also assessed. Adipogenesis of bovine and porcine adipocytes was compared by Oil Red O staining, and differentiation induced morphological changes in the cells. Bovine fibroblasts (Figure 3.4A) were switched to pre-adipocyte growth medium (Figure 3.4B), then switched to adipocyte differentiation medium for 3 days (Figure 3.4C), and finally switched to nutrition medium for 2 weeks (Figure 3.4D-F). Porcine cells underwent the same differentiation protocol and were imaged after 2 weeks (Figure 3.4G, H). Cultures underwent ORO staining to quantify lipid droplet formation (Figure 3.4E-H). The % of ORO staining in bovine adipocytes was 0.7% of the total image area, while porcine adipocytes stained for 7.6% of total area, a significant increase (Figure 3.4I). However, virtually all bovine cells underwent adipogenic differentiation as observed by universal cell morphology changes to rounded, vesicle containing phenotype (Figure 3.4D), compared to porcine cells (Figure 3.4G), which had much fewer differentiating adipocytes in the population. These results demonstrated that pork and beef cells differed in heterogeneity at the population level, as well as their requirements for robust lipogenesis.

3.4. Discussion

Skeletal muscle cells and pre-adipoblast cells can be co-isolated from porcine or bovine muscle tissue. The muscle fiber and intramuscular fat composition of the muscle organ will determine innate cell line properties. In this study, we showed that porcine and bovine skeletal muscle and fat cells can both be isolated from the *biceps femoris*. The morphology of bovine myoblasts and fibroblasts often presented in square-like

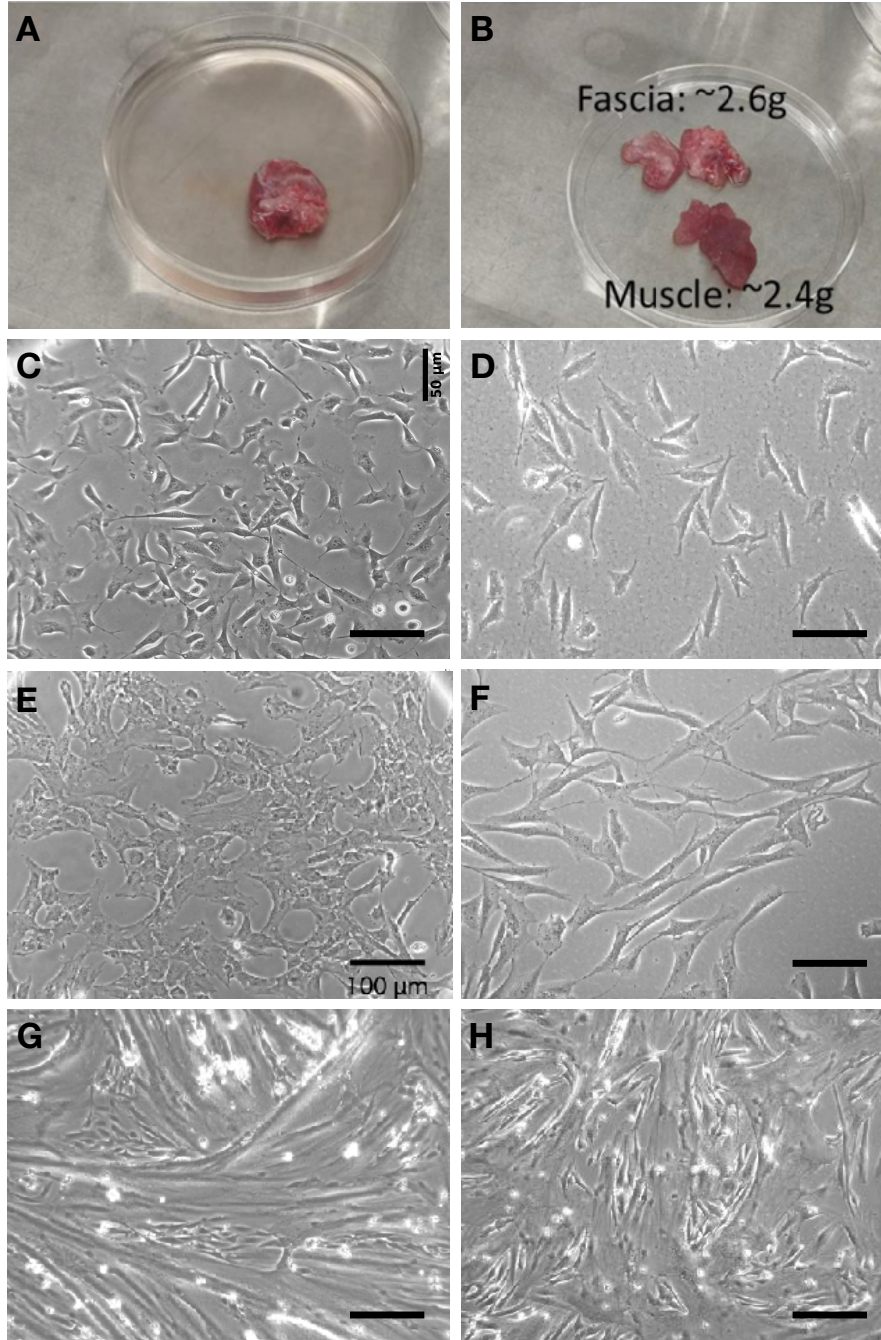


Figure 3.1. Bovine muscle tissue biopsy and cell morphology of bovine and porcine myoblasts and fibroblasts. (A) 5 gram sample of muscle from the hind leg and separation of connective tissue fascia from muscle (B). Passage 0 bovine (C) and porcine (D) myoblasts. Passage 0 bovine (E) and

porcine (F) intramuscular fibroblasts. Myogenesis assay of bovine (G) and porcine (H) myocytes. Scale bar (C-F) = 100µm, scale bar (G-H) = 150µm.

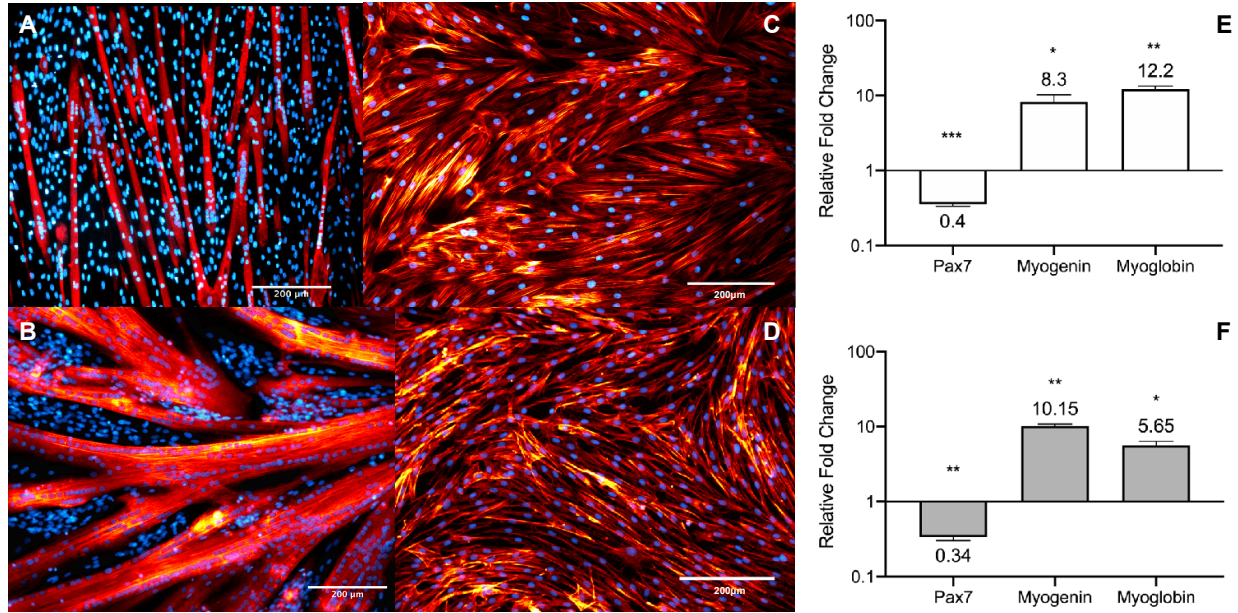


Figure 3.2. Immunocytochemistry of fibroblasts and differentiated muscle cells and myogenic gene expression. Porcine (A) and bovine (B) myocytes stained for myosin heavy chain and DAPI. Porcine (C) and bovine (D) fibroblasts are stained for α-smooth muscle actin and DAPI. Relative fold changes in Pax7, myogenin, and myoglobin gene expression in porcine (E) and bovine (F) skeletal muscle cells during myogenesis.

morphologies, whereas porcine cells were more elongated and spindle shaped. Myoblasts from both species followed typical myogenic gene expression patterns with elevating MYOG and decreasing Pax7, and showed nonsignificant differences in the capacity for multinucleation in live imaging studies. Digital holographic microscopy quantified differences in the rate of hypertrophy between species, with bovine myocytes increasing in volume faster than porcine cells, although porcine myocytes reached a higher maximum hypertrophy than bovine myocytes. This is likely due to variability in the dataset, since a smaller field of view was used to record volume changes in porcine versus bovine cultures.

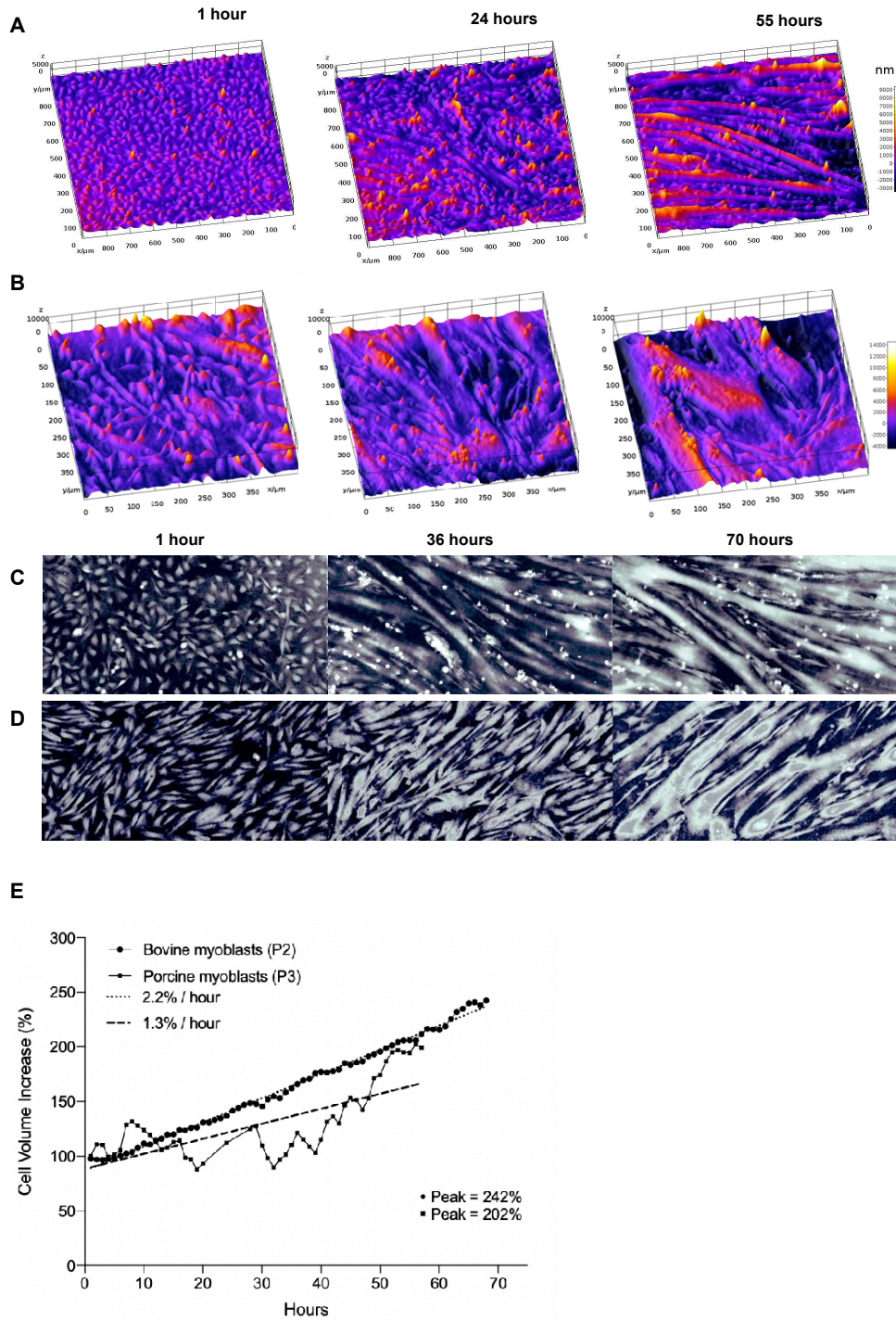


Figure 3.3. Digital holographic and phase microscopy live imaging of myogenesis. DHM analysis of hypertrophy in bovine (A) and porcine (B) muscle cells during myogenesis. Phase imaging recorded by DHM of bovine (C) and porcine (D) during differentiation. The % of volume increase in passage 2 bovine myoblasts and passage 3 porcine myoblasts (E). Please note the different scales between porcine and bovine DHM data in (A) and (B).

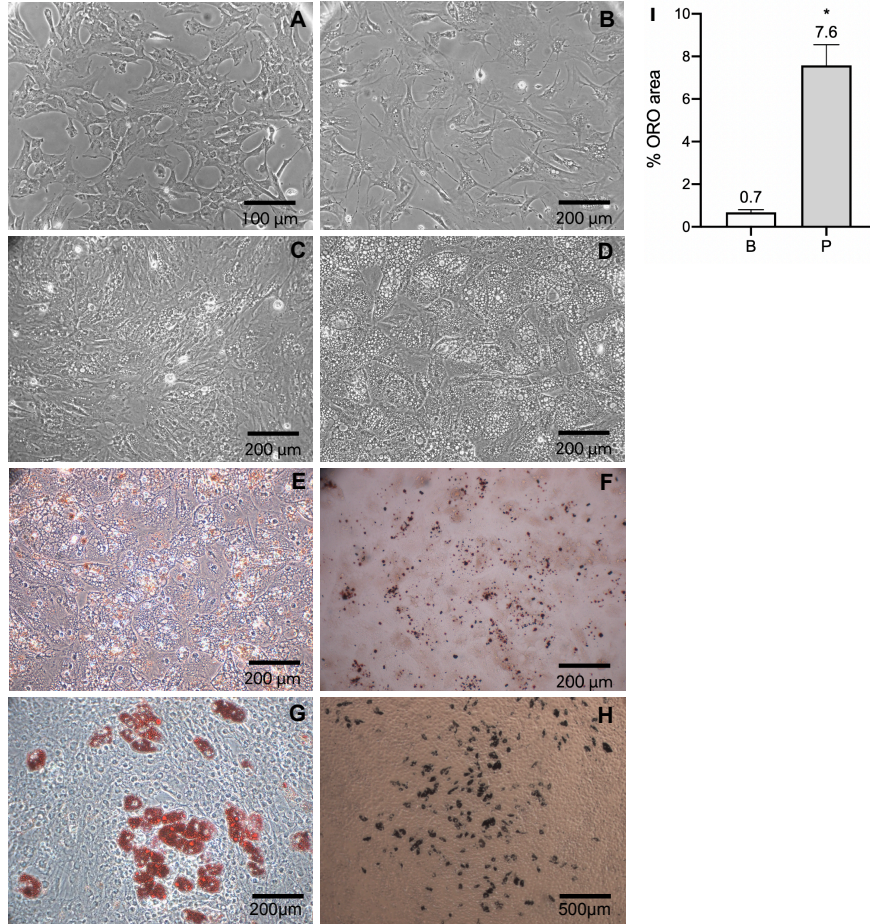


Figure 3.4. Adipogenesis of bovine and porcine intramuscular fibroblasts. Bovine fibroblast morphology before (A) and after (B) switching to adipogenic growth media, after 3 days in differentiation media (C), and after 2 weeks in adipocyte nutrition media (D). Oil Red O staining of lipid droplets in bovine adipocytes in phase (E) and brightfield (F), and porcine adipocytes in phase (G) and brightfield (H). (I) The % of ORO stained area within field of view of bovine and porcine adipocytes. (*) indicates $p < 0.01$ between bovine (B) and porcine (P) cells.

There were starker differences found in adipogenic outcomes of fibroblast populations derived from the *biceps femoris* of both species. A smaller population of differentiating adipocytes was observed in porcine cultures than bovine. This is perhaps due to differences in intramuscular fat depositions between species. Skeletal muscle in cattle has intramuscular fat deposits that can be visibly observed as

marbling, yet most pig breeds (except the duroc) lack marbling. Additionally, the IMF content of *biceps femoris* in pig meat is 1.4 +/- 0.4% at slaughter age³⁴, while it is 2.55% in the Dexter cattle breed⁹⁵. A different cell isolation technique could be used to improve the porcine pre-adipoblast isolation yield, due to difference in extracellular matrix composition and localization of pre-adipoblasts.

Despite nearly 100% adipogenic differentiation in bovine fibroblasts, there was a low level of lipogenesis observed via ORO stain compared to porcine cultures. Low level of lipogenesis levels may be due to the cattle Dexter breed, muscle organ selected, sex, age, and feed composition of the animal. The establishment of robust differentiation bovine adipoblasts may be improved by selecting another muscle organ to extract cells and an alternate breed known for high IMF visible in marbling. Marbling is the ratio of intramuscular fat to lean muscle mass. Increased marbling improves beef quality by affecting the tenderness and flavor of the meat.

Intramuscular Fat

The most savory beef cuts are from the ribs of the cow. Rib-eye steak (derived from the *longissimus*) is the most flavorful cut of beef due to the high intramuscular fat and marbling content, while the round (derived from the *biceps femoris*) contains less marbling and fat content than rib eye⁹⁶. The IMF% of the *biceps femoris* in animals fed a low fat diet is 2.5% in Dexter⁹⁵, 4.9% in Angus, and 6.8% in Wagyu x Angus crossbreeds (Table 3.2). In cattle fed a high fat diet, the fat content is 12.6% in Angus, 11.6% in Wagyu x Angus⁹⁷, and between 14.7-26.4% in the proximal and distal cranial head of Japanese Black Wagyu cattle⁹⁸. The IMF% of the *longissimus thoracis* is 2.3% in Dexter⁹⁵, 6.2% in Angus⁹⁷, 15.3% in Korean Hanwoo⁹⁹, and 31.5% in Japanese Black Wagyu animals⁹⁸. The total IMF% from 21 muscles of Wagyu steers is 32%¹⁰⁰.

Fatty Acid Compositions

The fatty acid composition of intramuscular fat impacts flavor, juiciness, and tenderness. This composition includes saturated fatty acids (SFAs), monounsaturated fatty acids (MUFAs), and polyunsaturated fatty acids (PUFAs). SFAs like myristic acid (14:0), palmitic acid (16:0), and stearic acid (18:0) are composed of carbon chains that lack double bonds; MUFAs like oleic acid (18:1) and

palmitoleic acid (16:1) contain one carbon double bond; and PUFAs have two or more carbon double bonds. Double bonds in fatty acids hinder the formation of the crystal structure of solidified fat.

Table 3.2. Average intramuscular fat % and muscle fiber type in the biceps femoris and longissimus thoracis

Breed	IMF (%)	Type I fiber (%)	Type 2A fiber (%)	Type 2B fiber (%)	Age (months)	Reference
<i>Biceps Femoris</i>						
<i>Dexter</i>	2.5	48.7	21.3	30.0	17	95
<i>Angus</i>	4.9				12	97
	12.6				20 (fattened)	
<i>Wagyu x Angus</i>	6.8				12	
	11.6				20 (fattened)	
<i>Japanese Black Wagyu</i>	14.7 - 26.4	36.5	26.0	37.6	29 (fattened)	98
<i>Longissimus Thoracis</i>						
<i>Dexter</i>	2.3	29.0	32.9	38.1	17	95
<i>Angus</i>	6.2				27.5 (fattened)	97
<i>Hanwoo</i>	15.3				31.7 (fattened)	99
<i>Japanese Black Wagyu</i>	31.5	34.3	17.6	48.0	29 (fattened)	98
<i>Total fat - 21 muscles</i>						
<i>Japanese Black Wagyu</i>	32				26 (fattened)	100

Consequently, every double bond lowers the melting point of the fatty acid. The melting point of lipids greatly influences the juiciness of beef. SFAs have melting points at ~70°C, MUFAs melt at ~20°C, and PUFAs a liquid at room temperature and melt at -20°C ¹⁰¹.

High SFA levels can be produced from high calorie feed and is associated with meat toughness⁹⁷ and flavor liking¹⁰². 16:0 and 18:0 are two FAs that determine meat hardness due to their high melting point. Lowering the total % of these SFAs will soften meat products¹⁰³. High oleic acid levels are found in animals with intense marbling, such as Wagyu and Hanwoo, which can be increased through high calorie feed. Oleic acid is associated with beef palatability due to its lower melting point, which improves tenderness, juiciness, and flavor. SFA and MUFA deposition increases total IMF% in muscle¹⁰⁴. The MUFA:SFA ratio increases over the life of the animal due to an increasing oleic acid and MUFA

composition, which improves the palatability and healthiness of beef¹⁰³. The MUFA:SFA ratio also determines the melting point of the fat in beef. In the US, the lowest fat melting point in beef is 30°C, which comes from animals fed a corn-based diet, while Japanese Wagyu beef melts at 24°C.

PUFAs have the lowest melting point of the FAs. PUFAs contribute minimally to IMF due to their slower deposition rate than SFAs and MUFAs, but have nutritional importance. Linoleic acid (18:2 n-6), also called omega-6, and linolenic acid (18:3 n-3), or omega-3, are essential PUFAs present in animal meat. 18:2 is produced in higher concentration with high calorie feeding and is positively correlated with flavor liking, while 18:3 is increased in animals with grass diets and is negatively correlated with liking¹⁰². A high C18:2/C18:3 ratio is positively correlated with flavor liking and overall liking¹⁰⁵.

Table 3.3 lists six of the most common FAs within intramuscular fat in the *longissimus* muscle of cattle breeds. Hard fats like 16:0 are more prevalent in Angus (29.79%), Holsteins (28.0%), and Hanwoo (28.2%) than Wagyu (26.1%, Table 3.3), but Wagyu and Hanwoo have lower 18:0% compositions than Angus and Holstein (10.48%, 9%, 14.16%, and 12.27%, respectively). Wagyu and Hanwoo cattle are genetically dispositioned to produce high levels of oleic acid (50.04% and 52.14%), which increases their MUFA levels compared to other cattle like Angus and Hosteins (47.62%, and 47.5%). Higher MUFA:SFA ratios are found in Wagyu and Hanwoo (1.37 and 1.44) compared to Angus and Holstein (1.10 and 1.19). These fatty acid compositions yield softer and more flavorful meat in Wagyu and Hanwoo beef than in Angus and Holstein, and has heart health benefits. Oleic acid is a heart healthy dietary fat that lowers low-density lipoprotein cholesterol (LDL-C) and increase high-density lipoprotein cholesterol (HDL-C). Meanwhile, saturated fats increase LDL-C while decreasing HDL-C¹⁰⁶. The link between red meat consumption and cardiovascular disease lies in high SFA composition. In human trials, supplementing a diet with ground beef high in oleic acid increased HDL-C but also increased total cholesterol¹⁰⁷. This is likely due to the already high concentration of SFA preexisting in beef.

Muscle Fiber Compositions

Varying muscle fiber type compositions within muscle organ also impacts fat composition and meat quality. Fiber type is influenced by animal age, sex, muscle group, diet, and exercise^{108, 109}. Each type of muscle fiber type has distinct contractile capacities and energy metabolism properties, yielding

unique textures and fat storage characteristics. Muscle fiber twitch types are found in 3 main varieties: slow twitch type I fibers and fast twitch type 2 fibers, which are split into 2A and 2B types. Type I fibers have the highest contraction speed and mitochondria density and are predominant in muscle used

Table 3.3. Intramuscular fatty acid compositions in the longissimus muscle in cattle feed high calorie diets.

Saturation	FFA	Total Lipid %	Japanese Black Wagyu	Angus	Holstein	Hanwoo
SFA	Myristic acid	14:0 %	2.84	2.56	2.72	3
	Palmitic acid	16:0 %	26.14	29.79	28.01	28.21
	Steric acid	18:0 %	10.48	14.16	12.27	9
MUFA	Oleic acid	18:1 %	50.04	47.62	47.47	52.14
	Palmitoleic acid	16:1 %	4.07	2.7	3.83	3.94
PUFA	Linoleic acid (o-6)	18:2 n-6 %	2.12	1.8	1.93	2.11
	Linolenic acid (o-3)	18:3 n-3 %	0.12	0.21	0.18	0.08
MUFA:SFA			1.37	1.10	1.19	1.44
PUFA:SFA			0.062	0.16	0.053	0.06
Age (months)			26	24	26	24
Reference			100	102	100	102

routinely that require high endurance¹¹⁰. Type I and 2A fibers have high oxidative potential for aerobic respiration due to increased mitochondrial levels, while 2B fibers have low mitochondrial levels but high glycolytic potential for anaerobic respiration. Type 2A muscle fibers have higher glycolytic potential than type I, but less than type 2B, which has high expression levels of enzymes that enhance the glycolytic pathway. Glycolytic 2B muscle fibers produce lactate as a result of producing ATP for muscle contraction from glycolysis.

Intramuscular fatty acid composition shows a relationship with muscle fiber compositions that is dependent on breed, feed, muscle group, and age of the animal. Dexter cattle on a low calorie diet have a low IMF% in the *biceps femoris*, a high density of type I muscle fibers (48.7%), and a lower density of type

2B fibers (30.0%)⁹⁵ (Table 3.2). In contrast, the fatty *longissimus thoracis* muscle of Japanese Black Wagyu contains 34.3% type I fibers and 48.0% type 2B fibers⁹⁸. In a study that averaged fatty acid and muscle fiber composition over 21 muscles in Wagyu, the percentages of type I muscle fibers were positively correlated with total IMF%, and the percentages of type 2A and 2B muscle fibers was negatively correlated with total IMF%. Type I muscle fiber presence was negatively correlated with SFAs with shorter chains (<C17) and positively correlated with longer MUFA chains (C18:1, 18:2 n-6, and 20:1). Type 2A and 2B muscle fibers were positively correlated with short SFA chains (C14:0, 15:0, and 16:0) and negatively correlated with longer MUFA chains. From this dataset, the ratio of MUFA:SFA is 1.44, indicating a higher % composition of type 1 muscle fibers and MUFAs overall in wagyu muscle, and a clear relationship between muscle fiber type metabolism and composition and IMF accumulation¹¹¹.

Multipotent Satellite Cells and Marbling

During fetal development, mesenchymal stem cells undergo myogenesis, adipogenesis, and fibrogenesis to produce myogenic, adipogenic, and fibroblastic cells. Wnt and β -catenin regulates MSC differentiation, where Wnt and β -catenin signaling will promote myogenesis, while suppression of Wnt and β -catenin signaling induces MSC adipogenesis¹¹². In 2001 Rudnicki et. al showed that rat satellite cells can differentiate into adipocytes without treatment of IBMX, dexamethasone, or insulin. Living muscle fibers were isolated and grown on Matrigel, which lacked adipogenic inducers. The satellite cells on the muscle fibers maintained a more stem-like state than they otherwise would on cell culture plates since they were still affiliated with signals from their tissue niche. After 10 days in culture, the satellite cells formed lipid droplets that was visualized with ORO and expressed PPAR γ gene, providing supporting evidence to the multi potency of satellite cells¹¹³. A study focusing on C2C12s showed that myoblasts also have transdifferentiation potential into adipocytes. C2C12s differentiated in adipogenic induction medium with TZD for 10 days showed a decrease in myotube formation, a simultaneous increase in adipoblast formation (indicated by transition to rounded morphology and lipid droplet formation in the cells), and expressed PPAR γ protein. There was not complete conversion into adipocytes, however, and myotubes were still present in the culture¹¹⁴.

In the highest grades of Black Japanese beef, multipotent satellite cells are suspected to contribute to the hallmark tenderness of the *longissimus*. Intramuscular marbling typically occurs in a connective tissue sheath called the *perimysium* in most cattle breeds. The perimysium wraps around muscle *fascicles* - bundles of muscle fibers embedded in honeycomb-shaped endomysium, another form of connective tissue. Preadipoblasts are associated with the perimysial connective tissue. However, in the *longissimus* of Japanese A grade cattle, IMF has been observed within the muscle fascicles along with mechanically disrupted *endomysium*, the connective tissue layer that covers individual muscle fibers¹¹⁵. These muscle fascicles have smaller and fewer muscle fibers¹⁰¹. The intrafascicular location, mechanically ruptured endomysium, and reduced number of muscle fibers suggests that a cell type within the muscle fascicles, such as satellite cells, are transdifferentiating into fat cells.

There is additional evidence that bovine myoblast cells are multipotent and can transdifferentiate into adipocytes. In one study, bovine skeletal muscle cells underwent myogenic differentiation through serum reduction, but were cultured in adipogenic media containing insulin, oleic acid, ciglitzone (a drug that serves as a PPAR γ ligand and adipogenesis stimulator for mesenchymal stem cells) and melengestrol acetate (MGA, a feed additive for cattle to improve feedlot performance). ORO-staining showed multicellular lipid droplets formed inside mononuclear myoblasts and multinucleated myotubes. PPAR γ and C/EBP β gene expression increased and myogenin gene expression decreased⁷³. In a follow up study, oleic acid was tested without a PPAR γ agonist to determine its efficacy to stimulate adipogenesis in bovine satellite cells. The authors found that oleic acid increased the % of lipid droplets in the cells; increased PPAR γ , C/EBP β , C/EBP α , and FABP4 gene expression; and adiponectin protein expression. The satellite cells were still able to undergo myogenesis to form multinucleated muscle fibers and expressed myogenin gene expression, but showed decreased gene expression of Pax3 and MYOD1¹¹⁶. These data indicate an incomplete conversion of bovine satellite cells to adipocytes, with both myogenic and adipogenic characteristics maintained in the cells. The authors also hypothesized that since Wagyu beef is so high in oleic acid, that perhaps oleic acid can act as a paracrine factor to transdifferentiate satellite cells located between the muscle fiber cell membrane and basal lamina into adipocytes. During fasting states and adipogenic differentiation, FFAs such as oleic acid are released by the adipocytes that regulate skeletal muscle energy metabolism⁶⁵. These studies highlight the potential to

create a myogenic cell line that can create both skeletal muscle and fat cells in the same culture, eliminating the need for developing two separate cell lines.

Future Directions

Given the poor adipogenic outcome observed in the bovine cells isolated from a dexter herd calf, a new starter cell line should be strategically chosen. Pre-adipocyte populations could be isolated from cattle with Wagyu genetic backgrounds, and the cells can be collected from the *longissimus*, given its higher IMF% in adult animals than the *biceps femoris*. A Wagyu cell line from *longissimus* muscle will likely have a better capacity for adipogenesis, since Wagyu are genetically bred to have high IMF. Selecting better starter cells will enhance speed and ease of research of cell-based beef, as well as ensure palatability of beef products.

Strategically supplementing bovine adipocyte cultures with MUFAs like oleic acid, but not SFAs, could improve differentiation and flavor of cell-based fat while removing the risk of cardiovascular disease development mediated by eating red meat containing high saturated fat. Studies have found oleic acid (100-500 μ M concentration) increases PPAR γ , G protein receptor 43 (GPR43) protein expression, and lipid droplet formation in bovine intramuscular adipocytes. GPR43 activation inhibits lipolysis and increases lipid accumulation in the adipose tissue¹¹⁷. However, differentiation may also be improved by adding SFAs like steric and palmitic acid, which increase C/EBP β gene expression that activates PPAR γ transcription. Another study found that bovine preadipocytes sourced from the subcutaneous stromal vascular cells treated with oleic acid supplementation induced lipogenesis⁴⁷.

Additionally, optimizing an appropriate MUFA:SFA ratio will improve the tenderness and mouthfeel of the product, as well as enhance juiciness while cooking. The meat might have a mouthfeel that's atypical for the product if there's too much or too little MUFA or SFA. Supplementation of adipocyte cultures with essential fatty acids like 18:2 n-6 and 18:3 n-3 can also enhance the health benefits of cell-based meat while promoting adipogenesis. The PUFA 18:2 n-6 also enhances adipogenesis by stimulates PPAR γ gene expression¹¹⁸.

Chapter 4

DRIVING FLAVOR AND PIGMENT PROFILES THROUGH PORCINE AND BOVINE MYOGENESIS

4.1. Introduction

Identifying culture processes that can improve meat quality while minimizing the necessity for high cost consumable reagents can further lower the cost of cell-based meat. Overcoming the high cost of media components, particularly FBS, is one of the technical hurdles of cell-based meat production. The development of animal and serum free medias is required for commercialization. Finding a chemically defined serum alternative is imperative to scaling up meat biomanufacturing. Fetal bovine serum is used because it contains high concentrations of growth factors that promote cell proliferation and low concentrations of factors that inhibit cell growth. Basic serum free media formulations include growth factors such as EGF, FGF, PDGF, NGF, IGF; cytokines such as interferons and interleukins; insulin and other hormones; proteins like transferrin and albumin; trace elements; and fatty acids¹¹⁹. Finding the right media composition can enhance flavor and performance of cell lines.

Animal-free growth factors, hormones, and proteins found in FBS can be produced from recombinant DNA technology, or collected from conditioned media of desired cell types. Conditioning media, without having to purify cell products, represents a low cost and scalable alternative to collecting and purifying cell products. Macrophage conditioned media has been thoroughly investigated, having shown to induce tissue regeneration mechanisms in skeletal muscle cells^{120, 121}. Using conditioned media with known growth factor compositions in proliferation and differentiation experiments of cell-based meat cell types can illuminate protein targets for serum free media development.

Electrical stimulation of myoblast cultures has been used in the past to improve differentiation of skeletal muscle cells^{59,122}. Using electrical stimulation equipment is a potential way to improve the flavor and taste of cells that simulates natural processes that don't add reagent costs to production. Since the cost of cell-based meat is such a significant hurdle to commercialization, the objectives of this chapter include the development of reagent-free culture processes is necessary to develop cell-based meat products. Additionally, conditioned media could be a potential source of serum-free media for cell-based meat if the media conditioning cell type has minimal media requirements of its own. PAMs are a robust SV-40T immortalized macrophage cell line with incredibly high proliferation rates. Macrophages can be M0 unpolarized type or polarized into pro-inflammatory M1 or anti-inflammatory M2 types, which shift their soluble protein expression profiles to enhance proliferation and differentiation of skeletal muscle cells. The paracrine protein factor network in conditioned media can be analyzed to optimize media compositions for cellular proliferation and differentiation.

4.2. Materials and Methods.

4.2.1. Cell culture protocols

Primary bovine and porcine myoblasts are grown in MGM and passaged upon reaching 50-60% confluency. All cells used for experiments were between passage 1-4. Immortalized porcine alveolar macrophage cells (PAMs), C2C12s, and hDFs were purchased from ATCC. PAMs were grown in RPMI, 10% FBS, 1% glutamate and 1% P/S; and C2C12s and hDFs were grown in high glucose DMEM, 10% FBS, 1% glutamate and 1% P/S. All cells are plated at a cell density of 6000 cells/cm².

4.2.2. Tissue synthesis and conditioned media culture

Porcine myoblasts, and porcine fibroblasts were plated on standard cell culture plates at 1 k/cm² in their respective growth medias. Cells were trypsinized, resuspended in GM, and combined at a 3:1 ratio of C2C12s to hDFs or 1:1 ratio of porcine myoblasts to fibroblasts into self-assembled into 3D tissue construct. To develop 3D self-assembled tissues, cell suspensions were added into custom 2% agarose molds that were prepared by casting molten agarose onto a patterned PDMS mask. After solidification of the gel, the molds were sectioned and added to cell culture plates. Each tissue mold is composed of a

hollow well with a 2 mm diameter central agarose post. When a cell suspension is added to the well, the cells will prefer to adhere to each other instead of the agarose, and self-assemble into a ring-shaped tissue structure that contracts around the central post. A cell seeding density of 350,000 cells/millimeter of post diameter is used per tissue sample. Tissues were then cultured for 7 days in M0, M1, or M2 conditioned media and harvested for immunostaining.

4.2.3. Beef and pork tissue sourcing

Beef and pork used to assess pigment and myoglobin content was sourced from a local butcher, who produced rib cuts. All samples were stored in closed containers at 4C before being used in experiments and were used within 24 hours of purchase.

4.2.4. Myogenesis protocol

Bovine and porcine myoblasts were cultured in MGM until reaching 80% confluency. Media was then switched to myoblast differentiation media (MDM, Advanced DMEM/F12, 2% horse serum, 1% glutamate, 1% P/S) and cultured for 72 hours.

4.2.5. Preparation of culture vessels for electrical stimulation

A 6 well cell culture dish lid was prepared with electrodes. Briefly, glass coated with indium tin oxide transparent electrodes were adhered to the inner surface of the lid along with wires that connect to a waveform generator. The lid was treated for 30 minutes with UV ozone for sterilization, assembled with the bottom half of the dish, and kept in a biosafety cabinet for storage until use.

4.2.6. Electrical stimulation of myocytes

Bovine myoblasts were grown in 6 well plates until reaching 70-80% confluency and switched to DM. Then, two types of electrical pulses were applied: 2 wells with alternating waveform pulses (D-A) and 2 wells with positive pulses (D-P). The pulse width is set to 10 ms and time between individual pulses is 100 ms. For D-A we apply voltage with alternating polarity and amplitude 10V, for D-P only positive pulses of 10 V are applied. The unstimulated control samples (D) in the last 2 wells were cultured and differentiated

together with D-A and D-P samples but with no application of the electrical field. As undifferentiated control (U) we used myoblasts grown for 2 days before they reach 70% confluency. Differentiated sample groups were harvested for qPCR and spectroscopy analysis after 48 hours.

4.2.7. Total myoglobin concentration with absorption spectroscopy

The assessment of total myoglobin (Mb) concentration of bovine myoblasts was performed using a spectroscopic assay (total myoglobin isobestic point assay) in fresh or cooked meat⁵¹, adapted for scale-down of cell cultures. Myoglobin in all forms (Deoxy-Mb, Oxy-Mb, and Met-Mb) is extracted into the buffer and the total Mb concentration is determined by absorbance at 525 nm, the isobestic point for all 3 forms of myoglobin.

Bovine myoblasts were grown in 6 well plates as previous described. After reaching 70% confluence, some undifferentiated cells were harvested for myoglobin analysis, while others were cultured in DM for 72 hours. All samples were collected in 0.25% trypsin, collected in 1.5mL tubes, centrifuged at 2000g for 1 minute. The supernatant is aspirated and the mass of the cell pellet is recorded, and the samples are consequently held on ice. 40 mM potassium phosphate buffer (KPB, pH 6.8) is prepared by mixing monobasic KH_2PO_4 (4.87 g) and dibasic K_2HPO_4 (2.48 g) potassium salts (purchased from Millipore Sigma) with 1 L distilled/deionized water and kept cold at 4C. 1 mL of ice cold KPB is added to the samples and myoglobin protein is extracted from cells by using ultrasonic homogenizer with medium amplitude pulses for 5 sec 3 times with 5 sec breaks in between. The samples are kept on ice for 30 min and then centrifuged at 20000×g for 30 minutes at 4C. We filter supernatant through a 0.22um syringe filter into spectroscopic cuvettes and measure absorbance A_{525} at 525 nm. Mb concentration is then calculated as (mg/g cells) = $(A_{525}/7.6 \times 17 \times \text{DF})$, where 7.6 is millimolar extinction coefficient for Mb at 525 nm (assuming path length is 1 cm, standard UV-vis cuvette), and DF is a dilution factor (1000 divided by the pallet mass). The average molecular mass of Mb is taken at 17 kDa.

4.2.8. Colorimetry analysis

We performed diffuse reflectance spectroscopy of meat samples meat samples and compared those to partially differentiated C2C12 cell palette. Absorption peaks are obtained from the spectra, as well as

color and position of the sample reflection on a CIE1931 chromaticity diagram. A portable UV-Vis spectrometer (Ocean Optics) equipped with tungsten-halogen lamp was used to illuminate the surface of meat or cell palette through an optical light guide with the aperture of 3 mm and large focal distance lens. The diffuse reflection spectrum in the range from 400-700 nm was recorded from the sample placed 5 cm from the lens. The recorded spectra was analyzed for coloration parameters (hue, contrast, saturation) and in placed in xy coordinates of colorimetry diagram. The reflection color on the CIE1931 chromaticity diagram is obtained in the form of chromaticity coordinates x,y that are normalization $x = X/(X + Y + Z)$; $y = Y/(X + Y + Z)$, where X, Y, Z values obtained from integration of reflection spectrum and normalized spectrum of human eye sensitivity (<http://www.techmind.org/colour/>). Values (x,y) are plotted on CIE1931 chromaticity diagram and the perception color is extracted.

4.2.9. Fusion index assay for differentiating myoblasts

Separate DAPI and myosin heavy chain images were obtained of skeletal muscle cell cultures. Images were processed in image J. Briefly, total nuclei were counter per sample by creating a binary image, using a watershed function to split up nuclei clusters into individual nuclei, and measuring nuclei counted by analyzing particles. Then, the myosin heavy chain image was converted to a binary image, the myosin and DAPI images were overlaid, and the nuclei overlapping myotubes were deleted. A final nuclei count was performed and the fusion index was obtained using the equation:

$$F = (\text{nuclei within multinucleated myotubes} / \text{total nuclei per field of view}) * 100$$

Fusion indices were averaged for each group. N=6 images for each sample.

4.2.10. Macrophage polarization and conditioned media collection

PAMs are plated at 2.5×10^4 / cm^2 and grown to 70% confluency in 10% FBS and RPMI, and then switched to serum-free polarization media for 24 hours. The polarization media consists of Advanced DMEM/F12 basal media and P/S/G: M1 macrophages are obtained by addition of 10 ng / mL INF γ and 10 ng / mL LPS and M2 macrophages are supplemented with 50 ng/mL IL-4, while M0 macrophages do not receive additional supplementation with polarizing factors. The polarization media is then collected, the cultures washed with 1x PBS, and fresh serum free Advanced DMEM/F12 is added to the M0, M1, and

M2 cultures. After 20 hours, the conditioned media is collected, sterile filtered, and stored for CM experiments at -80°C. Macrophage cultures are trypsinized, flash frozen in LN2, and stored at -80°C until gene expression is analyzed.

4.2.11. Myogenesis assay with macrophage conditioned media

pMyos are plated at 6.6×10^3 / cm^2 in plastic dishes and grown to 80% confluency in Advanced DMEM/F12 media with 20% FBS and 1ng/mL FGF-2. The growth media is then switched to CM from M0, M1, and M2 pMacros for 48 hours. Two control groups are also investigated: a negative control serum free media group that was not conditioned by macrophage culture, and a positive control supplemented with 10% FBS. The basal medias in this study for all groups was Advanced DMEM/F12 supplemented with insulin and transferrin. The cultures are then fixed and stained for myosin heavy chain and DAPI and samples were imaged and processed in Image J.

4.2.12. Proliferation assay for porcine myoblasts in macrophage conditioned media

Porcine myoblasts were grown on plastic culture dishes in M0, M1, and M2 CM for 48 hours. Immunostaining of cell nuclei with DAPI was used to determine differences of each respective media to induce cell proliferation. Cultures were fixed in PFA, stained with DAPI as previously described, and imaged. Six representative images were obtained from each culture condition and the total amount of nuclei for each image was determined in ImageJ software. Means were compared between samples.

4.2.13. Immunostaining

Myogenic cells and tissues were assessed qualitatively with immunostaining. 2D and 3D cultures were fixed with 4% formaldehyde for 20 min. 3D self-assembled tissues were then submerged in OCT media, frozen for cryosectioning, sectioned at 30 μm thick, and applied to glass slides. After fixing, samples were permeabilized with 0.1% Triton X-100 in PBS for 20 min, and then incubated with a blocking solution consisting of 5% FBS in PBS for 20 min. Following blocking, samples were stained with myosin heavy chain (MF-20, 1:50; Developmental Studies Hybridoma Bank, Iowa City, IA, USA) or α -SMA (A 2547, 1:1,000; Sigma-Aldrich, St. Louis, MO, USA) primary antibodies. Primary antibody staining was followed

by incubation with Alexa-Fluor 488 (1:250; Life Technologies, Carlsbad, CA, USA) and DAPI (1:50,000; Invitrogen, Carlsbad, CA, USA). Imaging of 2D samples was completed with an Olympus IX81 microscope (Olympus corporation of the Americas, Center Valley, PA, USA) and 3D self-assembled tissues were imaged with an Olympus Fluoview FV1000 Confocal Microscope. All images were processed with ImageJ (Version 1.48; National Institute of Health, Bethesda, MD, USA).

4.2.14. qPCR

Total RNA is isolated using MicroElute Total RNA Kit (OMEGA, R6831) according to the manufacturer's protocol. Briefly, after harvesting the cells were centrifuged and the tube with pellet is quickly immersed into the liquid nitrogen and stored at -80°C. Using 350 µL TRK Lysis Buffer (with 20 µL of 2-mercaptoethanol per 1 mL) to resuspend the cell pellet and extract RNA lysate. After a sequence of vortex, centrifugation, and washes the RNA concentration is determined using NanoDrop 2000 nucleic acid and protein quantification spectrometer. Synthesis of cDNA is carried out using qScript cDNA SuperMix (Quantabio) and PCR-grade water. The temperature profile of the cDNA synthesis protocol was as follows: 1) 25°C, 5 min; 2) 42°C, 30 min; 3) 85°C, 5 min. The samples were stored at 4°C until use for quantitative PCR (QPCR). We choose reference genes to be glyceraldehyde-3-phosphate dehydrogenase (GAPDH). Primer sets for porcine GAPDH, myogenin, myoglobin, and Pax7 are synthesized by Integrated DNA Technologies and sequence for forward and reverse primers is given below. The QPCR reaction (RealPlex 4, Eppendorf) was performed using SYBR Green Supermix (Bimake), primers (0.5 mM), PCR-grade water and cDNA in 20 µL volume samples. The temperature profile was as follows: 3 min at 95°C, 40× (20 s at 95°C, 20 s at 60°C, 30 s at 72°C), 1 min at 95°C, 1 min at 65°C, followed by a melt curve analysis. Target gene expression is evaluated using the $\Delta\Delta CT$ method with results being normalized to GAPDH housekeeping gene and compared to corresponding control cultures. List of forward/reverse primers used (Table 4.1).

Table 4.1. Sequences of primers used for PCR in this study

Species	Name	Sequence	
<i>Sus Scrofa</i>	GAPDH	F: TGGTGAAGGTCGGAGTGAAC R: GTACGACCACCCCATCCAAG	
	TNFa	F: CCTCACTCACACCATCAGCC R: GAAGACCCCTCCCAGGTAGA	
	FGF2	F: ATCTTCTCCAGGCTCCGACA R: ATTGGGGTGCAGGTACCAAAA	
	EGF	F: TTCAGTAGGGCGTTTGCCTG R: AATGGCTCACTCTCTCCGTG	
	LIF	F: GGCACCTAGTGAGACATTCCGG R: CATCTCTCCAACGGACCCTG	
	HGF	F: ATGCTGCTTCCCCTTCCTCT R: AGCAAGGCTCAGCCCAATAG	
	ANG I	F: CAAGCATAAGGGAGGGTCCA R: CAAAGTGGACAGGCAAGCCA	
	TGFB-1	F: GTCTGGAGCCGCAAACC R: AAAACCGAGATGGGCGAGAT	
	VEGF	F: CGGAGCGGAGAAAGCATTTG R: TTA ACTCAAGCTGCCTCGCC	
	INFG	F: GATCCAGCGCAAAGCCATCA R: TCTGGCCTTGGAACATAGTCTG	
	IL-6	F: ATGTCGAGGCTGTGCAGATT R: CAGGTGCCCCAGCTACATTA	
	<i>Bos Taurus</i>	GAPDH	F: TCCCAACGTGTCTGTTGTGGATCT R: TGTTGAAGTCGCAGGAGACAACCT
		MB	F: TCTGCATGGTACCTGGCCTC R: CAAGTGGAGAGCCTAGCGTG
		MYOG	F: AGCCTCCAAATCCACTCCCTGAAA R: AGCCACTGGCATAGGAAGAGATGA

4.2.15. Statistics

All data are presented as means and their standard error bars. One-tailed, one way ANOVAs were used to compare differences in gene expression levels, myoglobin concentrations, cell proliferation, and fusion index assays. Differences were considered significant at $p < 0.05$.

4.3. Results

4.3.1. In diffuse reflectance spectroscopy, C2C12s lack major wavelength peaks, while beef and pork have major wavelength peaks in the red wavelength spectrum

To compare colorimetry of cultured cells and meat from animals, pork, oxygenated and deoxygenated beef samples were homogenized, and a C2C12 cell mass collected for sample testing. Pork and both beef samples presented major wavelength peaks around 625nm (Figure 4.1A). Pork and deoxygenated

beef had additional minor wavelength peaks around 490nm and 550nm. In contrast to meat derived from animals, the color reflectance from the C2C12 myogenic mouse cell line cultured *in vitro* lacks major reflectance peaks. When reflectance wavelengths are plotted on a chromaticity graph, the oxygenated beef is deep red in color, pork and deoxygenated myoglobin in beef is reddish orange, and C2C12s are white (Figure 4.1B). This demonstrates that cultured cells lack the same degree of protein expression as animal meat that leads to proper product coloration.

4.3.2. Differentiated bovine myoblasts express more myoglobin protein than undifferentiated myoblasts, but have lower myoglobin levels than skeletal muscle tissue from a cow

Meat pigment is determined by myoglobin protein concentration in skeletal muscle cells. Consequently, myoglobin expression is important to assess in cell lines. The absorption spectroscopy analysis (Figure 4.1C) shows a typical myoglobin (Mb) protein concentration of 27.3 mg/g from adult cow muscle. Bovine muscle cells grown in cell culture produce lower levels of myoglobin protein than in beef from an animal, which is also dependent on whether the cells have undergone myogenic differentiation (6.1 mg/g) or remain in an undifferentiated progenitor state (0.6 mg/g). This indicates that myogenic differentiation may be important to myoglobin expression and product coloration.

4.3.3. Electrical stimulation with positive waveform increases myogenin gene expression and myoglobin protein expression in bovine cells

Myogenic differentiation can be improved by nerve impulses *in vivo* and does not require reagents *in vitro*, so we decided to test whether electrical stimulation would improve myoglobin expression in bovine cells. An electrical stimulation apparatus was prepared by modifying the lid of a 6-well plate with glass electrodes and conductive wire leads to generate a voltage field (Figure 4.2A, B). Two groups were differentiated in the presence of voltage fields which were either alternated with positive and negative charges or emitted positive charges only (Figure 4.2C and D, respectively), a third group underwent differentiation with no electrical stimulation, and an undifferentiated condition served as a negative control. Differentiation of bovine cells without electrical stimulation increased myoglobin gene and protein expression compared to undifferentiated samples (Figure 4.2E, F). Alternating electrical pulse waveforms

decreased myoglobin gene and protein expression below conditions with positive waveform pulses and differentiation without electrical stimulation. Positive waveform pulses yielded the highest myogenin and myoglobin gene expression and myoglobin protein expression with respect to all other groups. The results show that certain electrical stimulation waveforms can improve myoglobin gene and protein expression. differentiated samples (without electrical stimulation) (D), alternating waveform (D-A), and positive waveform samples (D-P). Gene expression of these samples is normalized to undifferentiated control (U). (D) Myoglobin protein concentration produced by U, D, D-A, and D-P samples. (*) indicates $p < 0.05$ significance vs control sample (U), and (**) indicates $p < 0.05$ significance between D-A and D-P samples.

4.3.4. M1 polarization increases gene expression of inflammatory cytokines and M2 polarization increases expression of tissue maturation factors

The immune response regulates skeletal muscle regeneration during wound healing through release of paracrine factors. Characterizing different macrophage polarization states can be used identify specific growth factors relevant to growing cell-based meat. Macrophages were polarized for 24 hours, then switched to serum free media to produce conditioned media. Macrophage polarization did not significantly alter gene expression patterns of HGF, EGF, FGF-2, and LIF (Figure 4.3A, B). M1 polarization increased VEGF, TGF- β 1, TNF α , INF γ , and IL-6 expression with respect to M0 and M2 macrophages. M2 polarization increased TGF- β 1 expression and angiopoietin 1 gene expression higher than M0 and M1 groups. Accordingly, gene expression patterns showed in increase in inflammatory cytokines during M1 polarization and an increase in tissue maturation factors during M2 polarization in macrophages prepared to produce conditioned media.

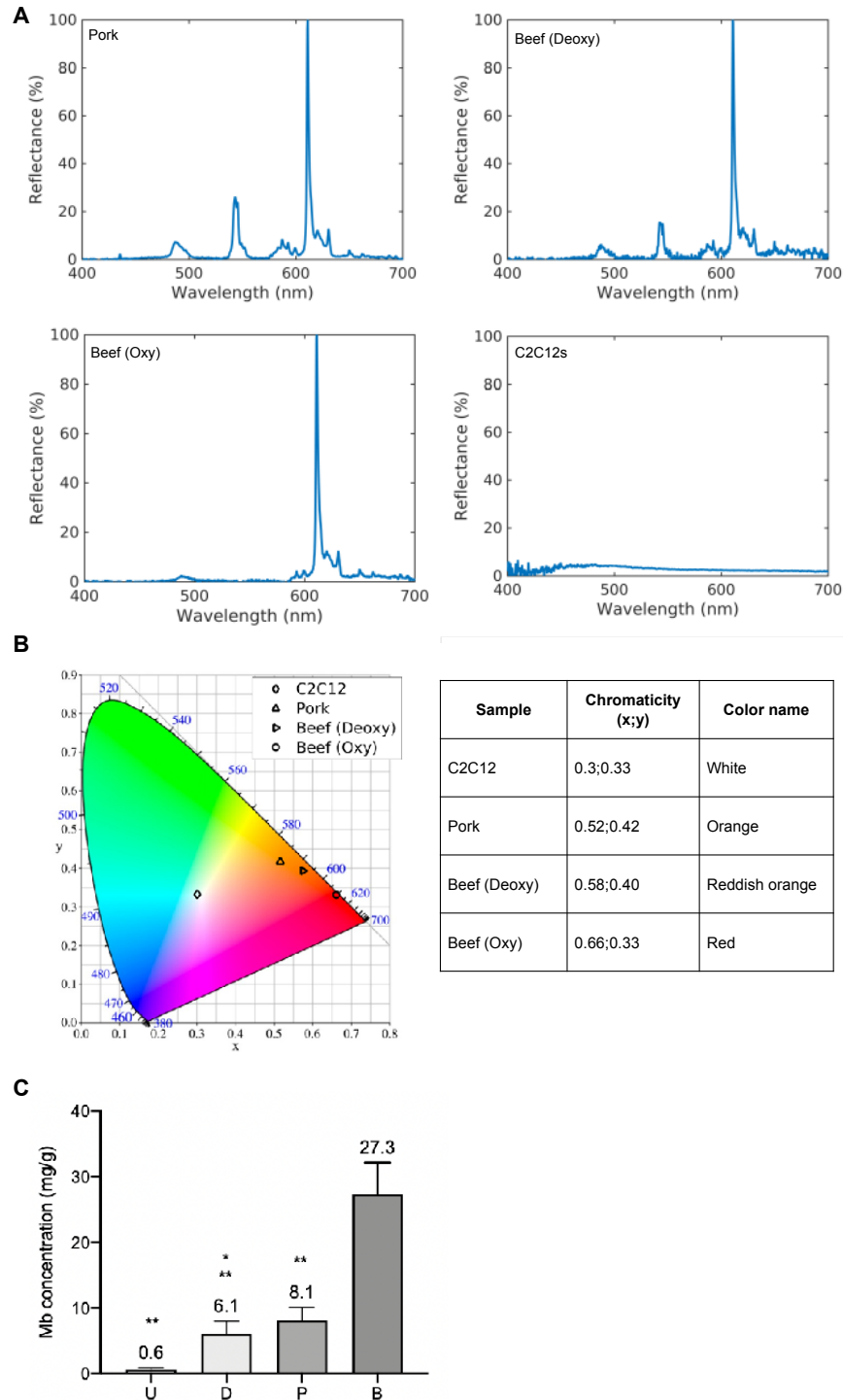


Figure 4.1. Colorimetry analysis and myoglobin protein concentration of cell cultures and meat samples. (A) Diffuse reflectance spectra for meat and cultured cell samples: pork, deoxygenated beef, oxygenated beef, and C2C12 cells. (B) CIE1931 chromaticity diagram and position of the reflection for C2C12 cells and meat samples, and sample color determination. (C) Total myoglobin concentration

obtained from absorption at isobestic point for undifferentiated (U) and differentiated (D) bovine myoblasts as well as pork shoulder muscle (P) and beef rear round muscle (B). (*) indicates $p < 0.001$ significance of (D) vs (U), and (**) indicates $p < 0.001$ statistical significance of samples vs (B).

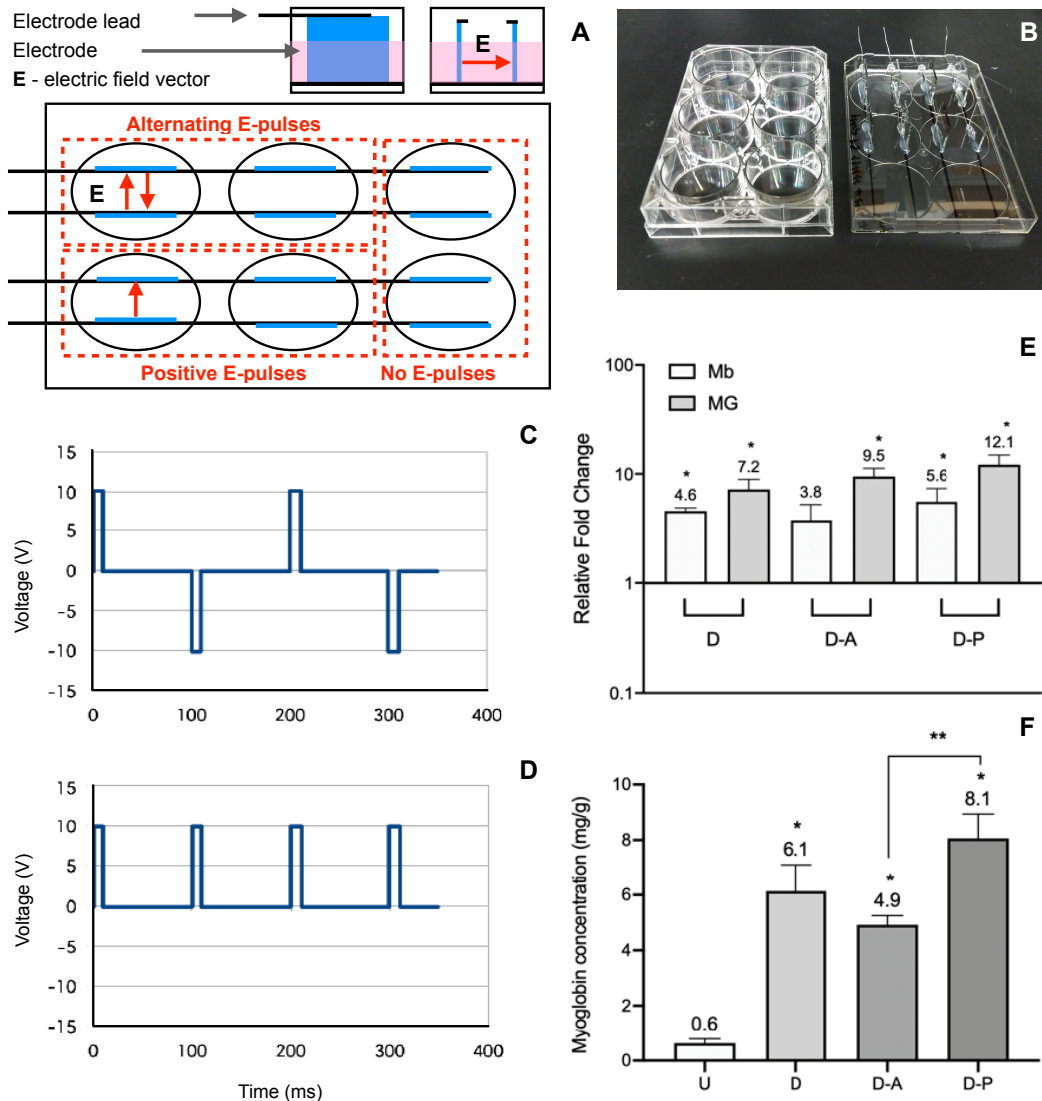


Figure 4.2. Gene and protein expression of bovine myoblasts under electrical stimulation regime.

(A, B) Schematic of stimulation apparatus in modified 6-well plates. Electrodes are attached to the top of the plate and current is transmitted through wire leads, creating an electrical field between electrodes. Some electrodes emit both positive and negative alternating voltage waveforms (C), or only positive voltage waveforms (D). (E) Gene expression analysis of myoglobin (Mb) and myogenin (MG) in

differentiated samples (without electrical stimulation) (*D*), alternating waveform (*D-A*), and positive waveform samples (*D-P*). Gene expression of these samples is normalized to undifferentiated control (*U*). (*D*) Myoglobin protein concentration produced by *U*, *D*, *D-A*, and *D-P* samples. (*) indicates $p < 0.05$ significance vs control sample (*U*), and (**) indicates $p < 0.05$ significance between *D-A* and *D-P* samples.

4.3.5. In porcine skeletal muscle cells, M0 and M2 conditioned media promote myogenesis and proliferation

Protein expression is under additional control circuits in the cell than gene expression alone. We decided to test the protein level expression of polarized macrophage conditioned media to elucidate which paracrine profile was most useful to proliferation and differentiation of myogenic cells. Porcine skeletal muscle cells were treated with 10% FBS (PC, positive control), serum free media (SF, negative control), or M0, M1, or M2 conditioned media. The positive control containing FBS media showed the highest degree of cell proliferation with respect to all other groups (Figure 4.4A, C), while the serum free negative control displayed the second lowest proliferation rate. M0 and M2 groups yielded proliferation rates that were not significantly different than the positive control or from each other, although proliferation in the M2 condition was higher than the M0 condition. The M1 conditioned media group showed the lowest decrease in mitosis of all conditions. Both M1 and the negative control had statistically lower proliferation rates than the positive control, M0, and M2 groups.

The degree of myogenesis was highest in the serum free group, which possessed the largest fusion index (Figure 4.4D, 62.5%) of the group. High fusion indices were found in M0 (53.6%) and M2 (58.2%) conditioned media condition, and PC, M0, and M2 groups were not significantly different from one another. The lowest fusion index was found in the M0 condition (0%), with a significantly higher fusion index in the control treated with FBS (16.6%). Additionally, M2 conditioned media was found to improve myogenesis in 3D samples of porcine skeletal muscle, which had multinucleate myotubes (Figure 4.4B). M0 media showed some muscle fiber formation (white arrow), while multinucleated myotubes were not

present in M1 conditioned media. The proliferation assay demonstrated that growth factors released during M0 and M2 polarization are useful to cell-based meat growth and myogenesis.

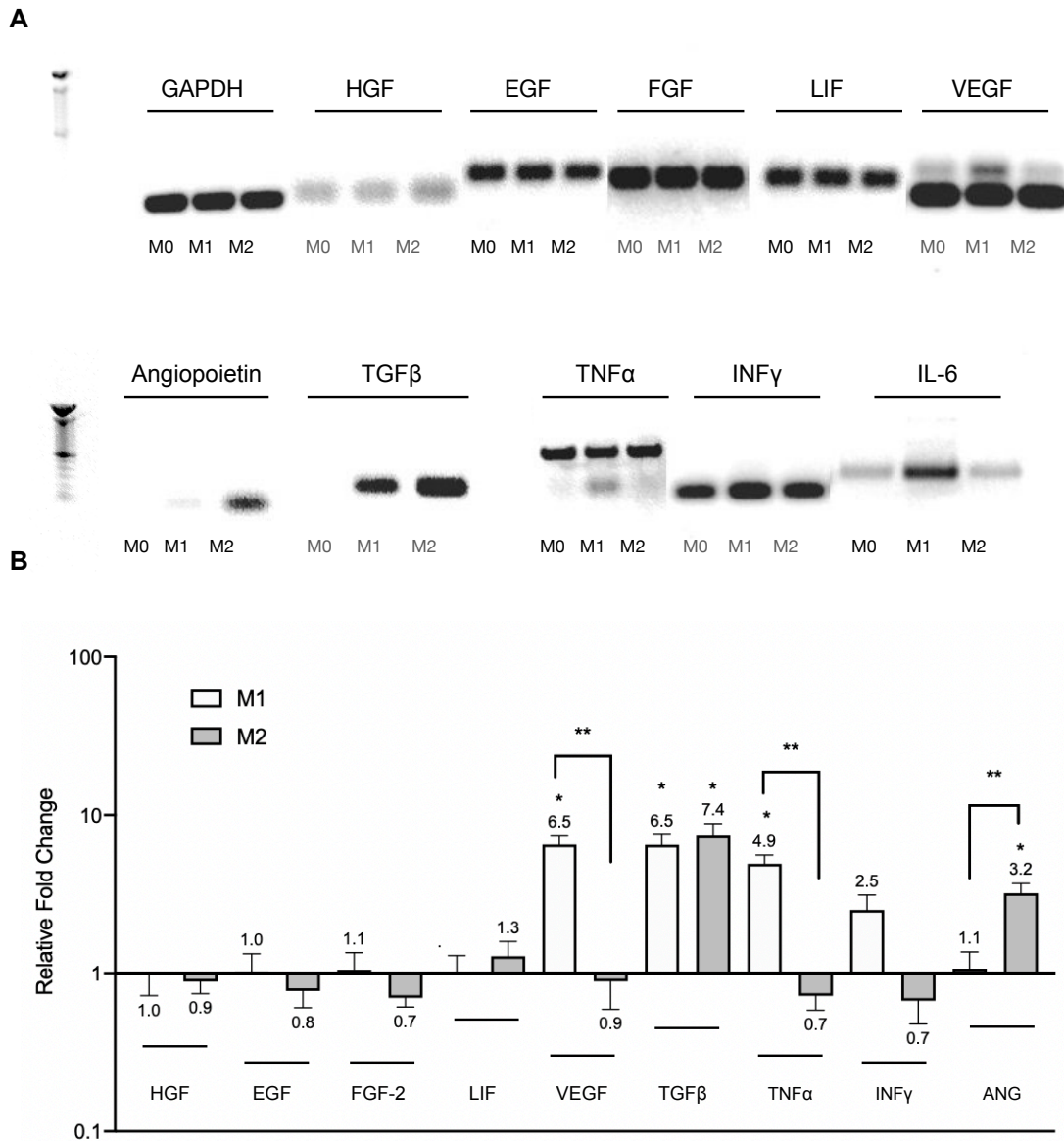


Figure 4.3. Gene expression analysis of M0, M1, and M2 polarized macrophages. (A) Gel-based PCR reactions for growth factors and cytokines visualized via gel electrophoresis. (B) Relative fold change values for M1 and M2 polarized macrophages, normalized to M0 gene expression. Average fold change values are reported with standard error bars. Significance values were defined at $p < 0.01$, (*)

indicates statistical difference from M0 condition, and (**) indicates statistical differences between M1 and M2 groups.

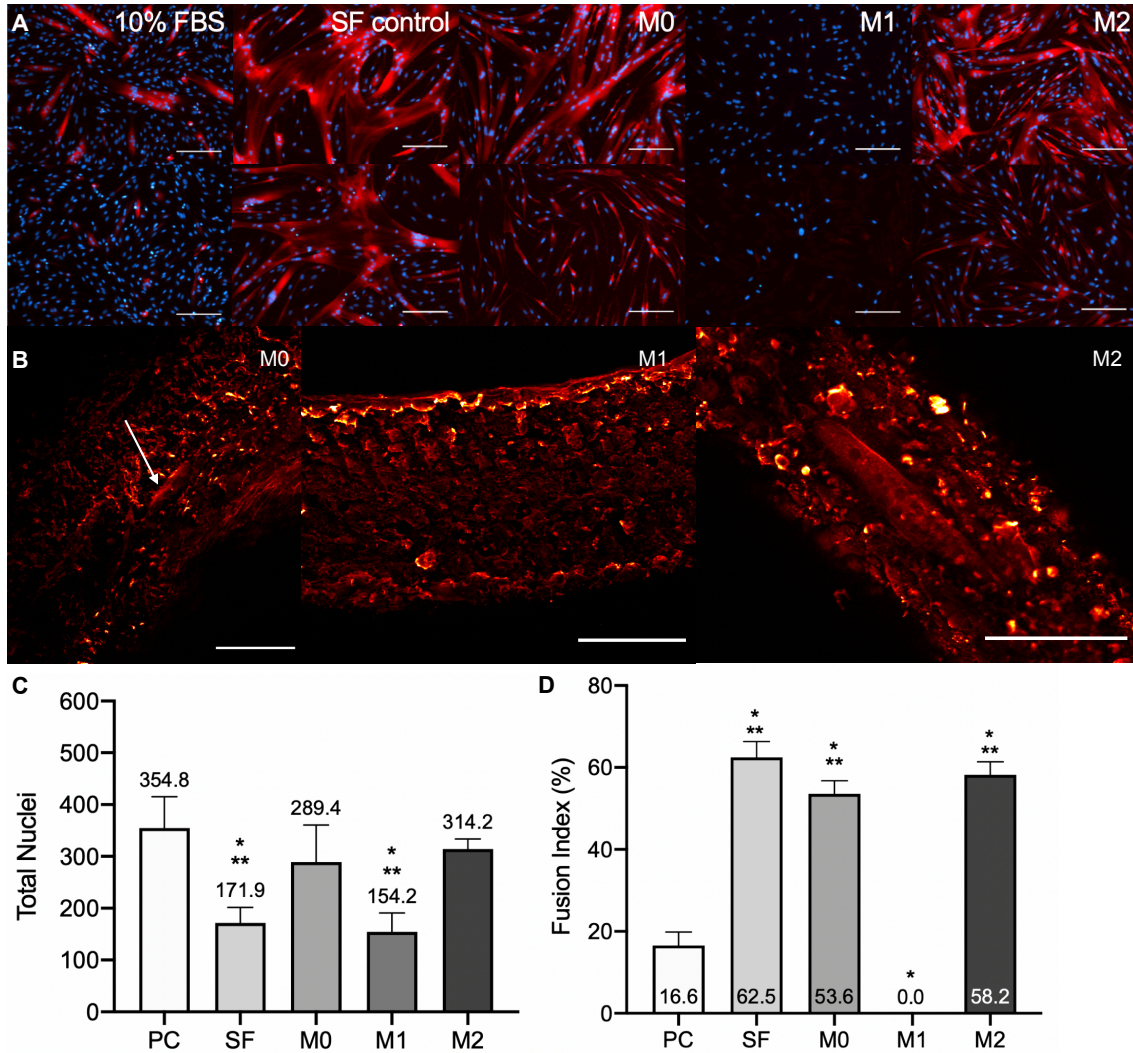


Figure 4.4. Macrophage conditioned media in 2D and 3D myogenesis and proliferation assays. (A) Myogenesis of porcine muscle cells in different media compositions. Cells were treated either with basal media containing 10% FBS; serum free basal media; or basal media conditioned by M0, M1, or M2 macrophages. The top row shows areas with high cell density in the cultures, while the bottom row shows areas of low cell density. Cultures were stained for myosin heavy chain and DAPI. Scale bar = 200µm. (B) Myosin heavy chain in porcine skeletal muscle and porcine fibroblasts tissues cultured in M0, M1, and

M2 media. Scale bar = 100 μ m. The white arrow points to a small myotube in M0 condition. (C) Porcine myoblast cell proliferation in PC (positive control), SF (serum free), and macrophage conditioned medias, measured by total nuclei count in DAPI stained samples. (*) indicates $p < 0.01$ vs PC, and (**) indicates $p < 0.05$ vs M2 condition. (D) Fusion index of porcine myoblasts in PC, SF, and macrophage conditioned medias. (*) indicates $p < 0.01$ vs PC, and (**) indicates $p < 0.05$ vs M1 condition.

4.4. Discussion

We assessed the reflectance spectra of C2C12 myocyte cells, OMb and DMb beef, and pork. C2C12 mouse myoblasts were white in color due to a lack of myoglobin protein present in the cells. Beef and pork meat samples showed typical wavelength spectra in the red-orange range. Like C2C12s, myoglobin protein concentration was also very low in undifferentiated bovine myoblasts. Differentiation brought a 10-fold increase in myoglobin concentration in bovine cells, although they were still only 22% of the myoglobin concentration found in beef. These data indicate that the color is dependent on myoglobin concentration, and myogenic cells grown in cell culture express lower levels of Mb compared to meat from an animal. Myogenic differentiation increased myoglobin concentration in bovine cells and electrical stimulation of cultures further improved myoglobin concentration during positive waveform electrical pulses. Myoglobin protein expression must be enhanced in cell culture to increase the pigment and flavor of cultivated meat to levels similar to meat derived from animal sources. Edible cell lines that stably express elevated Mb or culture processes that amplify Mb expression are necessary to reduce the cost and complexity of myoglobin upregulation strategies in cell production.

Harnessing the capacity of a single cell type to shift to different soluble protein expression profiles may be used to promote skeletal muscle cell and tissue manufacturing. Macrophage conditioned media represents a source of media for cultivated meat, or can be useful for screening the impact of known growth factors on cells. In polarized macrophage experiments, no significant differences were found in HGF, EGF, FGF-2, and LIF gene transcription, which are associated with satellite cell activation,

proliferation, and maintenance of stemness. Protein expression levels were not assessed for these growth factors, but translation likely occurred in M0 and M2 macrophages. M0 and M2, but not M1, conditioned media promoted proliferation of porcine skeletal muscle cells comparable to the control group containing 10% FBS, suggesting the presence of mitotic factors that stimulate cell proliferation in the conditioned medias. Previous studies have shown M1 macrophages induce proliferation and inhibit myogenesis in skeletal muscle cells *in vivo*¹²¹ and *in vitro*¹²⁰. However, the *in vitro* study used 0.5% FBS in the M1 media, which may have promoted proliferation beyond what this current studies' serum free M1 CM could perform. Additionally, proliferation in M1 CM was not statistically significantly different from the serum free control. The increase in TNF α , INF γ , TGF- β 1, and IL-6 gene expression in M1 macrophages may have led to too much inflammatory cytokine signaling in M1 CM and halted cell proliferation. There may also be species specific differences in growth factor effects, since previous studies looked at mouse or human models and this study used porcine cells.

Myoglobin

Visual perception of red meat quality is determined from myoglobin pigmentation. Myoglobin is a ~17 kDa cytoplasmic hemoprotein encoded by the "MB" gene. It possesses a single heme group, where hemoglobin contains four heme groups. Myoglobin reversibly binds to O₂ via the heme group and serves as an oxygen storage system for oxidative phosphorylation. The heme group in myoglobin provides a red pigment to meat, depending on the oxidation state of the Fe⁺ ion, which affiliates with O₂⁵¹. There are three basic myoglobin redox states that can be detected by reflectance spectra: oxymyoglobin (OMb), deoxymyoglobin (DMb), and metmyoglobin (MMb). In the presence of oxygen, O₂ is bound to Fe⁺² and OMb is generated, which produces a bright red color. When O₂ is absent from Fe⁺², DMb is formed and the heme ring is purplish in color. When meat is overexposed to oxygen for a prolonged period, Mb is oxidized to Fe⁺³, forming MMb and a dark brown color to the meat surface. The electron transport chain in mitochondria can reduce MMb back to Fe⁺² and is involved with color stability. Visual meat color acceptance follows the red > purple > brownness sequence¹²³.

Muscle Fiber Pigment and Flavor

Muscle fiber-type composition influences meat quality through myosin heavy chain isoform expression and myoglobin production, which affects meat flavor and pigmentation. The contractile properties of muscle fiber types result from myosin heavy chain isoform expression. Type 1 fibers express MyHC-1 (aka MyHC- β /slow) from the MYH6 and MYH7 gene, type 2A fibers express MyHC-2A from the MYH2 gene, and type 2B fibers express MyHC-2B from the MYH4 gene¹²⁴. Peak contractile power values and ATP consumption for myosin during sarcomeric contraction increase orderly from slow twitch to fast twitch 2A and fast twitch 2B fibers¹¹⁰. While higher contractile power is possible with fast twitch fibers, they fatigue more easily due to limited ATP regeneration possible from glycolysis. Conversely, slow twitch fibers can easily produce ATP from oxidative phosphorylation in mitochondria in addition to having lower ATP consumption demands, making these muscles fatigue resistant. High mitochondrial density in slow twitch fibers require supportive levels of intracellular myoglobin protein concentration to supply enough oxygen to stimulate oxidative phosphorylation. Myoglobin is highest in type I and 2A fibers that primarily utilize aerobic respiration, while myoglobin is virtually absent in type 2B fibers. High levels of myoglobin generate muscles with intense red color, such as found in red meat, while low myoglobin levels result in a lighter pink that's seen in white meat¹²⁵.

Once an animal is slaughtered meat undergoes a cell and tissue death before it become available to consumers. Biochemical reactions occur during rigor that give meat a more palatable flavor. Muscle fibers are subjected to an anaerobic environment during cellular rigor due to lack of oxygen, and begin using glycolysis to support intracellular activity. This lowers muscle pH and toughens meat, reduces water holding capacity and increases drip loss and exudation, which reduces juiciness and flavor^{126, 127}. High percentages of 2B muscle fibers will lead to higher levels of lactate buildup and steep pH decline that greatly reduces meat quality. Type I muscle fibers do not have the same capacity for glycolytic activity as type 2B fibers, making them less prone to steep drops in pH¹²⁷.

Electrical Stimulation

Electrical stimulation can attenuate both muscle fiber type and myoglobin protein expression via the calcineurin / NFAT pathway. NFAT transcription factor family serve as nerve-activity sensors. Calcineurin is a calcium-dependent phosphatase which can be activated from Ca²⁺ effluxes from the

sarcoplasmic reticulum during muscle contraction from nerve impulses. Once activated by Ca^{2+} , calcineurin dephosphorylates cytosolic NFAT, which is able to translocate to the nucleus. NFAT binds to an upstream promoter region of MB gene and activates expression of myoglobin¹²⁸. NFAT activity also controls fiber-type specification. In the absence of nerve impulses *in vivo*, type 2B fibers are predominantly present as the default fiber composition. However, reinnervation of skeletal muscle decreases the percentage of 2B fibers while gradually increasing 2A fibers and finally type I fibers, indicated through a transition from MyHC-2B > MyHC-2A > MyHC- β /slow isoform expression¹²⁹. *In vitro*, ES was found to increase expression of myosin heavy chain type 2 (MYH2) and decrease expression of myosin heavy chain type 4 (MYH4), indicating a switch from fast-to-slow MHC isoforms⁵⁹. Myosin isoform gene expression is coordinated by four NFAT isoforms: NFATc1, -c2, -c3, and -c4. NFATc1 dephosphorylation activates MyHC- β /slow gene expression; NFATc2, NFATc3, and NFATc4 activates MyHC-2A gene expression, and NFATc4 activates MyHC-2B expression. ES activates calcineurin to phosphorylate NFAT isoforms. NFATc1 is only translocated to the nucleus only during slow-type nerve impulse patterns to stimulate MyHC- β /slow isoform protein expression, leading to increasing type I fiber presence. NFATc3 will translocate to the nucleus during both fast- and slow-type nerve impulse patterns to increase MyHC-2A protein expression and type 2A fiber formation. NFATc4 however has constitutive nuclear localization, which continuously activates MyHC-2B gene expression and 2B fiber type composition. In the absence of electrical impulses, nuclear NFATc4 transcriptional activity specifies 2B fiber types, but impulses will translocate NFATc1 and NFATc3 to the nucleus to generate type I and 2A fibers¹²⁴.

Myoglobin expression and type I muscle fiber formation can be enhanced via ES in edible skeletal muscle cells to increase red pigment chroma and generate red cell-based meats. Alternatively, an absence of electrical stimulation can be used to design white meats with type 2B muscle fiber composition. ES can be used to generate specific meat products by mimicking muscle fiber compositions and myoglobin levels. For example, a lean cut of bottom round steak could be reproduced by generating a large type I to type 2 fiber ratio with high intracellular myoglobin concentration. Additionally, ES can increase cellular biomass without the additional reagent cost. ES increases muscle biomass through

improving hypertrophy¹²², force contraction¹³⁰, and maturation by enhancing sarcomeric assembly via increased expression of tropomyosin, sarcomeric α -actin and sarcomeric myosin heavy chain isoforms⁵⁹.

Macrophage Conditioned Media and Myogenesis

Developing an FBS-free macrophage-conditioned media manufacturing platform may support different phases of the meat manufacturing process. Resident tissue and bone marrow derived macrophage populations normally exist in an unpolarized M0 state, but are activated to an M1 pro-inflammatory phenotype in the presence of paracrine factors, such as lipopolysaccharide, a component of the cell walls of bacteria. After initially promoting inflammation, M1 polarized macrophages shift to a M2 tissue regenerative phenotype. M0 macrophage polarization into M1 and M2 phenotypes shifts the paracrine factory profile, resulting in expression of different proteins that impact cell metabolism, proliferation, and cell differentiation, and activate tissue regenerative mechanisms¹³¹.

Myogenesis is stimulated or inhibited by paracrine factors. Muscle regeneration is orchestrated by macrophages *in vivo*. The temporal pattern of macrophage recruitment and transitioning between M0, M1, and M2 polarized phenotypes coordinates muscle regeneration in part through attenuation of myogenic transcription factor expression¹³¹. M0 macrophages express HGF¹³², PDGF, FGF-2¹³³, LIF¹³⁴, and PPAR γ ; while pro-inflammatory M1 macrophages express cytokines such as VEGF¹³⁵, IGF-1, IL- β 1, TNF α ; and anti-inflammatory M2 macrophages express TGF- β 1¹³⁶. Early M1 polarization for 3 days post muscle injury is associated with hypertrophy of muscle fibers and higher force contraction of muscles, while early M2 polarization is associated with lower force contraction of regenerating muscles and persistent fibrosis from ongoing tissue remodeling. The temporal polarization of M1s peaks at day 3 and subsequently subsides, followed by more MYOD+ nuclei at day 4. M2 macrophage polarization increases over the course of 21 days, and peaks at day 21¹³⁶.

In line with previous studies¹²⁰, M1 CM inhibited myogenesis and M2 CM enhanced myogenic differentiation higher than any other CM group, although it was not significantly different from the M0 condition. The enhancement of myogenesis by M2 CM was present in both 2D and 3D cultures, similarly found in other literature^{131, 121}. In 3D tissue culture, M2 conditioned media promoted formation of highly multinucleated myotubes, in contrast to M0 and M1 samples.

Future Directions

Cell-based meat that includes skeletal muscle cells must account for the impact of muscle cell characteristics on the product. Differentiation improves myoglobin and myosin heavy chain protein expression over undifferentiated cells, which improves color and total protein content. Accordingly, cells that undergo myogenesis would likely improve umami and meat-like flavor. Culture protocols driving specific muscle fiber type expression of type I fibers would additionally have several benefits. Type 1 fibers have higher myoglobin protein concentrations than type 2A and 2B fibers due to their preference for oxidative phosphorylation rather than glycolysis. This will enhance the red pigment of harvested cells and improve meat flavor due to controlling the pH and protein profile. Alternatively, lowering pH in a muscle cell harvest may be a way to increase the viscosity of manufactured cells to improve material performance during product preparation. The use of electrical stimulation can control muscle fiber typing, myoglobin expression, and ultimately impact color and flavor. Bioreactors can be configured to include electrical stimulation apparatus without increasing the cost of reagents. This would improve product quality without impacting profit margins, although it would require advancements in bioreactor design.

Additionally, it may be possible to develop a macrophage cell line that can produce its own media, or a cell line's conditioned media could be helpful for various aspects of scale up. The PAM cell line from ATCC is SV40-T immortalized and can rapidly proliferate with low FBS requirements [data not shown]. Conditioned media from M0 and M2 polarized macrophage can be useful to replace FBS in scale up for co-culture applications. This media could improve cellular biomass harvest through enhancing proliferation and differentiation and umami flavor of cells. Conditioned media studies can also reveal useful growth factors or proteins to cell-based meat.

Chapter 5

EVALUATION OF TISSUE ENGINEERING METHODS FOR CULTIVATED MEAT

This work has been published in PeerJ

Krieger J, Park B, Lambert CR, Malcuit C. 2018. 3D skeletal muscle fascicle engineering is improved with TGF- β 1 treatment of myogenic cells and their co-culture with myofibroblasts. *PeerJ*. <https://doi.org/10.7717/peerj.4939>

5.1. Introduction

Tissue structuring has the potential to produce cell-based meat products that simulate meat from an animal by recapitulating the cellular architecture and connective tissue matrix of animal meat. The costs and complexity associated with these techniques must be minimized to become a viable option for manufacturing cell-based meat products. Tissue engineering in the regenerative medicine industry use high performance equipment to develop complex processes that are expensive to use and slow to produce a tissue product. Rapid and cheap tissue synthesis is required for scaling cultivated meat production.

Tissue can be self-assembled, prepared from a hydrogel scaffold, or embedded into a prefabricated scaffold; and edible materials will be necessary if using scaffolds. The cheapest, most readily available, and most scalable edible scaffolding materials are from plant sources. Typical ECM materials used by the regenerative medicine industry are either animal-derived¹³⁷ or inedible¹³⁸ - both are expensive and nonviable options for cell-based meat. Traditional plant-based scaffolds includes alginate and agarose, but these materials are well known for yielding limited growth and differentiation of cells due

to a lack of native mammalian RGD (Arg-Gly-Asp) sites in the polymer¹³⁹. RGDs are protein motifs found in ECM proteins that mammalian cells can recognize with integrins affiliated with the cytoskeleton. Integrin binding facilitates cell adhesion to the matrix and consequently mediates cell migration, proliferation, and differentiation¹⁴⁰. Plant-based alginate¹⁴¹ and agarose¹⁴² materials have to be modified with RGD motifs to mediate cell adhesion, and this increases the cost and complexity of material preparation. A new group of plant based scaffolds are being explored for their utility in cultivated meat, such as cellulose¹⁴³, TVP⁹⁰, and mycelium, which can be easily derived from nature in bulk. These materials need to be investigated for their performance ability as a scaffolding material and associated costs should be determined.

Tissue engineering faces challenges to maintain the integrity and stability of tissues, which can require the addition of supportive cell types along with adipocytes and myocytes, and should reliably drive myogenesis and adipogenesis for high quality cultured meats. Consequently, this study sought to first investigate the influence of co-culturing myogenic cells with connective tissue cells to stabilize and improve myogenesis in a scaffoldless tissue self-assembly model and in collagen-1 based hydrogels as a method to improve meat quality in muscle tissue samples. C2C12s and hDFs were used initially to develop the tissue engineering platforms, then porcine skeletal muscle myoblasts, fibroblasts, and myofibroblasts were used. Cellulose scaffolds from decellularized celery were also tested for application in cell-based meat. The rigidity of cellulose was stiffer [data not shown] than the muscle tissue niche ($\sim 12\text{kPA}$)¹⁴⁴, so a method to soften scaffolds was developed. The cellulose was first decellularized and the flexible scaffold was prepared by freezing plant material prior to decellularization. The scaffolds' ability to rapidly promote skeletal muscle tissue structuring through cell adhesion, proliferation, and differentiation was assessed. A method to improve mammalian cell adhesion and differentiation in plant-based scaffolds using connective tissue cell feeder layers was also investigated.

5.2. Materials and Methods

5.2.1. Cell and tissue culture for comparing 2D cultures to 3D self-assembled tissues

As shown in the experimental design listed in Figure 4.1A, cultures consisting solely of human neo-natal dermal fibroblasts (passage 4 hDFs, PCS-201-010; ATCC, Manassas, VA, USA) or mouse myoblasts

(pre-passage 4 C2C12s, CRL-1772, ATCC) were plated on standard cell culture plates at 1 k/cm² in growth media (GM) consisting of DMEM (Gibco, Waltham, MA, USA), 10% fetal bovine serum (FBS; Hyclone, Pittsburgh, PA, USA), 1% penicillin/streptomycin (P/S, Gibco). To promote differentiation of hDFs and porcine fibroblasts to myofibroblasts, some fibroblasts were incubated with 1 ng/mL TGF- β 1 (Peprotech, Rocky Hill, NJ, USA) for 6 days between P4 and P5. Porcine myoblasts were cultured as previously described. For both C2C12 / hDF and porcine myoblast / myofibroblast tissues, cells were trypsinized, resuspended in GM, and seeded at a 1:1 ratio on standard cell culture plates at 20 k/cm² or self-assembled into 3D tissue constructs. As mentioned previously, to develop 3D self-assembled tissues, cell suspensions were added into custom 2% agarose molds that were prepared by casting molten agarose onto a patterned PDMS mask. After solidification of the gel, the molds were sectioned and added to cell culture plates. Each tissue mold is composed of a hollow well with a 2 mm diameter central agarose post (Figure 5.1A). When a cell suspension is added to the well, the cells will prefer to adhere to each other instead of the agarose, and self-assemble into a ring-shaped tissue structure that contracts around the central post. A cell seeding density of 350,000 cells/millimeter of post diameter is used per tissue sample. This density was selected through a pilot experiment determining the concentration of cells required to self-assemble tissue around the circumference of the agarose post, which is a function of the post's diameter (C. Malcuit, personal communication, 2013). Hydrogels were produced from a protocol adapted from Langelaan et al. (2011)⁵⁹ where 1.5×10^6 C2C12s alone or a 1:3 ratio of fibroblasts/myofibroblasts and C2C12s were resuspended in 42% GM, 54% rat collagen type 1 (3 mg/mL; Corning Life Sciences, Corning, NY, USA), and 2.7% NaOH (0.1 M). 1.5×10^6 porcine myoblasts alone or a 1:3 ratio of porcine fibroblasts/myofibroblasts and C2C12s were resuspended in 42% GM, 54% bovine collagen type 1 (3 mg/mL; Corning Life Sciences, Corning, NY, USA), and 2.7% NaOH (0.1 M). The hydrogel mixture was poured between house-shaped Velcro anchors super glued to the bottom of a six well plate and gelled for 45 min before adding GM. After 24 h, the media were switched in both 2D and 3D conditions to differentiation medium (DM) composed of DMEM, 2% horse serum (Sigma-Aldrich, St. Louis, MO, USA), and 1% P/S, with or without 1 ng/mL TGF- β 1. Media was changed every 2–3 days for 7 days for C2C12 / hDF tissues, after which cells and tissues underwent qPCR, ICC or IHC, or mechanical

characterization. See Figure 5.1B for listing of experimental groups. Porcine tissues were cultured for 48 hours before collection for immunocytochemistry.

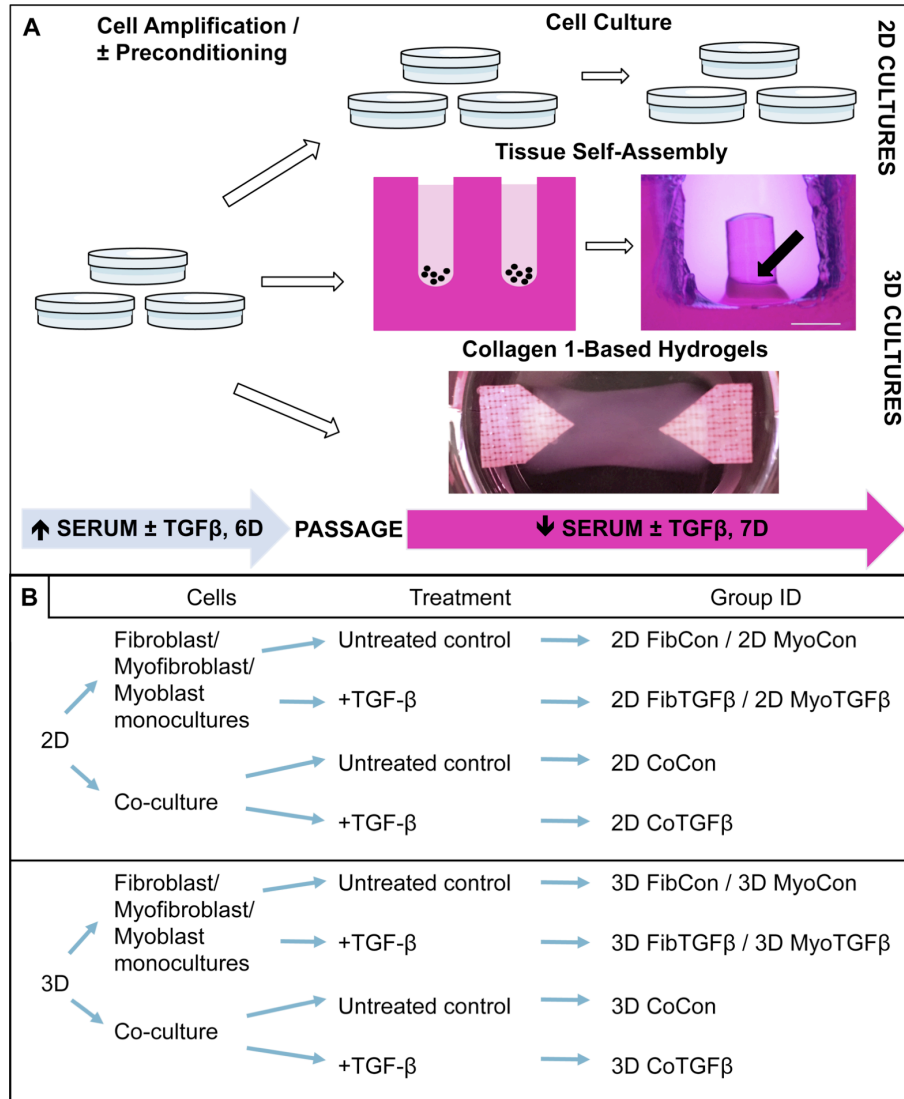


Figure 5.1. Technical protocol for 2D/3D culture systems and experimental conditions design. (A)

Technique: 2D cell culture and 3D tissue engineering protocols involve an initial high serum culture period on standard cell culture plates to separately amplify myoblast and fibroblast populations, with a subset of ‘preconditioned’ fibroblasts being treated with TGF- β 1 to differentiate them into myofibroblasts. After 6 days the cells are passaged and either replated on cell culture plates for 2D studies or used for 3D systems. 3D tissue-engineered models were produced either via scaffoldless self-assembly or collagen 1 hydrogel biofabrication. A low serum culture period subsequently followed, with some groups treated with

TGF- β 1 over 7 days. The black arrow denotes the location of a tissue construct around the annulus inside an agarose mold; scale bar = 2 mm. (B) Conditions: experimental design is defined by comparisons between culture systems (2D culture plates vs 3D agarose gels/collagen 1-based hydrogels), cellular content (co-culture or monoculture of myoblasts, fibroblasts, or myofibroblasts), and their biochemical treatment in culture (\pm TGF- β 1). The resulting group identification terms code for the conditions investigated in these experiments.

5.2.2. Gene expression analysis

Total RNA was isolated from cultures using TriZol reagent (Life Technologies, Carlsbad, CA, USA) according to the manufacturers recommended instructions. cDNA was reverse transcribed from 1 μ g total RNA using qScript SuperMix (Quanta Biosciences, Gaithersburg, MD, USA) according to manufacturer's instructions. qPCR was carried out using a 5 ng equivalent of cDNA in a 1X reaction of PerfeCTa SYBR Green SuperMix (Quanta Biosciences, Beverly, MA, USA) and 250nM each (forward and reverse) custom oligonucleotide primers (Integrated DNA Technologies, Coralville, IA, USA) generated by using PrimerBlast (National Center for Biotechnology Information, Bethesda, MD, USA). Reactions were carried out on an Eppendorf RealPlex2 qPCR system, and fold changes in gene expression were calculated using the $\Delta\Delta$ CT method using species-specific GAPDH primers. Primer sequences are listed in Table 5.1. Human collagen 1 and α -SMA expression levels in the 2D FibCon condition were used as the reference group for fibroblast gene expression, and mouse myogenin gene expression levels of 2D MyoCon were used as a reference for myoblasts. $N = 5$ for all groups.

Table 5.1. Sequences of primers used for PCR in this study

Species	Name	Sequence
<i>Homo sapien</i>	GAPDH	F: CCCCCGGTTTCTATAAATTGAGC R: AAGAAGATGCGGCTGACTGT
	α -SMA	F: CTTCCCTGAACACCACCCAGT R: CCTCTTCTTCACACATAGCTGGA
	Collagen 1A	F: TCCCCAGCCACAAAGAGTCTA R: CCTCTTCTTCACACATAGCTGGA
<i>Mus musculus</i>	GAPDH	F: CCAGCAAGGACACTGAGCAA R: CCCTAGGCCCTCCTGTTAT
	Myogenin	F: GCCATCCAGTACATTGAGCG R: TGGACGTAAGGGAGTGCAGA

5.2.3. Immunostaining

2D and 3D cultures were assessed qualitatively with immunostaining. 2D cultures were fixed with 4% formaldehyde for 20 min, and 3D cultures were fixed for 2 h. 3D self-assembled tissues were then submerged in OCT media, frozen for cryosectioning, sectioned at 30 μm thick, and applied to glass slides. Hydrogels remained unsectioned for whole-mount imaging. After fixing, 2D and 3D samples were permeabilized with 0.1% Triton X-100 in PBS for 20 min, and then incubated with a blocking solution consisting of 5% FBS in PBS for 20 min. Following blocking, samples containing myoblasts were stained with rhodamine phalloidin (R415, 1:40 dilution; Life Technologies, Carlsbad, CA, USA) and/or myosin heavy chain (MF-20, 1:50; Developmental Studies Hybridoma Bank, Iowa City, IA, USA), procollagen (M-38, 1:50; Developmental Studies Hybridoma Bank) or α -SMA (A 2547, 1:1,000; Sigma-Aldrich, St. Louis, MO, USA) primary antibodies. Primary antibody staining was followed by incubation with Alexa-Fluor 488 or 564 secondaries (1:250; Life Technologies, Carlsbad, CA, USA) and DAPI (1:50,000; Invitrogen, Carlsbad, CA, USA). Imaging of 2D samples was completed with an Olympus IX81 microscope (Olympus corporation of the Americas, Center Valley, PA, USA), 3D self-assembled tissues were imaged with an Olympus Fluoview FV1000 Confocal Microscope, and hydrogels were imaged with an Olympus Fluoview FV1000MPE multiphoton microscope. All images were processed with ImageJ (Version 1.48; National Institute of Health, Bethesda, MD, USA). The total area of procollagen staining was measured in 2D FibCon and FibTGF β images and divided by the total number of nuclei to find the average area of procollagen staining per cell. Increased area procollagen signal was extrapolated as a change of in cell shape and increased cell spreading. Circularity of DAPI stained fibroblast nuclei was measured to compare changes in cyto- and nucleoskeletal shape. $N = 13$ images for each group. 2D MyoCon and CoCon images were also processed to measure changes in myotube alignment. In each image, the myotubes formed angles with a common axis (x or y). The standard deviations of the angles from each image were measured to compare the variability in each group, with smaller averaged standard deviations for one sample image indicating higher myotube alignment. $N = 8\text{--}9$ images for each sample.

5.2.4. Slack tests

The slack test method has been adapted by our lab to indirectly measure and compare tissue integrity, ECM maturity, and muscle fiber development between engineered samples. Two slack test methods were employed. In the whole tissue slack test, self-assembled tissue constructs were released from tension in culture and their shortening lengths were recorded over time. The initial lengths (μm , L_i) of rings were recorded across their longest axis while they remained on their posts. Rings were then removed from the agarose posts, suspended in PBS (37 °C) on a submerged horizontal microbeam from the Microsquisher system (CellScale, Ontario, Canada), and points across their longest axis for 27 min. The final lengths (L_f) were recorded and percent shortening (%) was calculated with the formula $\% = 100*(L_f/L_i)$. Tissues were then stored in their respective medias for 24 h at 37 °C and imaged with a stereoscope. $N = 3\text{--}6$ samples per group.

The cleaved tissue slack test was performed to release the tissues from internal tension, which may arise from tissue structuring patterns building passive forces. 3D MyoCon, MyoTGFB, CoCon, and CoTGFB tissue rings were cut with a scalpel to generate linear muscle constructs freed from their agarose posts and placed in a 37 °C bath of cell culture media. Tissue lengths were measured every 3 min for 15 min, then samples were allowed to slack over 24 h at 37 °C to give the final length (L_f). The initial length (μm , L_i) for each construct, the length of the uncut tissue sample still mounted on its post, was calculated as the circumference of the 2 mm agarose posts using the formula: $L_i = 2 \pi r$. The percent of original size (%) was determined with the formula: $\% = 100*(L_f/L_i)$. $N = 4\text{--}5$ samples per group.

5.2.5. Tissue elastic moduli assessments

For calculations of the elastic stiffness of self-assembled engineered tissues, two methods of mechanical characterization were used: a compression-based system to generate slopes from stress–strain curves and atomic force microscopy (AFM). Tissue constructs were sectioned into 4–5 pieces with diameters between 250 and 500 μm and were compressed in a PBS fluid bath (pH 7.4, 37 °C) using a Microsquisher (Cellscale, Waterloo, Ontario, Canada). Tissues were compressed to 40% of their original diameter at a rate of 1% per second using microbeams with diameters between 0.2 and 0.3048 mm. Force–displacement curves were generated and the slope of the linear portion of the curve was

extrapolated as the elastic modulus of the tissue. Slopes were averaged for each 3D condition with $N = 8-12$ section samples per group.

Tissue elastic moduli were measured by an Asylum MFP3D-Bio AFM (Asylum Research, Santa Barbara, CA, USA) through a nano-indentation method using MFP-3D software (Version 13.04.77). Force-distance curves were determined using equations (1) and (2):

$$F(\delta) = \frac{4\sqrt{R}}{3} \frac{E}{1-\nu^2} \delta^{3/2} \quad (1)$$

$$F(\delta) = \frac{E}{1-\nu^2} \frac{2 \tan \alpha}{\pi} \delta^2. \quad (2)$$

Where F is the measured force, E is the local Young's modulus, R is the cantilever's tip radius (for a spherical tip), α is the cantilever's tip angle (for a cone tip), ν is the Poisson's ratio of the sample (assumed as 0.5 for an incompressible material), and δ is the sample indentation. Pyramidal tips with a nominal tip radius 20 nm, 200 μm in length, 20 μm in width, and a tip semi-angle of 15° on silicon nitride triangular V-shaped cantilevers with a nominal spring constant of 0.06 N/m (DNP-10; Bruker Inc., Camarillo, CA, USA) were employed. The recorded force-distance curves were analyzed in MATLAB and statistical analysis was done using SPSS (Ver. 17.0; IBM, Somers, NY, USA).

5.2.6. Celery scaffold preparation and decellularization

Scaffolds were prepared using a modified protocol from Modulevsky et al. (2014)¹⁴³. Celery scaffolds were prepared by sectioning ~1mm thickness of celery and a tissue biopsy punch was used to generate circular samples. The samples were placed in water and either stored overnight at 4C or frozen overnight at -10C. Then the celery punches were placed in sterilized 1.5 mL microcentrifuge tubes with 1 mL of 0.5% sodium dodecyl sulphate (SDS) (Sigma-Aldrich) and shaken for 12 hours at 160 RPM at room temperature. The decellularized cellulose scaffolds were then transferred into new sterile microcentrifuge tubes, washed and incubated for 6 hours in PBS (Sigma-Aldrich) with 1% streptomycin/penicillin (HyClone) and 1% amphotericin B (Wisent). Samples were then stored in PBS at 4C until use.

5.2.7. Schiff staining of cellulose scaffolds

To label the cellulose cell walls, decellularized samples were rinsed with water and incubated in 1% periodic acid (Sigma-Aldrich) for 40 minutes at room temperature. Samples were then rinsed with water and incubated in Schiff reagent (100 mM sodium metabisulphite and 0.15 N HCl) along with 100 mg/mL propidium iodide (Invitrogen) for 2 hours. The samples were then washed with PBS and imaged with a multiphoton microscope.

5.2.8. Cell seeding and culture in cellulose scaffolds

A cell seeding protocol for all samples was used as follows: 5×10^5 cells were seeded into scaffolds in 60 μ L droplets of media and incubated for 6 hours. Then, growth media was gradually added to the well to limit disruption to the cell layer and submerge the samples. GFP-3T3s were seeded into unfrozen scaffolds and grown for 3 days in growth media, then imaged with a multiphoton microscope. 5×10^5 C2C12s were seeded into frozen and unfrozen scaffolds. After 2 weeks in 10% FBS-containing growth media, the samples were switched to differentiated media containing either 2% horse serum or 2% horse serum with 1 ng/mL TGF-B1 for one week. Samples were harvested, stained with myosin heavy chain antibody, and imaged with a multiphoton microscope, as described previously.

5.2.9. Porcine myogenesis on fibroblast and myofibroblast feeder layers

Porcine fibroblasts were seeded into a 12 well plate and grown in FGM to complete confluency. Two of the samples were grown in FGM supplemented with 1 ng/mL TGFB for myofibroblast differentiation. After 3 days in culture, porcine myoblasts were seeded to the feeder layers at concentrations of 5×10^3 /cm², 10×10^3 /cm², or 20×10^3 /cm² onto fibroblast feeder layers (FibMyo) or 5×10^3 /cm² and 10×10^3 /cm² onto myofibroblast feeder layers (MyoMyo). Cultures were incubated in DM for 3 days, then underwent immunostaining.

5.2.10. Fusion index assay for differentiating myoblasts

Separate DAPI and myosin heavy chain images were obtained of differentiated skeletal muscle cells seeded onto fibroblast or myofibroblast feeder layers. Images were processed in image J. Briefly, total nuclei were counted per sample by creating a binary image, using a watershed function to split up nuclei clusters into individual nuclei, and measuring nuclei counted by analyzing particles. Then, the myosin heavy chain image was converted to a binary image, the myosin and DAPI images were overlaid, and the nuclei overlapping myotubes were deleted. A final nuclei count was performed and the fusion index was obtained using the equation:

$$F = (\# \text{ of nuclei within multinucleated myotubes} / \text{total} \# \text{ of nuclei per field of view}) \times 100$$

Fusion indices were averaged for each group. N=5 images for each sample.

5.2.11. Statistics

Statistical analyses were performed with two-tailed unpaired *t*-tests and one-way ANOVAs using GraphPad Prism (Version 4; GraphPad Software) and statistical significance was defined as $p < 0.05$. Means are reported with standard error bars in bar graphs. Skew coefficients were calculated in Excel (Version 14.6.4; Microsoft).

5.3. Results

5.3.1. Fibroblast to myofibroblast differentiation is observed in 2D cultures treated with TGF- β 1, regardless of myoblast presence

2D fibroblast-only cultures displayed increased α -SMA staining in TGF- β 1-treated samples (Figs. 5.2 A, B) and increased α -SMA gene expression ($p < 0.01$, Fig. 5.3 A), indicating their differentiation to myofibroblasts. There was no significant difference in collagen 1 transcription between any 2D conditions containing fibroblasts or myofibroblasts (Fig. 5.3. B), but post-translational control of the protein differed with TGF- β 1 treatment. Fibroblasts in the control group were spindle-shaped and displayed smaller areas of procollagen signal per cell nuclei (Figs. 5.2 C, I), while TGF- β 1 treatment significantly increased the area of procollagen staining per nuclei by 32.2 % ($p < 0.0001$, Fig. 5.2 D, I) and enhanced the secretion of

procollagen out of the cell (red arrow in 2D). Nuclei circularity was also increased in 2D FibTGF β samples ($p < 0.0001$, Fig. 5.2. J), indicating a widening of the nucleoskeleton accompanying increased cell spreading, compared to the more elongated nuclear shape in control conditions. Enhanced cell proliferation was also observed with TGF- β 1 treatment ($p < 0.0001$, Fig. 5.2. K), as recorded by average number of nuclei per field of view. α -SMA gene expression in 2D CoCon samples was similar to transcript levels of the fibroblast-only control group, but was significantly upregulated in 2D CoTGF β conditions ($p < 0.01$, Fig. 5.3A).

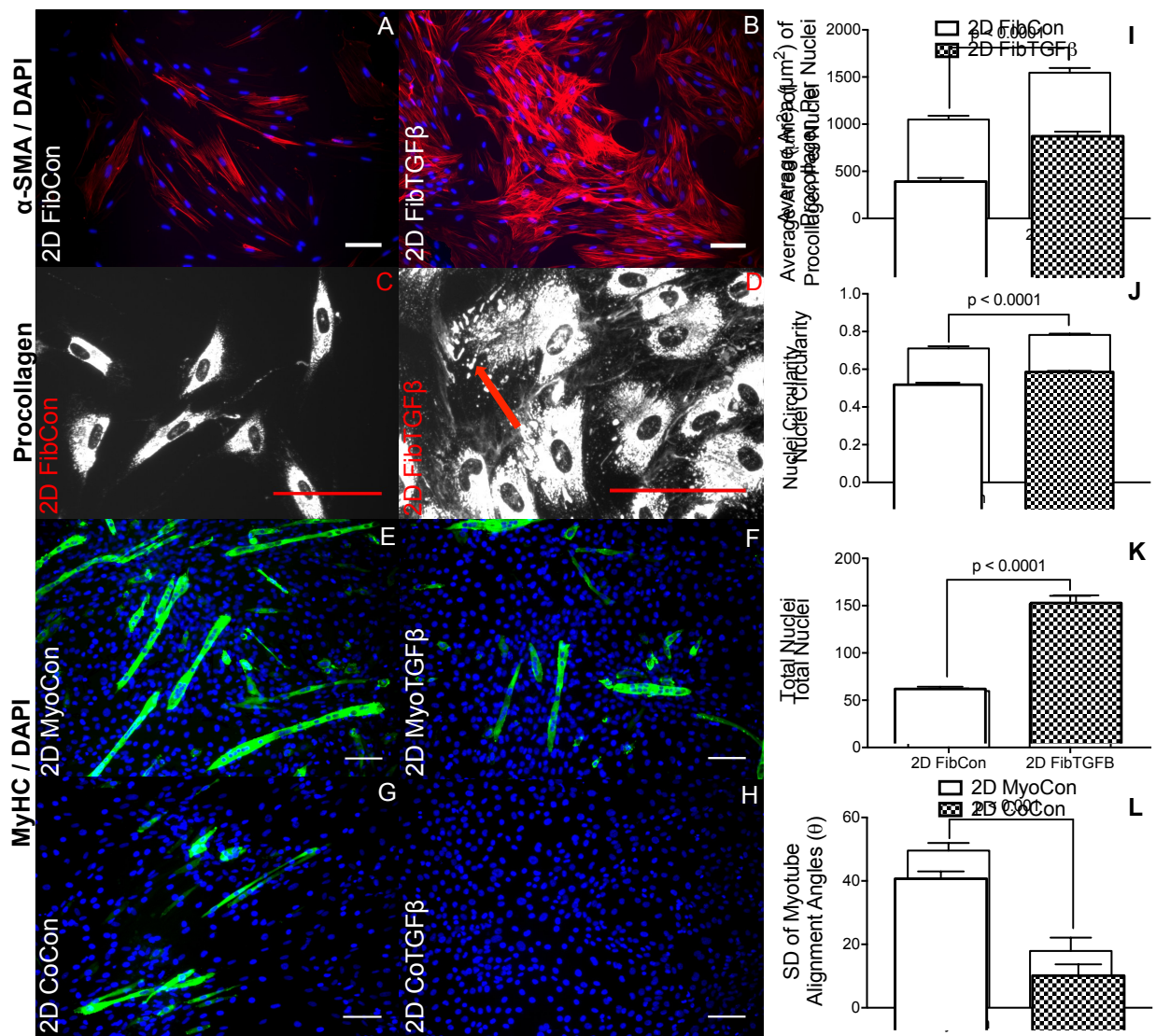


Figure 5.2. Immunostaining and morphological characterization of 2D cultures. 2D FibCon (A) and

FibTGF β (B) stained for α -SMA and DAPI, and FibCon (C) and FibTGF β (D) stained for procollagen. 2D MyoCon (E), MyoTGF β (F), CoCon (G), and CoTGF β (H) conditions stained for myosin heavy chain (MyHC) and DAPI. Scale bars = 100 μ m for all images. Quantitative analysis of average area of procollagen signal/average number of nuclei per field of view (I), nuclei circularity (J), and average number of total nuclei per field of view (K) in FibCon and FibTGF β samples. Quantitative analysis of myotube alignment (L) in MyoCon and CoCon cultures, reported as the standard deviation of myotube alignment angles. Graphs display group averages with standard error bars.

5.3.2. Myogenesis is suppressed in 2D cultures with TGF- β 1 supplementation and in the presence of fibroblasts and myofibroblasts, yet fibroblasts increase myotube alignment

Robust myotube formation was present in 2D MyoCon samples (Fig. 5.2. E), decreased with exposure to TGF- β 1 (Fig. 5.2. F) or in co-culture with fibroblasts (Fig. 5.2. G), and completely inhibited in myofibroblast co-cultures supplemented with TGF- β 1 (Fig. 5.2. H). MYOG gene expression in the 2D MyoTGF β and 2D CoCon conditions were similar to each other and both displayed significant MYOG downregulation in comparison to 2D MyoCon. 2D co-cultures exposed to TGF- β 1 showed the lowest MYOG expression of any group ($p < 0.01$, Fig. 5.3. C). Despite diminishing myogenesis, fibroblasts organized myotube formation by increasing their alignment in 2D CoCon samples ($p < 0.001$, Fig. 5.2. L).

5.3.3. In comparison to fibroblasts grown on plastic, self-assembled tissues containing only fibroblasts have a suppressed ability to assume a myofibroblast phenotype

In comparison to 2D fibroblast-only controls, expression of procollagen was dramatically downregulated in fibroblast-only tissues, and this was not improved by TGF- β 1 exposure ($p < 0.01$, Fig. 5.3. B). 3D FibCon and FibTGF β α -SMA gene expression was transcriptionally downregulated to an even greater degree than procollagen, yet these values were not significantly different from each other ($p < 0.01$, Fig. 5.3. A). Fibroblast/myofibroblast-only tissues were quite fragile; they would easily rupture during handling (arrow, Fig. 5.4. D) and would sometimes collapse, losing their annular shape (Fig. 5.4. C, F). The average thickness of constructs containing myofibroblasts treated with TGF- β 1 was 33.2% larger than respective controls ($p < 0.01$, Fig. 5.5. F), similar to the myofibroblast hypertrophy seen in 2D FibTGF β .

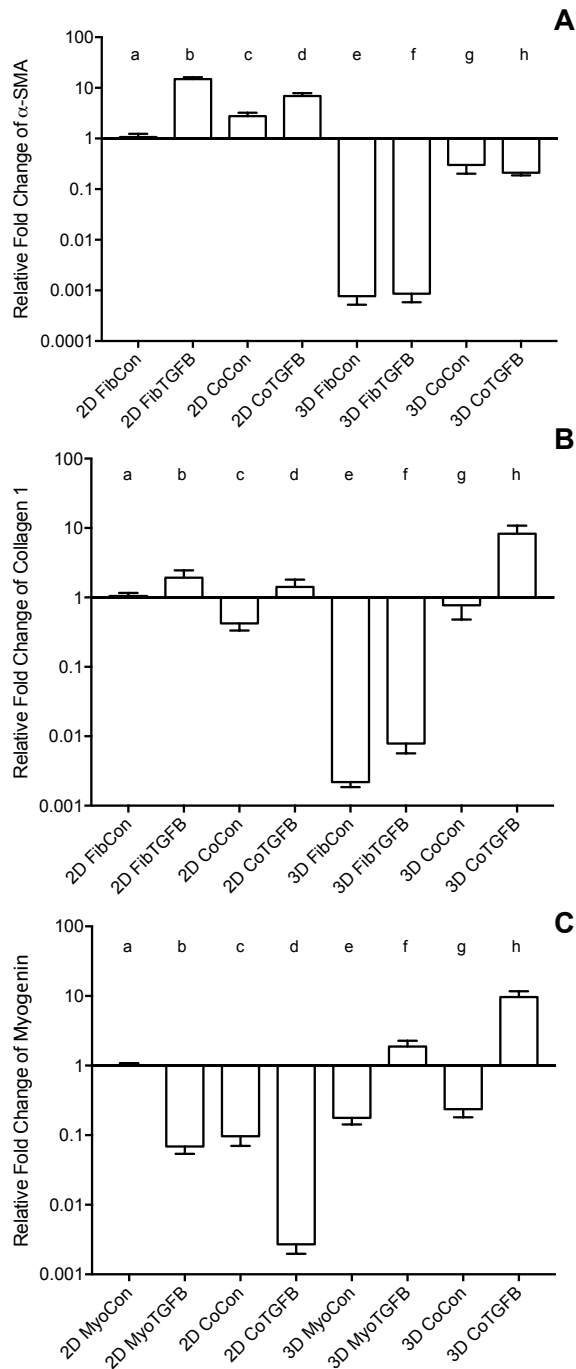


Figure 5.3. Gene expression of fibroblast collagen 1 and α -SMA and myoblast myogenin in 2D cell cultures and 3D self-assembled tissue conditions. Species-specific gene expression for all groups is normalized to gene expression for group (a), 2D FibCon or MyoCon samples. Average fold change values are reported with standard error bars. Significance values were defined at $p < 0.01$. (A) α -SMA: (a)

is significantly different from (b), (d), (e), (f), (g), and (h); (b) is significantly different from (c), (e), (f), (g), and (h); (c) is significantly different from (e), (f), (g), and (h); (d) is significantly different from (e), (f), (g), and (h); (e) is significantly different from (g) and (h); and (f) is significantly different from (g) and (h). (B) COL1: (a) is significantly different from (e), (f), and (h); (b) is significantly different from (c), (e), (f), and (h); (c) is significantly different from (e), (f), and (h); (d) is significantly different from (e), (f), and (h); (e) is significantly different from (g) and (h); (f) is significantly different from (g) and (h); and (g) is significantly different from (h). (C) MYOG: (a) is significantly different from (b), (c), (d), (e), (g), and (h); (b) is significantly different from (d), (f), (g), and (h); (c) is significantly different from (d), (f), and (h); (d) is significantly different from (e), (f), (g), and (h); (e) is significantly different from (f) and (h); (f) is significantly different from (g) and (h); and (g) is significantly different from (h).

5.3.4. TGF- β 1 supplementation improves myoblast differentiation and alignment in myoblast-only self-assembled tissues

3D myoblast-only groups differed in their degree of myogenesis and their myotube formation patterns. 3D MyoCon contained myotubes that had some degree of organization but generally weren't aligned (Fig. 5.6. A, B), whereas myoblast samples treated with TGF- β 1 had myotubes that were aligned along their circumferential axis (white filled arrow, Fig. 5.6. E, F). Gene expression profiles indicated that 3D MyoCon samples had significantly lower myogenin expression than both the 2D MyoCon control and 3D MyoTGF β condition ($p < 0.01$, Fig. 5.3. C), but the 2D control and 3D TGF β treated condition were not significantly different from each other. α -SMA was present in both untreated (Fig. 5.6. C, D) and TGF- β 1 treated (Fig. 5.6. G, H) myoblast constructs. Observable in the α -SMA stained sections are fissures and breaks in the tissue (white asterisks, Fig. 5.6. C, G). Additionally, the surfaces of myoblast-only tissues presented nodular syncytium of fused myoblasts lacking the anchorage necessary to elongate and form myotubes (arrow, Fig. 5.6. I, K), and this was macroscopically observable (unfilled arrows, Fig. 5.4. T). Heterogeneous tissue patterning is also seen here, with many ripples along the tissue surface, large buds (filled arrow, Fig. 5.4. T), and regions of varying density.

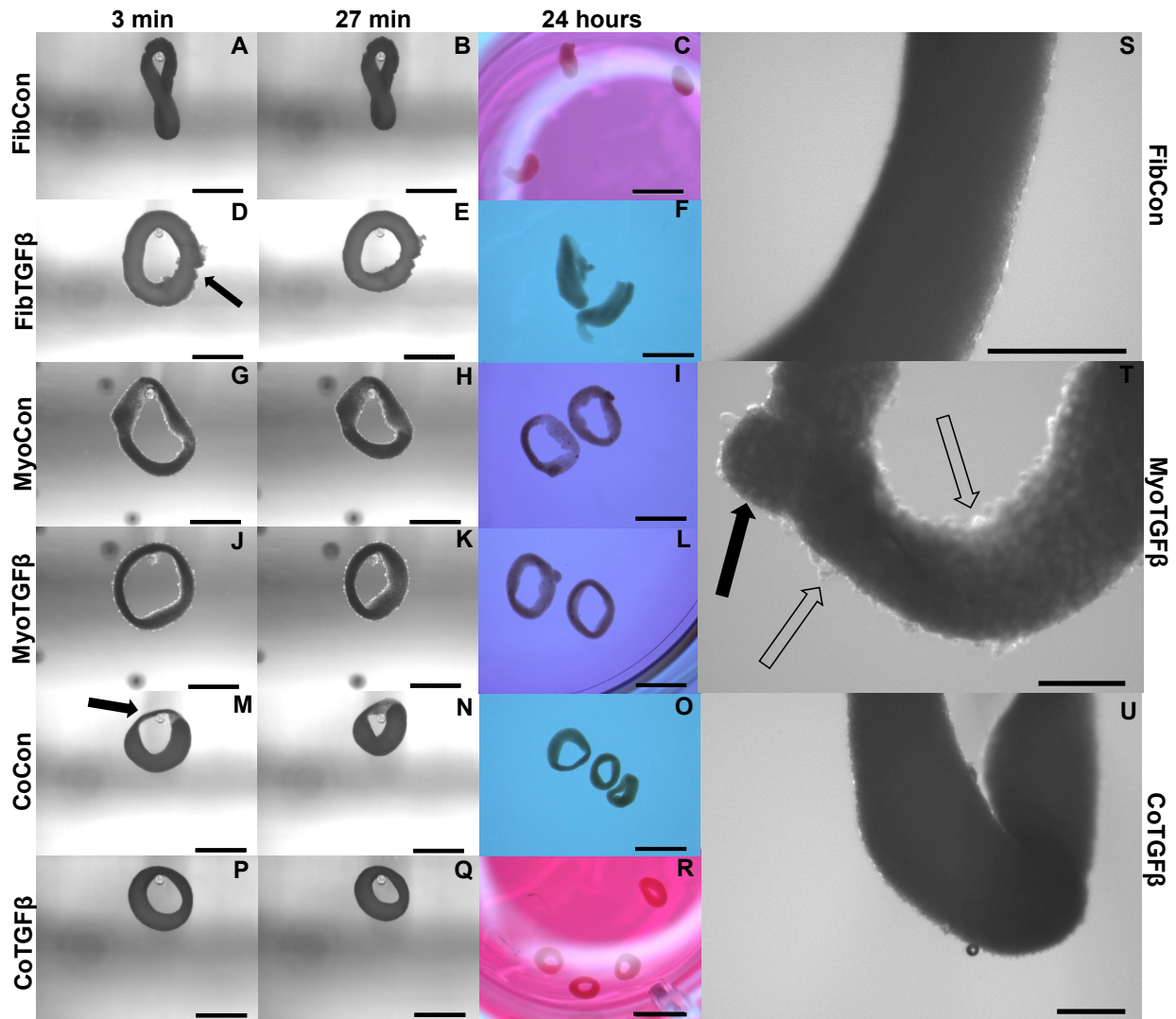


Figure 5.4. Zero force shortening of self-assembled tissues and their surface characteristics.

Tissue shortening was assessed when removed from agarose molds after 3 min, 27 min, and 24 h. 3D FibCon (A–C), FibTGF β (D–F), MyoCon (G–I), MyoTGF β (J–L), CoCon (M–O), and CoTGF β tissue rings (P–R), with scale bars = 1,000 μm . The filled arrow in (D) indicates a structural rupture in the tissue, and the black arrow in (M) indicates thinned myoblast-free region of sample. Higher magnification images of FibCon (S), MyoTGF β (T), and CoTGF β tissues (U) show surface texture. In (T), the filled arrow is a large nodule on a MyoTGF β sample, and unfilled arrows indicate smaller syncytium; scale bars = 300 μm .

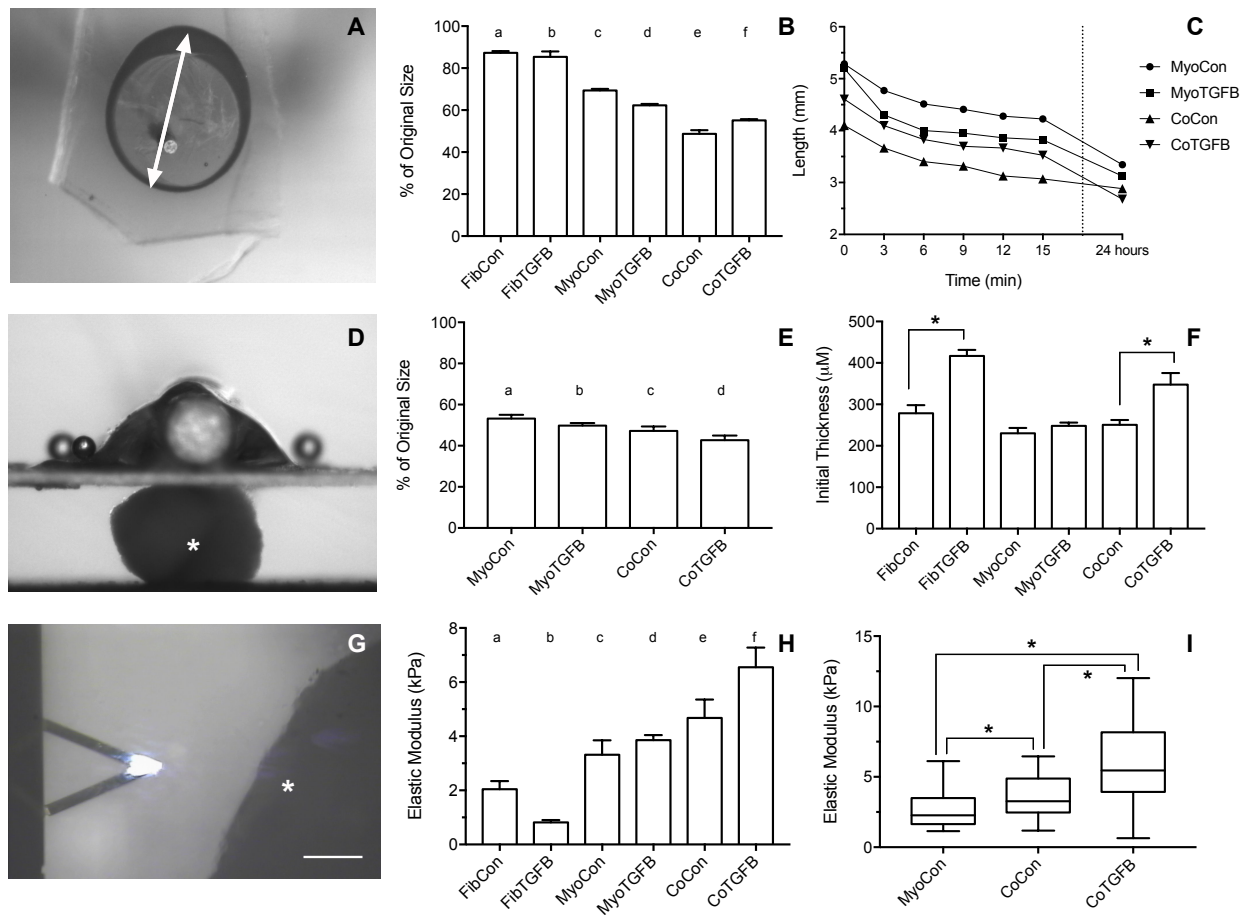


Figure 5.5. Biomechanical and elastic properties of 3D tissue constructs. (A) An agarose gel mold with central post and tissue of tissue skewered onto a microbeam from the Microsquisher system. The white arrow denotes the longest axis of the tissue constructs used to track slacking from initial length in the whole tissue slack test, scale bar = 1,000 μm . (B) Percent (%) of initial length of the longest axis of tissue samples in the whole tissue slack test 27 min after their removal from agarose gels. All groups shortened from their original size significantly ($p < 0.001$), with significant differences between each group ($p < 0.05$), except for (a) and (b). (C) The shortening length of tissue samples over 3 min intervals in the cleaved tissue slack test. Note the final data point is at 24 hours, and the Y-axis origin is 2 mm. (D) Image of the Microsquisher system used to obtain elastic's modulus of tissue sections (white asterisk); scale bar = 300 μm . (E) Percent (%) of initial length of tissue samples in the cleaved tissue slack test after 24 h. All groups shortened from their original size significantly ($p < 0.001$), with significant differences between

each group ($p < 0.05$), except for (b) and (c). (F) Initial thickness of tissue samples, asterisks indicate $p < 0.001$. (G) Screenshot of AFM cantilever and sample (white asterisk), scale bar = 100 μm . (H) Young's modulus of tissues generated from Microsquisher force-displacement data. (a) is significantly softer than (e) and (f); (b) is significantly softer than (c), (d), (e), and (f); and (c) and (d) are significantly softer than (f), with $p < 0.001$. (I) Young's modulus of MyoCon, CoCon, and CoTGF β tissues calculated by AFM, asterisks indicate $p < 0.01$. Graphs display group averages with standard error bars.

5.3.5. In self-assembled co-cultures, fibroblasts and myofibroblasts homogenize tissue surfaces, myofibroblasts improve myotube formation, and TGF- β 1 enhances myogenesis

Addition of fibroblasts or myofibroblasts smoothed the surface of co-culture tissues (Fig. 5.4. U), similarly to fibroblast- or myofibroblast-only samples, and these constructs lacked the studding of nodular syncytium seen in myoblast-only tissues. Co-culture conditions (Fig. 5.4. M, P) appeared visually denser than their fibroblast- (Fig. 5.4. A, D) and myoblast-only (Fig. 5.4. G, J) counterparts. Similar to the hypertrophy observed in 2D and 3D myofibroblast conditions treated with TGF- β 1, CoTGF β tissues were 27.9% thicker than CoCon ($p < 0.01$, Fig. 5.5. F). While human fibroblast/myofibroblast α -SMA gene expression was decreased in all 3D conditions compared to the 2D FibCon group, it was significantly higher in 3D CoCon and CoTGF β compared to 3D fibroblast-only tissues ($p < 0.01$, Fig. 5.3. A), and co-culture transcription levels were not influenced by TGF- β 1 supplementation. A non-species specific α -SMA antibody was visible within myotubes, where CoCon samples showed α -SMA within punctate and short myotubes (Fig. 5.7. A), while those in CoTGF β tissues were elongated and more mature (Fig. 5.7. C), indicating that TGF- β 1 facilitated the development of bundles of myotubes aligned in parallel. Additionally, collagen 1 expression was increased in 3D co-cultures compared to 3D fibroblast/myofibroblast-only cultures ($p < 0.01$, Fig. 5.3. B), but CoCon constructs were not significantly different from the 2D FibCon condition. Interestingly, collagen 1 gene expression was highest in 3D CoTGF β samples, which was also the condition of highest MYOG expression ($p < 0.01$).

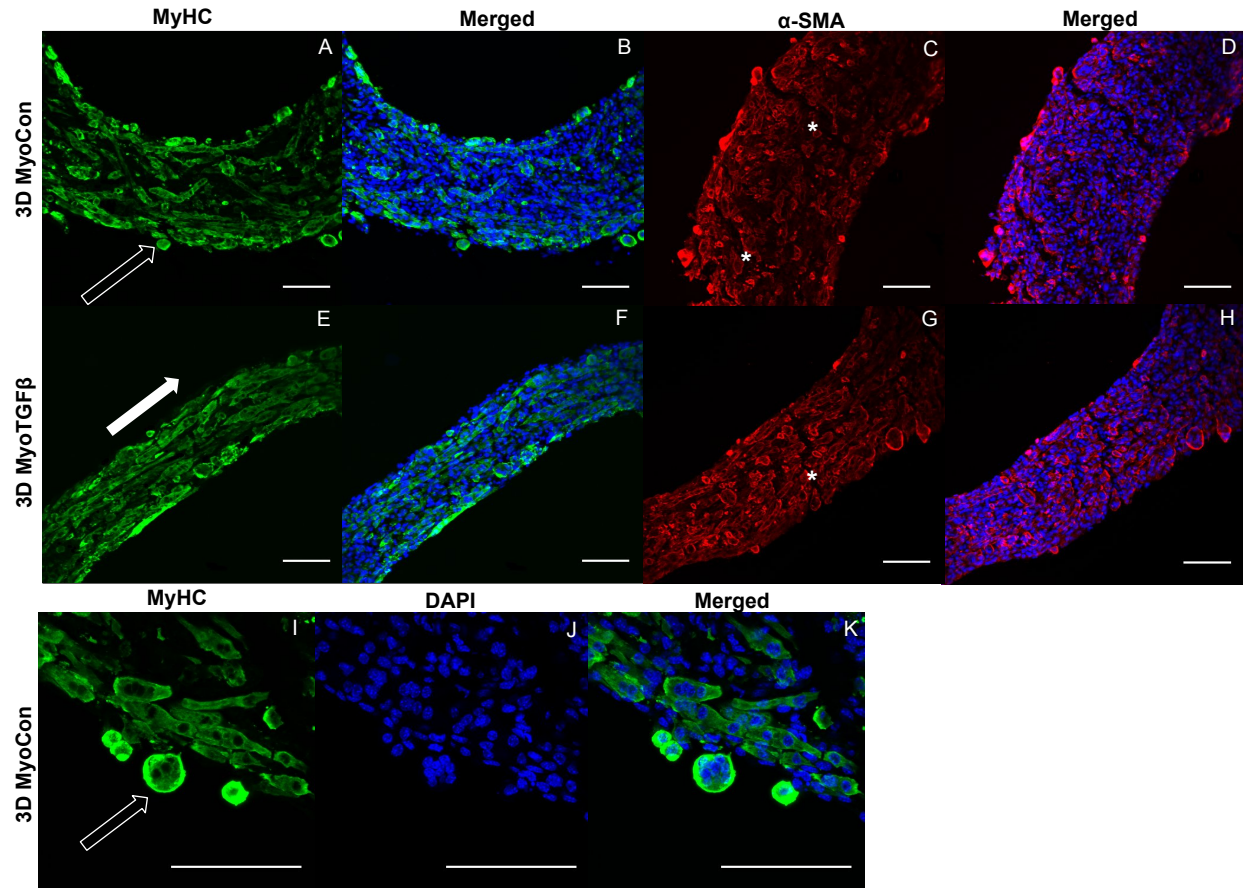


Figure 5.6. Histology of self-assembled myoblast monocultures. 3D MyoCon (A–D, I–K) and MyoTGF β constructs (E–H) are displayed with myosin heavy chain (A, E, I), MyHC merged with DAPI (B, F, K), and DAPI alone (J). α -SMA (C, G) and α -SMA merged with DAPI (D, H). White filled arrows indicate direction of alignment and anisotropy of myotubes (E), while unfilled arrows indicate unanchored syncytium (A, I), and white asterisks identify regions of tissue breakage (C, G), scale bars = 100 μ m.

3D CoCon constructs containing fibroblasts frequently presented dense bulges with thickened regions of cells composed of differentiating myoblasts (Fig. 5.7, E, F) between thinner regions absent of MyHC staining (Fig. 5.7. H, I); this heterogeneous tissue architecture can also be seen macroscopically (arrow, Fig. 5.4. M). CoCon constructs contained myotubes that were short but numerous. Some myotubes fused from one wall of the tissue to another, so that during sectioning, cross sections of myotubes are apparent (filled arrows, Fig. 5.7. E, F). In contrast, CoTGF β samples containing myofibroblasts had

myotubes that were thicker and more multinucleated (Fig. 5.7. G, J, K). These tissues also had many cross-sections of myotubes (filled arrow, Fig. 5.7. J), but additionally contained much longer circumferentially aligned myotubes than in control co-culture samples (unfilled arrow, Fig. 5.7. G). MYOG expression in 3D CoTGF β constructs was significantly higher than all other groups ($p < 0.01$, Fig. 5.3. C), while MYOG

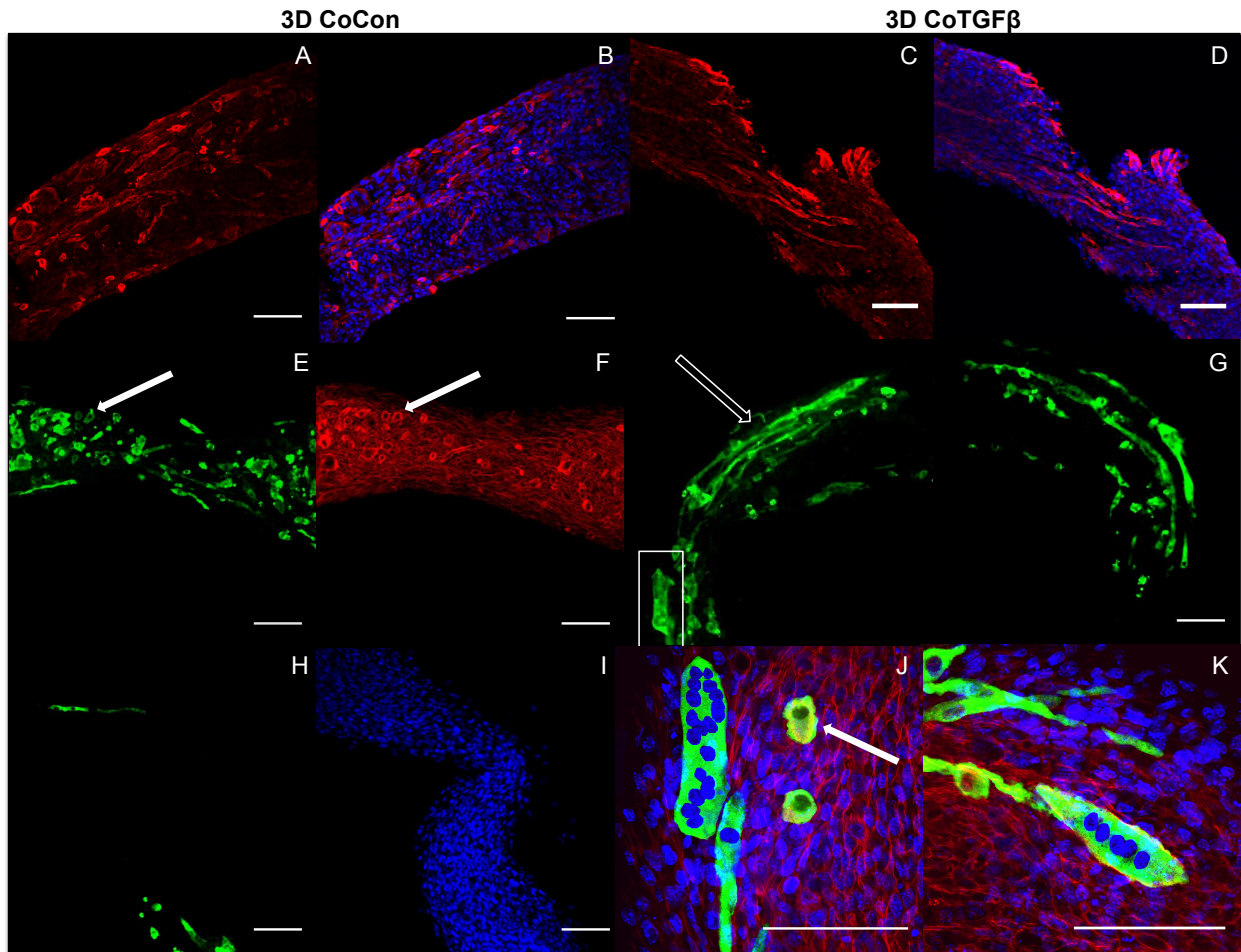


Figure 5.7. Histology of self-assembled co-cultures. 3D CoCon (A, B, E, F, H, I) and CoTGF β tissues (C, D, G, J, K). α -SMA (A, C) and α -SMA merged with DAPI (B, D). Myosin heavy chain staining of CoCon constructs (E, H), f-actin staining of E (F), and DAPI staining of H (I). MyHC staining of CoTGF β tissues (G, J, K) with DAPI and f-actin staining (J, K). (J) is an inset of G. White arrows indicate cross sections of myotubes observed with MyHC and actin staining, while unfilled arrows show elongated myotubes fused along circumferential axis of tissue rings, scale bar = 100 μ m.

expression in 3D CoCon constructs was suppressed compared to 2D MyoCon ($p < 0.01$), and was not significantly different from 3D MyoCon. This data demonstrates that addition of fibroblasts with myoblasts in 3D co-culture does not improve myogenesis beyond what is observed in cultures consisting solely of myoblasts, and TGF- β 1 supplementation is a myogenesis-promoting factor.

5.3.6. Zero-force velocity is greatest in co-culture with TGF- β 1 supplementation in slack tests

Slack tests are a measurement of zero force velocity tissue shortening resulting from the recoil of stretched elastic elements and myofibrillar filament sliding in sarcomeres. Slack tests assess acto-myosin kinetics that are independent of Ca²⁺ activation, which provides biomechanical information about extracellular matrix networking, MHC isoform and muscle fiber type, and muscle organ characteristics^{145, 146, 147}. In whole tissue slack tests, the initial maximum lengths of self-assembled tissue constructs were recorded prior to removal from their posts (white arrow, Fig. 5.5. A). Constructs were then released from tension (Fig. 5.4. A, D, G, J, M, P), their lengths measured after 27 min (Fig. 5.4. B, E, H, K, N, Q), and allowed to slack over 24 h (Fig. 5.4. C, F, I, L, O, R). While all groups shortened significantly from their original size after 27 min ($p < 0.001$, Fig. 5.5. B), tissues containing only fibroblasts or myofibroblasts shortened the least, with 3D FibCon remaining 87.3% and FibTGF β 85.4% their original size. Fibroblast/myofibroblast tissues were the only cell-content matched tissue group that did not display significantly different final length values due to TGF- β 1 treatment. Myoblast tissues underwent significantly greater shortening than fibroblast/myofibroblast samples: MyoCon rings shrank to 69.4% and MyoTGF β to 62.2% their initial diameter. Co-culture tissues underwent the greatest alteration, however. CoCon samples had the most significant shortening compared to all other groups (48.7%), and CoTGF β was the second most shortened group (55.1%). Interestingly, after 24 h, CoTGF β tissues (Fig. 5.4. R) showed a greater degree of sample shortening than CoCon (Fig. 4.4. O).

Since reference points for tracking changes in length were not conserved overnight in ring-shaped tissues, a cleaved tissue slack test was performed by cutting tissues containing C2C12s into linear constructs and plotting slacking lengths over time (Fig. 5.5. C). Most of the length shortening occurred within the first 3 min and slowed considerably by 9 min, with co-culture samples displaying the highest velocities. After 24 h, 3D MyoCon samples shortened to 53.2% of their initial length, MyoTGF β to

49.8%, CoCon to 47.2%, and CoTGF β to 42.7% (Fig. 5.5. E). Each experimental group was significantly different from the others ($p < 0.01$), except for MyoTGF β and CoCon. The slack tests demonstrated that while TGF- β 1 exposure for fibroblast-only samples did not lead to significantly more zero-force shortening in comparison to untreated controls, TGF- β 1 positively impacted shortening of myotubes within myoblast-containing tissues, and the interactions between TGF- β 1-treated myofibroblasts and myoblasts promoted the greatest degree of shortening over time.

5.3.7. Tissue elastic moduli increase in co-cultures and with TGF- β 1 exposure

Using the parallel plate compression system, the Young's modulus for sectioned self-assembled tissues was determined to be 2.04 kPa for FibCon, 0.81 kPa for FibTGF β , 3.32 kPa for MyoCon, 3.86 kPa for MyoTGF β , 4.47 kPa for CoCon, and 6.55 kPa for CoTGF β (Fig. 5.5. H). FibCon and FibTGF β tissues were significantly softer than CoCon and CoTGF β ($p < 0.001$). While MyoCon and MyoTGF β were also significantly softer than CoTGF β ($p < 0.001$), TGF- β 1 did not significantly increase stiffness of samples containing only myoblasts. Similarly, while TGF- β 1 treatment increased the stiffness of CoTGF β , it was not a significant increase with respect to CoCon. Consequently, AFM was used to increase the sensitivity of measurements of elasticity at the tissue surface. AFM generated Young's moduli of 2.66 kPa for MyoCon, 3.64 kPa for CoCon, and 6.02 kPa for CoTGF β , with all groups being significantly different from one another ($p < 0.01$, Fig. 5.5. I).

5.3.8. Supplementation with TGF- β 1 and addition of myofibroblasts enhances myogenesis in collagen 1-based hydrogels

MyoCon, MyoTGF β , CoCon, and CoTGF β hydrogels were imaged for myosin heavy chain. In the myoblast control condition lacking TGF- β 1 supplementation, some MyHC was present in unfused mononuclear cells, but observable myotube formation was absent (Fig. 5.8. A). In contrast, TGF- β 1-treated myoblast hydrogels showed robust myotube formation, with somewhat inconsistent alignment orientations (Fig. 5.8. B). Without supplementation with TGF- β 1, co-cultures with fibroblasts and myoblasts showed small and immature myotube-shaped cells (Fig. 5.8. C), in contrast to its TGF- β 1-treated counterpart containing myofibroblasts (Fig. 5.8. D). CoTGF β hydrogels yielded the thickest and

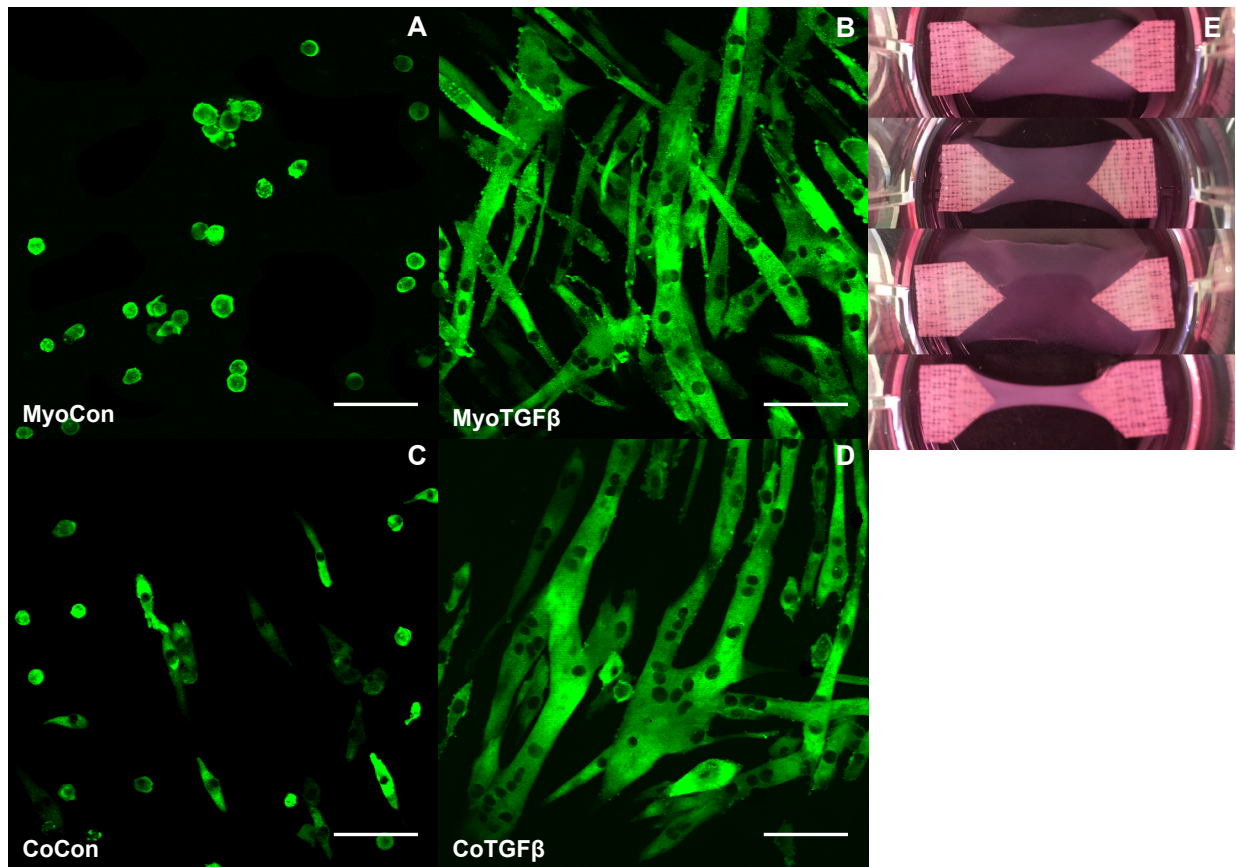


Figure 5.8. Histology of mono- and co-cultures in collagen 1-based hydrogels. Myosin heavy chain staining of MyoCon (A), MyoTGFβ (B), CoCon (C), and CoTGFβ (D) hydrogels. Scale bar = 100 μm. (E) are images of the hydrogels from culture wells of a 6-well plate, in descending order: MyoCon, MyoTGFβ, CoCon, and CoTGFβ hydrogels.

longest muscle fibers of any condition and possessed the highest degree of multinucleation. These muscle fibers also demonstrated the best alignment. CoTGFβ hydrogels were also more visibly contracted in their culture wells than other conditions (Fig. 5.8. E), although MyoTGFβ hydrogels displayed a lesser degree of contraction. Contraction of MyoCon and CoCon hydrogels was not observed.

5.3.9. Porcine tissues undergo myogenesis, but are unstable in long term tissue culture

Self-assembled and hydrogel-based tissues containing porcine myoblasts and myofibroblasts underwent myogenesis as evident by myosin heavy chain expression after 48 hours in culture (Fig. 5.9. A). After 24

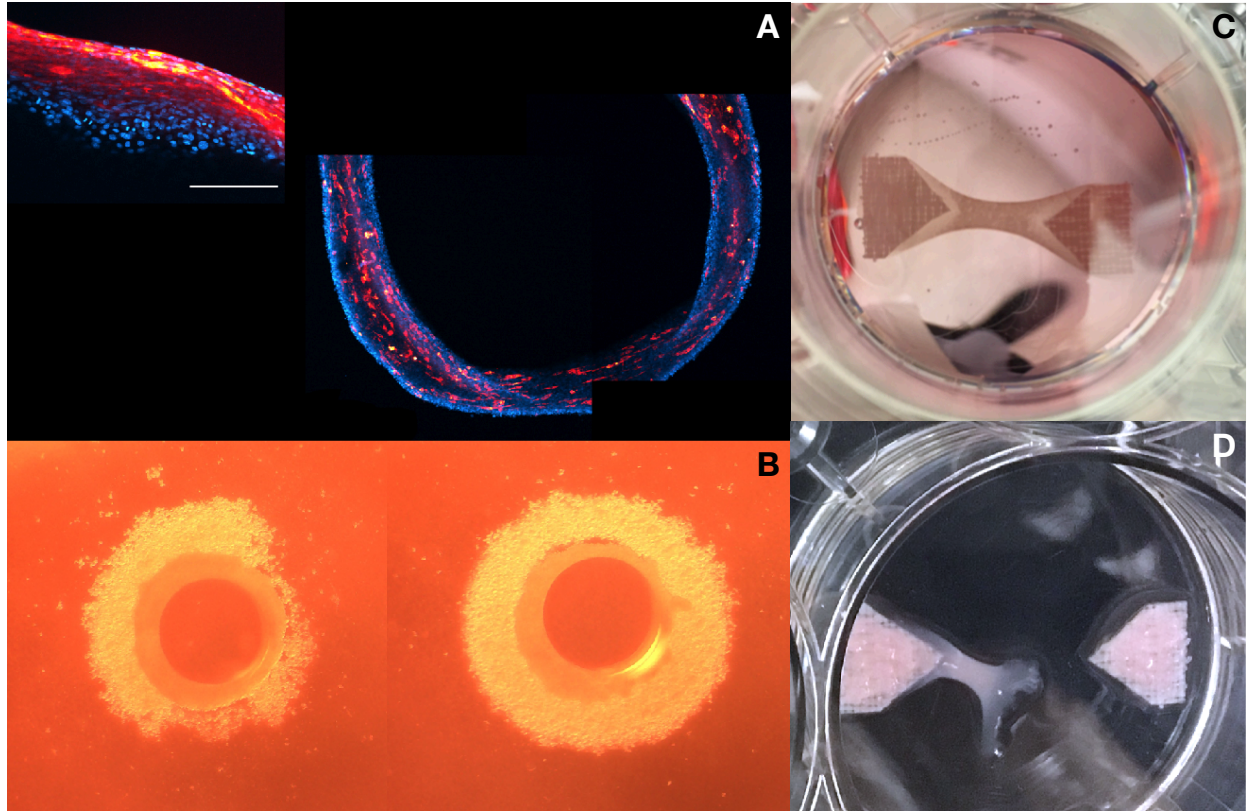


Figure 5.9. Histology and integrity of self-assembled and hydrogel-based porcine tissue. Myosin heavy chain and DAPI staining of porcine myotubes in self-assembled tissue (A), photographs of self-assembled tissue after 24 hours (B), photographs of hydrogel-based porcine tissues after 24 (C) and 48 hours (D). Scale bar = 100 μ m.

hours of self-assembly, tissues showed poor integration (Fig. 5.9. B), where many cells were lost during synthesis. Self-assembled tissues would contract or fall apart post 48 hours. In hydrogel conditions, constructs remained intact after 24 hours but underwent dramatic remodeling, increasing the tension of the hydrogel on the Velcro anchors until samples contracted off the Velcro (Fig. 5.9. C, D).

5.3.10. Freezing celery prior to decellularization creates a more flexible scaffold

Cellulose scaffolds were investigated for usefulness in cell-based meat. Freezing scaffolds created ice crystals that pierced cell membranes and cell walls, disrupting the overall structure of the cellulose (Figure

5.10A). This softened the celery tissue and allowed capillary forces to draw dye throughout the entire tissue section (Figure 5.10B). Multiphoton imaging was used to create 3D reconstructions of the cellulose to investigate microscopic structure. The unfrozen scaffold remained rigid and structurally defined, maintaining usual shape, while the frozen scaffold showed a collapse of the rigid structure, becoming rippled and flexible (Figure 5.10C, D). Cross sectional views of the frozen and unfrozen samples (Figure 5.10E, F) supported the loss of structural rigidity in frozen celery scaffolds.

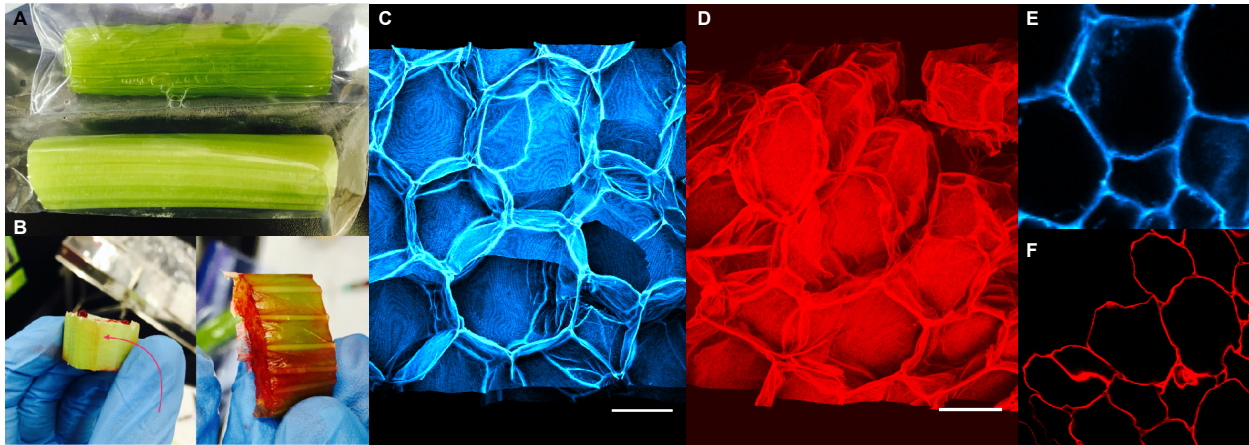


Figure 5.10. Frozen and unfrozen celery scaffold structures. (A) Prior to decellularization, samples were either frozen overnight at -20°C (top sample) or chilled at 4°C (bottom sample). Frozen samples were soft to the touch during subsequent handling, while unfrozen samples remained stiff. (B) Perfusion of Congo red dye was enhanced by freezing samples (right panel). 3D reconstructions of decellularized cellulose samples was visualized with a Schiff stain with unfrozen (C) and frozen (D) samples. Cross-sectional view of cellulose scaffold in unfrozen (E) and frozen samples (F). Scale bar = $100\mu\text{m}$.

5.3.11. Cellulose surface properties result in poor cell adhesion and promote cell aggregation of 3T3s and C2C12 cells on scaffold surfaces

At a seeding density of 5×10^5 , 3T3s and C2C12s had a higher adhesion affinity for other cells than the scaffold and cell aggregates would develop. GFP expression in 3T3s was visualized on a cellulose scaffold after 3 days in culture, indicating that cells had poor adhesion and spreading after 3 days (Figure 5.11A). C2C12s would form visible myogenic tissue aggregates on the scaffolds $\sim 1\text{mm}$ in diameter in 12

well plates (Figure 5.11B, green arrow) and showed cell migration into the interior of the cellulose after 3 weeks (Figure 5.11C). Myosin heavy chain staining indicated robust differentiation of C2C12s. Myotubes that migrate down into the cellulose anchor the aggregate to the scaffold. The formation of tissue aggregates prohibited even cell seeding throughout the scaffolds, and migration was mostly confined around the aggregate. In a rotated view of a 3D construction of myotubes, myotubes tended to form in the concave angles inside the cellulose tube and form bridges through fusion (left, Figure 5.11D, white arrows).

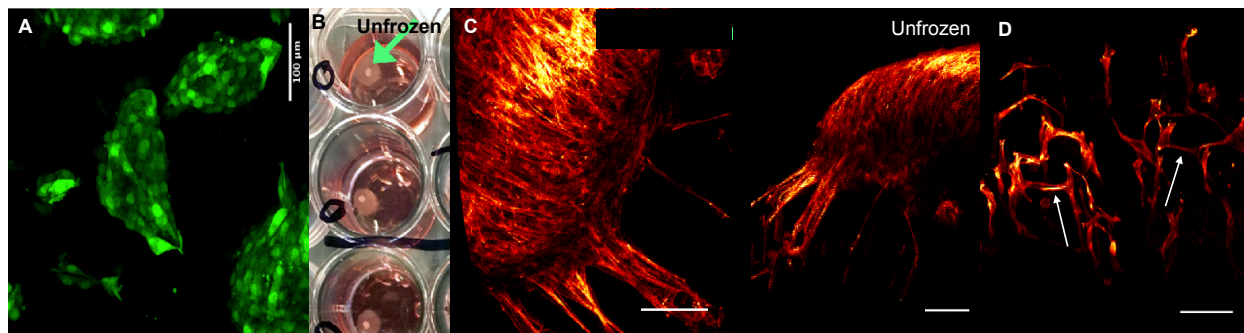


Figure 5.11. 3T3 and C2C12 seeding into unfrozen and frozen cellulose scaffolds. (A) GFP expressing 3T3s imaged 3 days after seeding into decellularized cellulose scaffold. (B-C) are differentiated C2C12s after 2 weeks in growth medium and 1 week in differentiation medium in frozen and unfrozen scaffolds. (B) Photograph of cellulose scaffolds with C2C12 tissue aggregate 3 weeks post seeding. (C) A C2C12 tissue aggregate from top and side views showing myotubes extending down into the scaffold, stained with myosin heavy chain. (D) Myotube fusion patterns in cellulose channels. Scale bars = 100μm.

5.3.12. Freezing scaffolds prior to cell seeding and treatment with TGF-B1 improve myogenesis of C2C12s

In comparison to the untreated control group, TGF-B1 treatment during differentiation enhanced networking of myotubes by improving fusion rates (Figure 5.12A-F). TGF-B1 treatment also increased the length, frequency, and depth penetration of myotubes (Figure 5.12G). Frozen scaffolds yielded myotubes that formed along a more flexible substrate than the unfrozen control, and thus presented different

morphology. Freezing scaffolds improved cell adhesion, cell spreading, and myotube fusion at the surface of the substrate. However, this also decreased the capacity for myotube migration into scaffold depths.

5.3.13. Porcine myofibroblast feeder layers improve adhesion and myogenic differentiation of myoblasts

All porcine cultures underwent myogenic differentiation after 3 days producing myosin heavy chain positive myocytes (Figure 5.13A). The cellular composition of the feeder layer and the number of myoblasts seeded determined the degree of myogenesis for each condition. Fusion indexes (Figure 5.13B) were low for fibroblast feeder layers with myoblasts seeded at 5k / cm² (14.8%) and 10k / cm² (12.6%). When myoblasts were seeded onto fibroblast feeder layers at 20k / cm², the fusion index increased to 23.7% and was significantly elevated compared to the FibMyo 10k / cm² condition. Myofibroblast feeder layers improved cell adhesion and differentiation of myoblasts with respect to equivalent seeding densities in fibroblast feeder layer conditions. The MyoMyo 5k / cm² group had a fusion index of 23.9%, which was significantly increased compared to both FibMyo 10k / cm² and FibMyo 10k / cm² conditions.

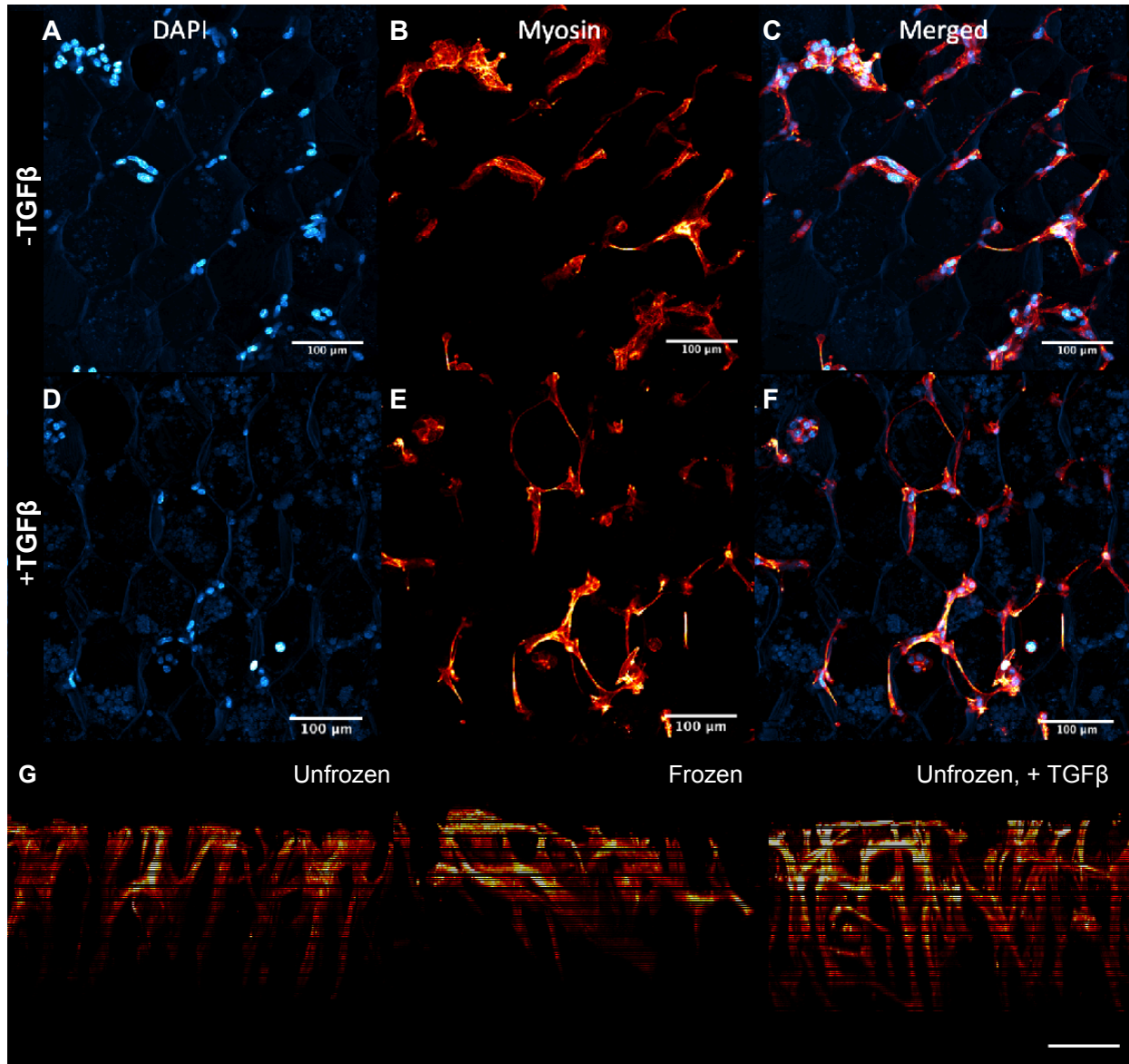


Figure 5.12. Cross sectional view of C2C12 myogenesis with and without TGF β treatment in unfrozen scaffolds. All samples were cultured in growth media for 2 weeks and switched to differentiation media for 1 week. (A-C) was not treated with TGF β , and (D-F) received TGF β treatment. (A, D) shows DAPI stain, (B, E) is myosin heavy chain, and (C, F) are merged channels. (G) Side views of myotube morphology and migration into scaffold depths in unfrozen and frozen scaffolds, with an addition of TGF β supplement in the differentiation media in the righthand image. Scale bars = 100 μ m.

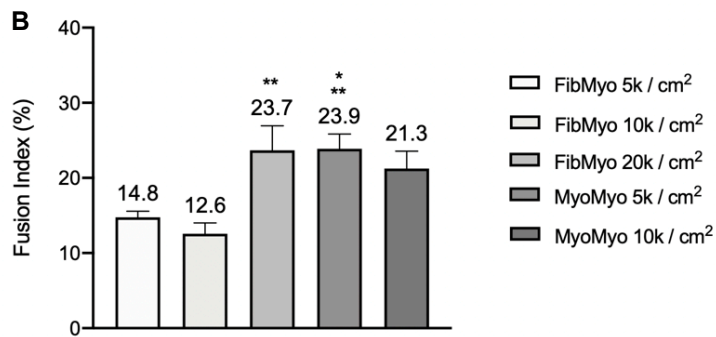
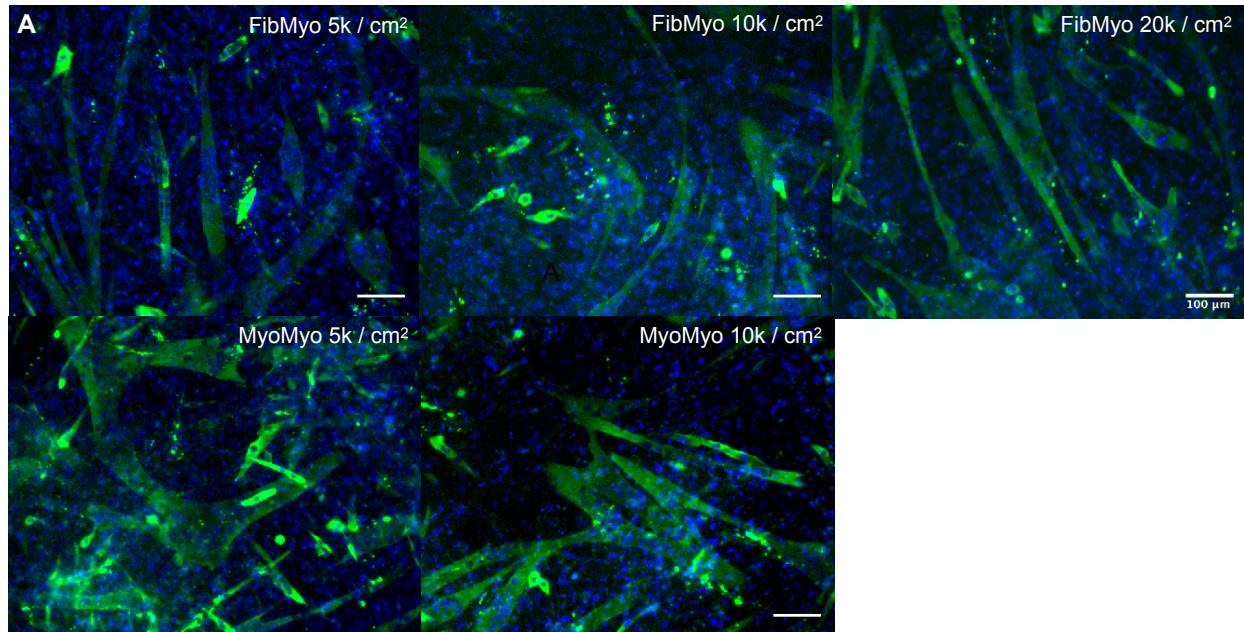


Figure 5.13. Porcine fibroblast and myofibroblast feeder layer cultures with porcine skeletal

muscle cells. (A) Myosin heavy chain and DAPI images of fibroblast feeder layers (top row) and myofibroblast feeder layers (bottom row). Myoblasts were seeded onto feeder layers at concentrations of 5k / cm², 10k / cm², or 20k / cm². Scale bars = 100μm. (B) Fusion index of feeder layer cultures. (*) indicates p < 0.05 statistical significance of samples vs the FibMyo 5k / cm² condition, and (**) indicates p < 0.05 statistical significance from the FibMyo 10k / cm² condition.

5.4. Discussion

Co-culturing myogenic and connective tissue cells can improve meat quality. The robustness of myogenesis influences flavor while connective tissue cells provide ECM to create texture and mouthfeel of meat products. Our results also show that supplementation of growth factors like TGF- β 1 can improve myogenesis in certain culture systems: TGF- β 1 signaling in 3D improves myogenesis in myoblast monocultures and co-cultures with myofibroblasts. In co-cultures, myofibroblasts enhanced muscle differentiation to a greater extent than fibroblasts. Scaffoldless self-assembled tissues and hydrogels containing C2C12s both similarly displayed enhanced myogenesis with inclusion of myofibroblasts and TGF- β 1 treatment, indicating this technique has wide applicability across a variety of 3D platforms. However, 2D experiments demonstrated TGF- β 1-mediated inhibition of myogenesis in both mono- and co-culture conditions. Our data highlights that 2D *in vitro* models of skeletal muscle obscure a complete understanding of cell signaling mechanisms that can enhance myogenesis in other growth platforms, in addition to the usefulness of TGF- β 1 treatment and inclusion of myofibroblasts in improving tissue engineered cultured meat.

The mechanism for TGF- β 1-mediated increases in myogenic differentiation and contractility highlights a differential effect of TGF- β 1 on myofibrillogenesis in 2D and 3D systems. Myofibrillogenesis initiates sarcomere development by increasing the dense packing of contractile and cytoskeletal proteins in muscle cells. During myofibrillogenesis, myofibrils are assembled from the framework of the actin cytoskeleton and undergo maturation by successive incorporation of proteins with increasing contractility. This process is driven by transmitting mechanical tension in the actin cytoskeleton to surrounding ECM through costameres¹⁴⁸ and results in the development and alignment of sarcomeres¹⁴⁹. TGF- β receptor activation increases cytoskeletal polymerization of α -SMA stress fibers in 2D culture platforms¹⁵⁰, but also simultaneously has an inhibiting effect on myogenesis. However, since α -SMA is a precursor protein to sarcomeric actin in myofibrillogenesis, moderate TGF- β 1 levels in 3D may accelerate myofibrillogenesis through an α -SMA-mediated upregulation mechanism that could increase the tensional forces cells exert on their environment.

In 3D, fibroblasts and myofibroblasts benefit muscle regeneration through depositing ECM for force transmission, organizing myoblast differentiation and myotube fusion, and stimulating myofibrillogenesis^{148, 151}. Myotube formation dynamically remodels the biomechanical environment within muscle to further attenuate fibroblast and myofibroblast activity. *In vitro* cell traction studies have shown that C2C12 myotubes exert five to eight times greater traction forces on their substrates than fibroblasts, and these forces increase as myotubes mature¹⁵². Contracting myotubes transmit their forces to surrounding ECM through costameres and exert tensional forces throughout the muscle organ to facilitate contraction¹⁵³. This mechanism of force transmission could explain the greater recoil and shortening capacity co-culture tissues in contrast to myoblast-only samples with a suppressed ability to disperse forces to the surrounding ECM. Lower levels of supportive ECM for myotubes in self-assembled monocultures decreases the availability for integrin connections to the tissue microenvironment and reduces tensional forces applied to surrounding structures, resulting in less elastic recoil after being released from tension. Additionally, our data showing lower elastic moduli in 3D myoblast monocultures than co-cultures is congruent with the findings of Meyer and Lieber, who found the elastic stiffness of skeletal muscle fibers to be significantly dependent on the presence of ECM. In their study, dissected muscle fibers stripped of their extracellular matrix sheaths had four-fold lower elastic moduli than fascicles that retained their ECM¹⁵⁴. The CoTGF β group was approximately half of the native muscle tissue elastic modulus, which could result in very similar meat quality if the sample sizes were scaled.

3D fibroblast and myofibroblast co-cultures were distinct in their morphology, force transmission capacities, and biomechanical properties. The bundling of highly multinucleated myotubes in parallel within CoTGF β constructs was more similar to *in vivo* muscle fascicle morphology than fibroblast co-cultures, and was accompanied by the greatest upregulation in myogenin expression of all groups. Enhanced muscle fiber maturation and patterning likely increased the magnitude of zero-force shortening in CoTGF β samples due to acto-myosin kinetics. Our experiments identify that TGF- β 1 has both individual and synergistic benefits to skeletal muscle engineering. These data show that TGF- β 1 treatment in 3D monocultures of myoblasts boosts myoblast fusion and differentiation. In co-cultures with myoblasts, TGF- β 1 activates fibroblasts to differentiate into myofibroblasts, which are better accelerators

of myogenesis than fibroblasts, due in part to their enhanced ECM synthesis. TGF- β 1 shows promise to drive myogenesis in meat production bioprocesses as a media supplement.

Although the self-assembled CoTGF β model of skeletal muscle achieved structural similarity to muscle fascicles, utilizing this self-assembly strategy for tissue engineering is not practical at scale for whole muscle organs. It can be used for small samples, and the process parameters change greatly when switching from C2C12s to primary porcine skeletal muscle cells. The porcine cells likely exerted higher tensional forces on surrounding cells and the collagen matrix than C2C12s. This increased the complexity of the tissue engineering approach and reduced the viability of these low cost and simple tissue engineering techniques for pork. Microtissues can be formed this way, however, that can possibly be used to enhance differentiation in suspension culture in bioreactors. A self-assembly technique would need to be developed that could be utilized at scale.

Cellulose Scaffolds

Cellulose from celery was used as an edible scaffolding material to grow C2C12s and test feasibility for use in cell-based meat products. Plant-based scaffolds, like other non-animal derived matrix materials, face several challenges to become suitable materials for growing edible cell lines: surface functionalization to promote cell adhesion, optimizing scaffold stiffness (which can impact product mouthfeel as well as cell behavior), and uneven cell seeding density throughout the scaffold. Cell adhesion to the cellulose in these experiments was poor. 3T3s had not yet begun to migrate onto the scaffold after 3 days in culture and showed preference to adhere to other cells compared to the scaffold. C2C12 cells showed a similar response and would form microtissues on top of the scaffold after 24 hours. After 3 weeks of culture C2C12s began to deposit their own ECM onto the substrate, migrate unevenly through the scaffold, and differentiate into multinucleated muscle cells. Other experimenters have used similar time frames of 14⁹⁰ to 28 days^{143, 155}, which is too long to lead to an affordable production process. Using collagen and gelatin can improve the seeding efficiency and adhesion rate to cellulose scaffolds¹⁵⁶, as can fibronectin¹⁵⁷, fibrin⁹⁰, and RGD cell adhesion peptide coatings¹⁵⁵. ECM proteins must be animal-free for usage in cell-based meat products, and recombinant sources are not yet currently scalable in

manufacturing. However, RGDs and similar short peptides can be chemically synthesized cheaply and easily, making them a more cost-effective option for scaffold functionalization.

Different plants have unique cellulose structures that result in stiff cell substrates. The E' modulus of an apple is 4kPa, but the E' of celery is 590 kPa¹⁵⁸. Since muscle stiffness is 12-16kPa¹⁵⁹, the cellulose was softened by overnight freezing prior to decellularization to decrease E' modulus and improve flexibility. The results show that freezing decreased the rigidity of the cellulose and caused a visible increase in scaffold flexibility. This facilitated cell seeding, migration, and differentiation of C2C12s. Interestingly, in the same experiment, TGF- β 1 treatment C2C12s in cellulose scaffolds improved myogenesis, as indicated by myosin heavy chain expression and multi nucleation of myotubes - more evidence that TGF- β 1 can facilitate the growth and development of skeletal muscle in small amounts.

One possible solution to bypass the adhesion limitations of plant-based scaffolds may be to prepare scaffolds with connective tissue cell type feeder layers. Our study tested the efficacy of porcine fibroblast and myofibroblast feeder layers to facilitate myoblast adhesion in the absence of laminin coating. Myofibroblast feeder layers improved adhesion and fusion indices in comparison to fibroblast feeder layers. This is perhaps due to increased collagen secretion in myofibroblasts, and possibly other ECM proteins that facilitated cell adhesion, which was previously demonstrated with collagen staining in 2D FibTGFB hDF cultures. By using myofibroblast feeder layers, less myoblasts are required for cell adhesion and robust differentiation, providing optimized conditions for cell-based meat growth on plant-based scaffolds.

Future directions

True tissue structuring of cell-based meat is will be cost-prohibitive and technologically out of reach for decades and may never end up being necessary as other food structuring technologies mature. However, tissue engineering strategies and principles can be adapted for scale up if the process uses tissue self-assembly (or cell aggregation), cell encapsulation, or microcarriers as platforms for cell growth and differentiation. Cell aggregation is a common phenomenon occurring in suspension bioreactors where cells that come into contact will naturally clump together due to the interaction of cadherins. This research showed that myogenesis could be enhanced in suspension bioreactors where TGF- β 1 is present in the

media. Cell encapsulation is another viable option to design a bioprocess for differentiation due to the existence of cell encapsulation equipment and techniques¹⁶⁰, the current limitations of decellularized plant based scaffolding materials, the reduction of sheer forces that reduce cell viability in cell aggregates¹⁶¹, and the possibility of developing hypoxic cores in cell aggregates¹⁶². Alginate, or alginic acid, is an edible polysaccharide derived from the cell walls of brown algae and can also be produced from microbial culture¹⁶³. Sodium alginate, the sodium salt of alginic acid, is an interesting material for cell encapsulation. Sodium alginate is composed of mannuronic and guluronate blocks, and the guluronate can undergo ionic bonding when exposed to Ca^{2+} to polymerize the alginate into a hydrogel¹⁶⁴. Alginate can be dissolved at the end of a production cycle by rinsing with a chelating agent such as EDTA to remove the Ca^{2+} , which has been approved for food applications¹⁴¹. The cell mass can be collected and used for products.

Alginate lacks functional cell binding motifs, however. Adipose cells can differentiate in encapsulated form without the need to migrate through the hydrogel⁴⁷, but skeletal muscle cells require cell adhesion and migration for differentiation¹⁴⁸. Adipogenesis is promoted on laminin-coated surfaces¹⁶⁵, similar to myogenesis of skeletal muscle cells. Laminin enhances myotube numbers, myotube length, and fusion index more than fibronectin¹⁶⁶. RGD is present in fibronectin, collagen, and laminin proteins. It is the most common binding motif used to functionalize biomaterials with cell adhesion sites. Both laminin and fibronectin are important ECM found in the muscle tissue niche, but the RGD sequence in laminin can be inaccessible to integrins depending on the protein's conformation¹⁶⁷. Ile-Lys-Val-ala-Val (IKVAV) is an alternative peptide sequence derived from the $\alpha 1$ cell binding domain of laminin that can facilitate cell adhesion instead and shows additional potential as a signaling mechanism to promote adipogenesis and myogenesis.

Functionalization of alginate with RGD and IKVAV peptide sequences can be achieved through chemical reactions for cell encapsulation applications¹⁶⁸ to improve cell adhesion, migration, adipogenesis, and myogenesis. In an adipogenesis study on MSCs, adipogenic differentiation was best on RGD:IKVAV (10:90% ratio) functionalized substrates compared to RGD alone, as was indicated by ORO staining, cell morphology change from spindle shape to rounded morphology, and lipoprotein lipase gene expression. However, the presence of RGD was found necessary to promote cell survival on

substrates. Adipocytes increased their expression of $\alpha 6$ integrin, which binds to laminin, during differentiation and began secreting laminin onto the surfaces¹⁶⁹. This creates a positive feedback loop for adipogenesis. RGD:IKVAV peptides also improved cell adhesion and proliferation in muscle cell cultures in a plate-based model¹⁷⁰. Another study found despite RGD improve cell proliferation in peptide functionalized hydrogels, IKVAV functionalization improved myoblast migration and increased satellite cell activation via activating MyoD and Pax7 gene expression¹⁷¹. Accordingly, alginate gel functionalized with IKVAV and RDG peptide sequences has potential to improve adipogenic and myogenic differentiation for cell-based meat applications and provide a cell harvesting mechanism by dissolving alginate with a chelator.

Chapter 6

SUMMARY AND FUTURE STUDY

6.1. Summary

The scope of this work explored principles of cell line development, improving palatability of cell lines, and using tissue engineering strategies for cell-based meat. The research was guided by material considerations relevant to culturing edible cells for commercial products, in contrast to the material restrictions of regenerative medicine therapies. For cell-based meat, food considerations include ensuring materials are food safe, would be acceptable to consumers, and don't need or can receive regulatory approval for use in food. The source of materials should be low cost, animal free, and scalable enough to match demand. Materials should also perform well by having high efficacy, be compatible for use in upstream processes, and should not have unwanted downstream effects.

All cell line development begins with the characteristics of the starting cell population. We outlined cell isolation strategies that can be used to successfully culture bovine and porcine myoblasts and adipoblasts that can be used for further cell line development, although changes should be made in protocols to improve cell performance due to differences in bovine and porcine differentiation. Bovine cells underwent more hypertrophy during myogenesis than porcine cells. This could be due to specific-specific differences, or perhaps the FBS composition of the growth media was better suited for bovine cells and this had a beneficial impact on the differentiation phase. Porcine muscle fibers may naturally produce less biomass than differentiating bovine muscle fibers, which has implications for the bioprocess and cell line requirements for each respective cell type. Porcine adipocytes matured more rapidly than bovine adipocytes, although the population frequency of differentiating cells was much less than in bovine samples. This indicates that different media profiles should be used to enhance maturation in bovine cells and the cell isolation protocol for porcine cells should be tailored to further enrich the isolated population of preadipocytes.

The animal products used in this stage of cell isolation and characterization consist of FBS and mouse laminin. Laminin was used to adhere the myoblasts to cell culture plates, and without it the cells show poor proliferation, migration, and differentiation [data not shown]. While the amounts of these reagents used at this stage is negligible compared to the overall scale up process, alternatives should still be developed, such as recombinant laminin and serum-free cell isolation media. A source of recombinant laminin may be particularly important for scale up of myogenic cells from livestock if there is difficulty incorporating the cells into a bioprocess that requires adhesion for an aspect of the bioprocess. A cheap and scalable recombinant supply of an extracellular matrix component like laminin may not be available for many years.

Improving the sensory properties of myogenic cells was explored in these studies. Palatability and perception of cultivated meat products will determine their success or failure in the market. Products that do not look like meat, such as if they produce an off-color compared to the animal meat product they are simulating, may be rejected by consumers. Additionally, cultivated meat products have to possess noticeably improved flavor over plant-based competitors and have to be likable enough to replace meat from animals in the diets of consumers. Presentation and sensory characteristics should be optimized by identifying which characteristics define an animal meat product and enhance those in the cell-based meat product.

We focused on increasing the expression of a muscle-specific protein, myoglobin, that is known improve meat color and perceived quality. We first characterized cultured cells by their color to demonstrate the need for focusing on myoglobin, where we showed myogenic cells in culture are white in color. Then we identified processes for increasing myoglobin protein through both differentiation of muscle fibers and their electrical stimulation. Undifferentiated cells may be less beneficial for cultured meat products than differentiated cells due to lower myoglobin levels and muscle-specific protein density, which may change flavor as well as pigment. Electrical stimulation was shown to improve myoglobin concentration in the cells, but only when certain vector patterns were applied. Electrical stimulation does not require the use of reagents, although it does require electrodes, a stimulation apparatus, and a power source. Consequently, there would be associated equipment and energy consumption costs.

We also examined a serum-free media replacement for growth and differentiation media using macrophage conditioned media. M0 and M2 CM had comparable proliferation rates to FBS, but also facilitated differentiation. The current CM compositions would need to be modified for growth or differentiation. Media conditioning represents a form of serum free media production that would possibly only require basal media. It may be possible to develop a co-culture model where a spatially segregated population of conditioning cells produces media for edible cells. This could be possible with a fed-batch system, where a small amount of starting media supplemented with growth factors could support cell survival in the beginning phase of cell culture, and as the conditioning cells increase the concentration of growth factors then more basal media could be added.

Conditioning cells can be seeded into porous membranes or encapsulated into hydrogels that have good permeability and diffusion characteristics, such as alginate¹⁶⁰. Porous membranes can retain viable cells for ~15-30 days^{172, 173}. Cell-encapsulated alginate microgels can be produced from microfluidic platforms that use a high throughput production approach to generate highly uniform droplets. This method supports long term cultures of ~15 days^{174, 175}. The typical pore size of alginate hydrogels is dependent on the degree of cationic crosslinking¹⁷⁶, the rate of G-blocks to M-blocks, and the concentration of alginate, but is typically big enough to allow ~650kDa proteins to diffuse out, such as hemoglobin¹⁷⁷. Microgels have been previously used for sustained release of growth factors like TGF- β ¹⁷⁸.

Finally, we assessed the utility of low-cost tissue engineering strategies for cultivated meat using self-assembly, hydrogel-based, and plant-based scaffolding. We found that the techniques themselves face challenges for scale up for tissue engineering, but these techniques could be useful for creating microtissues to facilitate differentiation during a bioprocess. In particular, self-assembly can be used to develop cell aggregates in low agitation rate environments. Agitation rates can be optimized to keep the size of the micro tissues small enough to still be able to diffuse oxygen into the core and prevent hypoxia and necrosis¹⁷⁹. Hydrogel-based approaches to cell encapsulation show promise as long as they use scaffolding materials that are not animal derived, such as recombinant ECM or plant-based components like alginate. Plant-based scaffolds, such as cellulose or TVP, require additional functionalization with synthetic or recombinant cell adhesion peptides to promote cell seeding, proliferation, and differentiation.

6.2 Future study

Cell-based meat products must be assessed according to meat quality standards established by their countries of sale. Many countries view intramuscular fat to be important content in meat, such as Korea, Japan, Australia, and the US. European countries, such as France and Germany, prefers leaner cuts of meat. The USDA establishes meat quality with the US Beef Grading System¹⁸⁰ and the Japanese Meat Grading Association (JMGA) establishes meat quality in Japan¹⁸¹. Both systems assess quality via intramuscular fat percentage, color, and maturity, and the yield of usable meat on the carcass. These systems differ in how they use quality metrics, however. Understanding the differences between these quality evaluation systems is critical for US competition with Japanese exports.

In the JMGA meat scale, the marbling score of the *longissimus* muscle is evaluated at the 6th-7th rib interface, in comparison to the USDA marbling score, which is evaluated at the 12th-13th rib interface¹⁰⁰. The JMGA uses an overall meat quality scale 1-5 based on four meat quality assessments: beef marbling score (BMS); beef color standard (BCS); firmness and texture of meat; and beef fat standard (BFS). The BMS score is an estimate of minimum IMF% and ranks 1-12, with 1 being the least amount of marbling and 12 being the highest degree of marbling (Table 6.1). The meat must be graded at BMS 3 or above to reach the acceptable minimum IMF of wagyu: 21.4%, and a BMS score of 12 contains at least 56.3% IMF¹⁸² (Table 6.2, Figure 6.1A). BCS assesses meat color and brightness using a 1-7 scale, where number 1 is a pale red and number 7 is a dark red. The best BCS is 3 or 4, where color and brightness are most strongly correlated (Table 6.1, Figure 6.1B). The firmness of meat is determined by the amount of exudate on the surface of the cut, and the degree of depression of the indented surface. Meat with high BMS should be firm and have less exudate, since it has higher water holding capacity. The texture reflects a smooth or coarse surface of the cut (Table 6.1). Meat is graded best when it is very firm with a smooth texture. The BFS measures color, luster and quality of fat using a score between 1-7, where 1 is pale white and 7 is dark cream (Table 6.1, Figure 6.1C). The BFS is best between 1-4¹⁸³. After each of the quality scores are evaluated according to the 1-5 scale, the lowest of the scores becomes the overall meat quality score for the beef.

Table 6.1. Japanese and US beef quality scoring metrics.

Japanese Meat Grading Association								
Grade		BMS	BCS	Brightness	Firmness	Texture	BFS	Luster & Quality
5	Excellent	8-12	3-5	Very Good	Very Good	Very Fine	1-4	Excellent
4	Good	5-7	2-6	Good	Good	Fine	1-5	Good
3	Average	3-4	1-6	Average	Average	Average	1-6	Average
2	Bellow Average	2	1-7	Below Average	Below Average	Below Average	1-7	Below Average
1	Poor	1	BCS outside range 1-7		Inferior	Coarse	BFS outside range 1-7	

US Beef Grading System				
Grade	Marbling	Color	Firmness	Age (Months)
Prime	Very abundant - Slightly Abundant	Light cherry red	Moderately firm	9-42
Choice	Moderate - small	Light cherry red - slightly dark red	Slightly soft	9-42
Select	Slight	Moderately light red - moderately dark red	Moderately soft	9-30

Table 6.2. Japanese and US beef quality grades determined by intramuscular fat %.

Japanese Beef ¹⁸²			US Beef ¹⁸⁴		
Grade	BMS	Minimum IMF %(*)	Marbling Grade	USDA Grade	
5	Excellent	12	Abundant	Prime +	
		11			
		10			
		9			
		8			
4	Good	7	Abundant	Prime +	
		6			
		5			
3	Average	4	Abundant	Prime +	
		3			
2	Bellow average	2	Abundant	Prime +	
1	Poor	1	12.3	Moderately Abundant	Prime
			9.9	Slightly Abundant	Prime -
			7.7	Moderate	Choice +
			5.8	Modest	Choice
			4.0	Small	Choice -
			2.3	Slight	Select

The USDA beef standard assesses meat quality through marbling score, meat color, and texture of cuts (which is associated with age) and grades good quality beef into three categories: select, choice, and prime (Table 6.1). Above 21.4% IMF%, marbling is 'very abundant' and graded prime+. Typically, prime US beef has 9.9-12.3% IMF, the marbling is 'moderately abundant' to 'slightly abundant', it's bright red in color, and moderately firm in texture (Table 6.2, Figure 6.1D). Choice beef has a 'moderate' to 'small' amount of marbling (4-7.7% IMF), is light cherry red to slightly dark red in color, and is slightly soft in firmness. Select beef has a 'slight' amount of marbling (2.3-3.9%), moderately light red to moderately dark red color, and a moderately soft texture, since it comes from younger animals on average¹⁸⁴.

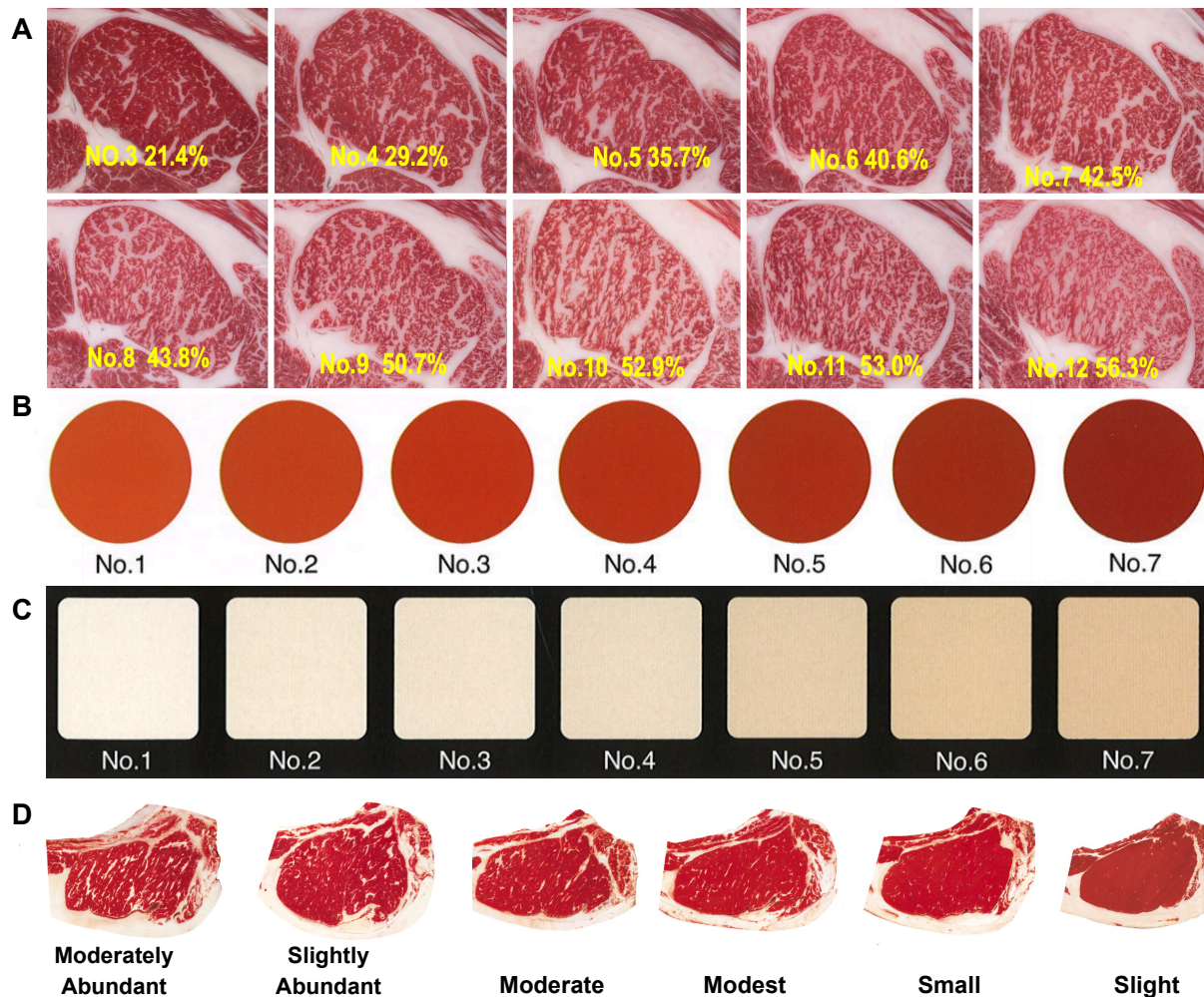


Figure 6.1. Japanese Meat Grading Association and USDA meat quality standards. (A) Official picture standard of BMS (Beef Marbling Standard), (B) BCS (Beef Color Standard), and (C) BFS (Beef

Fat Standard) by the Japan Meat Grading Association¹⁸¹. (D) Official picture standards of the USDA beef grade shield¹⁸⁰.

Wagyu Beef Product Development Strategy

US beef has much lower IMF% than Japanese beef. The average highest prime grade contains ~12% IMF, and the average Wagyu BMS is a minimum of 21.4% IMF. Cell-based meat will give US beef a way to compete with Japanese Wagyu beef global market. Cells for cell-based Wagyu can be sourced from an American Wagyu calf and grown *ex vivo*. The intramuscular fat composition can be simulated by adding 21% or greater adipocytes to the meat product.

Determine target product characteristics: Designing a cell-based Wagyu rib eye steak first requires assessing meat characteristics that influence sensory properties, such as muscle fiber type composition, fatty acid composition, IMF%, and chemical composition of the *longissimus thoracis*. The average IMF of the thoracic muscle is 31.5% and the muscle fiber ratio is 34.3% type I fibers and 48.0% type 2B fibers⁹⁸. The fatty acid composition of the top 5 FFAs are 50.0% 18:1, 26.1% 16:0, 10.4% 18:0, 4.0% 16:1, and 2.8% of 14:0¹⁰⁰. The chemical composition consists of 22% crude protein, 31% crude fat, and 47% moisture.

Design bioprocess to meet product characteristics: The cell isolation, cell line development strategy, culture process, and product formulation would be determined by the previous characteristics. First, skeletal muscle and preadipocytes could be isolation from the *longissimus thoracis* muscle of a Wagyu calf. These two cell lines would undergo development to increase mitotic capacity for scale up. The skeletal muscle cells would be grown in single cell suspension for scale up, then undergo a differentiation step. The cells would first undergo cell aggregation into micro tissues with low agitation rates inside the vessel. Then after sufficient tissue synthesis (below ~300um in thickness, the O₂ diffusion limitation), differentiation media would be supplemented to the culture and an electrical stimulation regimen would begin. Differentiation would increase myoglobin, myosin heavy chain, and other myogenic protein

expression by muscle fibers. The electrical stimulation would switch the muscle fibers from primarily type 2B to having ~30% type I fibers. This would improve myoglobin and protein levels to a similar state to the *longissimus*.

Preadipocytes would be grown in single cell suspension and differentiated with an adipogenic differentiation media to activate PPAR γ expression, which would mature the cells into adipocytes. 18:1, 16:0, 18:0, 16:1, and 14:0 FFAs would be supplemented in the culture media at rates that reflect the fatty acid composition of the muscle. If the adipocytes uptake each FFA at the same rate then a MUSA:SFA ratio be obtained. This ratio, and the fatty acid composition, will improve tenderness, flavor, palatability, and fat melting in cooked meat.

Production formulation: The product formulation would require recreating the chemical composition of the *longissimus thoracis*. Adipocytes and skeletal muscle cells could be grown to volumes that could yield a 2:3 ratio of skeletal muscles to fat cells. Cultured cells would not need to compose the entire 22% of crude protein and 31% of crude fat, since plant-based ingredients can add bulk and texture. However, since IMF is the hallmark of Wagyu beef, cell-based products would be held up to the JMGA standard of BMS, and require higher % of crude fat. Then, the cells and plant-based ingredient can be blended and hydrated to optimize the moisture content closer to 47%. A food printer can then be used to print the skeletal muscle blend with a network of intramuscular fat.

Market Entry: In 2016, Japan exported 504,384 tons of Wagyu beef primarily to Hong Kong, Cambodia, USA, Singapore, and Thailand, where Japanese Wagyu is sold at higher prices, and imported around 62% of its beef requirement¹⁸⁵. Since Wagyu is a premium product, there is a lower burden on cell-based meat production to reach price parity compared to commodity beef. US companies could export American Wagyu to Japan and other countries, and sell cell-based Wagyu within US at a cheaper price than Japanese Wagyu. Previously this would not have been possible due to the need to rely on using entire animals and being subject to their genetics. This is just one example of how cell-based meat technology will be a disrupting force on the future economy.

REFERENCES

1. Krieger, J. *et al.* Producing Food Products from Cultured Animal Tissues. (2020).
2. Friedrich, B. Cultivated Meat: Why GFI Is Embracing New Language. (2019).
3. Specht, E. A., Welch, D. R., Rees Clayton, E. M. & Lagally, C. D. Opportunities for applying biomedical production and manufacturing methods to the development of the clean meat industry. *Biochemical Engineering Journal* **132**, 161–168 (2018).
4. Purdy, C. The idea for lab-grown meat was born in a prisoner-of-war camp. *qz.com* <https://qz.com/1077183/the-idea-for-lab-grown-meat-was-born-in-a-prisoner-of-war-camp/> (2017).
5. Van Eelen, W. F. Industrial production of meat using cell culture methods. (2007).
6. Benjaminson, M. A., Gilchrist, J. A. & Lorenz, M. In vitro edible muscle protein production system (mpps): stage 1, fish. *Acta Astronautica* **51**, 879–889 (2002).
7. Edelman, P. D., McFarland, D. C., Mironov, V. A. & Matheny, J. G. Commentary: In Vitro -Cultured Meat Production. *Tissue Engineering* **11**, 659–662 (2005).
8. PETA's 'In Vitro' Chicken Contest. <https://www.peta.org/features/vitro-meat-contest/>.
9. Kupferschmidt, K. Lab Burger Adds Sizzle to Bid for Research Funds. *Science* **341**, 602–603 (2013).
10. Singer, P. *Animal Liberation*. (Harper Collins, 1975).
11. Taylor, L. H., Latham, S. M. & Woolhouse, M. E. J. Risk factors for human disease emergence. *Phil. Trans. R. Soc. Lond. B* **356**, 983–989 (2001).
12. Riedel, S. Edward Jenner and the History of Smallpox and Vaccination. *Baylor University Medical Center Proceedings* **18**, 21–25 (2005).
13. Barry, J. M. The site of origin of the 1918 influenza pandemic and its public health implications. *J Transl Med* **2**, 3 (2004).
14. H5N1 Influenza Virus Vaccine, manufactured by Sanofi Pasteur, Inc. Questions and Answers. *FDA.gov* <https://www.fda.gov/vaccines-blood-biologics/vaccines/h5n1-influenza-virus-vaccine-manufactured-sanofi-pasteur-inc-questions-and-answers> (2018).
15. General Information about 2009 H1N1 Vaccines. *cdc.gov* <https://www.cdc.gov/h1n1flu/vaccination/general.htm>.

16. Luo, V., Junqing, X. & Feng, C. Ten years after SARS: where was the virus from? *J Thorac Dis* **5**, S163–S167 (2013).
17. Andersen, K. G., Rambaut, A., Lipkin, W. I., Holmes, E. C. & Garry, R. F. The proximal origin of SARS-CoV-2. *Nat Med* **26**, 450–452 (2020).
18. Zhang, T., Wu, Q. & Zhang, Z. Probable Pangolin Origin of SARS-CoV-2 Associated with the COVID-19 Outbreak. *Current Biology* **30**, 1346-1351.e2 (2020).
19. Landers, T. F., Cohen, B., Wittum, T. E. & Larson, E. L. A Review of Antibiotic Use in Food Animals: Perspective, Policy, and Potential. *Public Health Rep* **127**, 4–22 (2012).
20. ANTIBIOTIC RESISTANCE THREATS in the United States. (2013).
21. Engberg, J. Quinolone and Macrolide Resistance in *Campylobacter jejuni* and *C. coli*: Resistance Mechanisms and Trends in Human Isolates. *Emerg. Infect. Dis.* **7**, 24–34 (2001).
22. New Animal Drugs and New Animal Drug Combination Products Administered in or on Medicated Feed or Drinking Water of Food Producing Animals: Recommendations for Drug Sponsors for Voluntarily Aligning Product Use Conditions with GFI #209.
23. IPCC. Climate Change 2014 Synthesis Report. Contribution of Working Groups I, II and III to the Fifth Assessment Report of the Intergovernmental Panel on Climate Change. (2014).
24. The World Bank. Turn Down the Heat: Why a 4°C Warmer World Must be Avoided. A Report for the World Bank by the Potsdam Institute for Climate Impact Research and Climate Analytics. (2012).
25. Food and Agriculture Organization of the United Nations. Tackling Climate Change through Livestock: A global assessment of emissions and mitigation opportunities. (2013).
26. Environmental Protection Agency. Inventory of U.S. Greenhouse Gas Emissions and Sinks: 1990–2016.
27. Harwatt, H., Ripple, W. J., Chaudhary, A., Betts, M. G. & Hayek, M. N. Scientists call for renewed Paris pledges to transform agriculture. *The Lancet Planetary Health* **4**, e9–e10 (2020).
28. Griscom, B. W. *et al.* Natural climate solutions. *Proc Natl Acad Sci USA* **114**, 11645–11650 (2017).
29. The Bonne Challenge. <https://www.bonnchallenge.org/>.
30. Poore, J. & Nemecek, T. Reducing food’s environmental impacts through producers and consumers. *Science* **360**, 987–992 (2018).

31. Simsa, R. *et al.* Extracellular Heme Proteins Influence Bovine Myosatellite Cell Proliferation and the Color of Cell-Based Meat. *Foods* **8**, 521 (2019).
32. Langelaan, M. L. P. *et al.* Meet the new meat: tissue engineered skeletal muscle. *Trends in Food Science & Technology* **21**, 59–66 (2010).
33. Araujo de Vizcarrondo, C., Carrillo de Padilla, F. & Martín, E. Fatty acid composition of beef, pork, and poultry fresh cuts, and some of their processed products. *Archivos Latinoamericanos De Nutricion* **48**, 354–358 (1998).
34. Mourot, J. & Hermier, D. Lipids in monogastric animal meat. *Reprod. Nutr. Dev.* **41**, 109–118 (2001).
35. Jakab, K. *et al.* Tissue engineering by self-assembly and bio-printing of living cells. *Biofabrication* **2**, 022001 (2010).
36. Campuzano, S. & Pelling, A. E. Scaffolds for 3D Cell Culture and Cellular Agriculture Applications Derived from Non-animal Sources. *Front. Sustain. Food Syst.* **3**, 38 (2019).
37. Koffler, J. *et al.* Improved vascular organization enhances functional integration of engineered skeletal muscle grafts. *Proceedings of the National Academy of Sciences* **108**, 14789–14794 (2011).
38. DiLoreto, R. & Murphy, C. T. The cell biology of aging. *MBoC* **26**, 4524–4531 (2015).
39. Shay, J. W. & Wright, W. E. Hayflick, his limit, and cellular ageing. *Nat Rev Mol Cell Biol* **1**, 72–76 (2000).
40. Genovese, N. J., Domeier, T. L., Telugu, B. P. V. L. & Roberts, R. M. Enhanced Development of Skeletal Myotubes from Porcine Induced Pluripotent Stem Cells. *Sci Rep* **7**, 41833 (2017).
41. Tanaka, A. *et al.* Efficient and Reproducible Myogenic Differentiation from Human iPS Cells: Prospects for Modeling Miyoshi Myopathy In Vitro. *PLoS ONE* **8**, e61540 (2013).
42. Zheng, J. K. *et al.* Skeletal myogenesis by human embryonic stem cells. *Cell Res* **16**, 713–722 (2006).
43. Irfan Maqsood, M., Matin, M. M., Bahrami, A. R. & Ghasroldasht, M. M. Immortality of cell lines: challenges and advantages of establishment: Immortality of cell lines. *Cell Biol Int* **37**, 1038–1045 (2013).
44. Post, M. J. Cultured meat from stem cells: Challenges and prospects. *Meat Science* **92**, 297–301 (2012).

45. Le Grand, F. & Rudnicki, M. A. Skeletal muscle satellite cells and adult myogenesis. *Curr Opin Cell Biol* **19**, 628–633 (2007).
46. Agley, C. C., Rowleson, A. M., Velloso, C. P., Lazarus, N. R. & Harridge, S. D. R. Human skeletal muscle fibroblasts, but not myogenic cells, readily undergo adipogenic differentiation. *J Cell Sci* **126**, 5610–5625 (2013).
47. Mehta, F., Theunissen, R. & Post, M. J. Adipogenesis from Bovine Precursors. *Methods Mol Biol* **1889**, 111–125 (2019).
48. Krieger, J., Park, B.-W., Lambert, C. R. & Malcuit, C. 3D skeletal muscle fascicle engineering is improved with TGF- β 1 treatment of myogenic cells and their co-culture with myofibroblasts. *PeerJ* **6**, e4939 (2018).
49. Iida, F., Saitou, K., Kawamura, T., Yamaguchi, S. & Nishimura, T. Effect of fat content on sensory characteristics of marbled beef from Japanese Black steers. *Anim Sci J* **86**, 707–715 (2015).
50. Tedesco, F. S., Dellavalle, A., Diaz-Manera, J., Messina, G. & Cossu, G. Repairing skeletal muscle: regenerative potential of skeletal muscle stem cells. *J. Clin. Invest.* **120**, 11–19 (2010).
51. American Meat Science Association. Meat color measurement guidelines. (2012).
52. Myhre, J. L. & Pilgrim, D. B. At the Start of the Sarcomere: A Previously Unrecognized Role for Myosin Chaperones and Associated Proteins during Early Myofibrillogenesis. *Biochemistry Research International* **2012**, 1–16 (2012).
53. Miller, K. J., Thaloor, D., Matteson, S. & Pavlath, G. K. Hepatocyte growth factor affects satellite cell activation and differentiation in regenerating skeletal muscle. *American Journal of Physiology-Cell Physiology* **278**, C174–C181 (2000).
54. Kästner, S., Elias, M. C., Rivera, A. J. & Yablonka-Reuveni, Z. Gene Expression Patterns of the Fibroblast Growth Factors and Their Receptors During Myogenesis of Rat Satellite Cells. *J Histochem Cytochem.* **48**, 1079–1096 (2000).
55. Christov, C. *et al.* Muscle Satellite Cells and Endothelial Cells: Close Neighbors and Privileged Partners. *MBoC* **18**, 1397–1409 (2007).
56. Engert, J. C., Berglund, E. B. & Rosenthal, N. Proliferation precedes differentiation in IGF-I-stimulated myogenesis. *J Cell Biol* **135**, 431–440 (1996).

57. Kurek, J. B. *et al.* The role of leukemia inhibitory factor in skeletal muscle regeneration. *Muscle Nerve* **20**, 815–822 (1997).
58. Kami, K. & Senba, E. Localization of leukemia inhibitory factor and interleukin-6 messenger ribonucleic acids in regenerating rat skeletal muscle. *Muscle Nerve* **21**, 819–822 (1998).
59. Langelan, M. L. P. *et al.* Advanced maturation by electrical stimulation: Differences in response between C2C12 and primary muscle progenitor cells. *J Tissue Eng Regen Med* **5**, 529–539 (2011).
60. Murphy, M. M., Lawson, J. A., Mathew, S. J., Hutcheson, D. A. & Kardon, G. Satellite cells, connective tissue fibroblasts and their interactions are crucial for muscle regeneration. *Development* **138**, 3625–3637 (2011).
61. Sandbo, N. & Dulin, N. Actin cytoskeleton in myofibroblast differentiation: Ultrastructure defining form and driving function. *Translational Research* **158**, 181–196 (2011).
62. Sanes, J. R. The basement membrane/basal lamina of skeletal muscle. *J Biol Chem* **278**, 12601–12604 (2003).
63. Karalaki, M., Fili, S., Philippou, A. & Koutsilieris, M. Muscle regeneration: cellular and molecular events. *In Vivo* **23**, 779–796 (2009).
64. Mendias, C. L. *et al.* Transforming growth factor-beta induces skeletal muscle atrophy and fibrosis through the induction of atrogin-1 and scleraxis: TGF- β Induces Atrogin-1 and Scleraxis. *Muscle Nerve* **45**, 55–59 (2012).
65. Kovalik, J.-P. *et al.* Metabolic Remodeling of Human Skeletal Myocytes by Cocultured Adipocytes Depends on the Lipolytic State of the System. *Diabetes* **60**, 1882–1893 (2011).
66. Kersten, S. Mechanisms of nutritional and hormonal regulation of lipogenesis. *EMBO Rep* **2**, 282–286 (2001).
67. Rosen, E. D., Walkey, C. J., Puigserver, P. & Spiegelman, B. M. Transcriptional regulation of adipogenesis. *Genes & Development* **14**, 1293–1307 (2000).
68. Hellerstein, M. K. De novo lipogenesis in humans: metabolic and regulatory aspects. *European Journal of Clinical Nutrition* **53 Suppl 1**, S53-65 (1999).
69. Nye, C., Kim, J., Kalhan, S. C. & Hanson, R. W. Reassessing triglyceride synthesis in adipose tissue. *Trends in Endocrinology & Metabolism* **19**, 356–361 (2008).

70. Tyagi, S., Sharma, S., Gupta, P., Saini, A. & Kaushal, C. The peroxisome proliferator-activated receptor: A family of nuclear receptors role in various diseases. *J Adv Pharm Tech Res* **2**, 236 (2011).
71. Barish, G. D. PPAR : a dagger in the heart of the metabolic syndrome. *Journal of Clinical Investigation* **116**, 590–597 (2006).
72. Seo, K., Suzuki, T., Kobayashi, K. & Nishimura, T. Adipocytes suppress differentiation of muscle cells in a co-culture system. *Anim Sci J* **90**, 423–434 (2019).
73. Chung, K. Y. & Johnson, B. J. Melengestrol acetate enhances adipogenic gene expression in cultured muscle-derived cells. *Journal of Animal Science* **87**, 3897–3904 (2009).
74. Pearce, J. Fatty acid synthesis in liver and adipose tissue. *Proc. Nutr. Soc.* **42**, 263–271 (1983).
75. Villacorta, L., Schopfer, F. J., Zhang, J., Freeman, B. A. & Chen, Y. E. PPAR γ and its ligands: therapeutic implications in cardiovascular disease. *Clinical Science* **116**, 205–218 (2009).
76. Allan, S. J., De Bank, P. A. & Ellis, M. J. Bioprocess Design Considerations for Cultured Meat Production With a Focus on the Expansion Bioreactor. *Front. Sustain. Food Syst.* **3**, 44 (2019).
77. Barbano, D. M. & Rasmussen, R. R. Cheese Yield Performance of Fermentation-Produced Chymosin and Other Milk Coagulants. *Journal of Dairy Science* **75**, 1–12 (1992).
78. Sung, B., Krieger, J., Yu, B. & Kim, M. Colloidal gelatin microgels with tunable elasticity support the viability and differentiation of mesenchymal stem cells under pro-inflammatory conditions. *J. Biomed. Mater. Res.* **106**, 2753–2761 (2018).
79. Verbruggen, S., Luining, D., van Essen, A. & Post, M. J. Bovine myoblast cell production in a microcarriers-based system. *Cytotechnology* **70**, 503–512 (2018).
80. Ben-Arye, T. & Levenberg, S. Tissue Engineering for Clean Meat Production. *Front. Sustain. Food Syst.* **3**, 46 (2019).
81. Kang, H.-W. *et al.* A 3D bioprinting system to produce human-scale tissue constructs with structural integrity. *Nat Biotechnol* **34**, 312–319 (2016).
82. Levenberg, S. *et al.* Engineering vascularized skeletal muscle tissue. *Nat Biotechnol* **23**, 879–884 (2005).

83. Lieber, R. L. & Ward, S. R. Cellular Mechanisms of Tissue Fibrosis. 4. Structural and functional consequences of skeletal muscle fibrosis. *American Journal of Physiology-Cell Physiology* **305**, C241–C252 (2013).
84. Mann, C. J. *et al.* Aberrant repair and fibrosis development in skeletal muscle. *Skeletal Muscle* **1**, 21 (2011).
85. Leprince, P., Popov, A. F., Simon, A. R., Benk, C. & Siepe, M. *Ex vivo* perfusion of the heart with the use of the Organ Care System. *Eur J Cardiothorac Surg* **49**, 1318–1320 (2016).
86. Davis, B. N., Yen, R., Prasad, V. & Truskey, G. A. Oxygen consumption in human, tissue-engineered myobundles during basal and electrical stimulation conditions. *APL Bioeng* **3**, 026103 (2019).
87. Kačarević, Ž. P. *et al.* An Introduction to 3D Bioprinting: Possibilities, Challenges and Future Aspects. *Materials (Basel)* **11**, (2018).
88. Forgacs, G. Tissue engineering: Perfusable vascular networks. *Nat Mater* **11**, 746–747 (2012).
89. Ding, S. *et al.* Maintaining bovine satellite cells stemness through p38 pathway. *Sci Rep* **8**, 10808 (2018).
90. Ben-Arye, T. *et al.* Textured soy protein scaffolds enable the generation of three-dimensional bovine skeletal muscle tissue for cell-based meat. *Nat Food* **1**, 210–220 (2020).
91. MacQueen, L. A. *et al.* Muscle tissue engineering in fibrous gelatin: implications for meat analogs. *npj Sci Food* **3**, 20 (2019).
92. Suman, S. P. & Joseph, P. Myoglobin Chemistry and Meat Color. *Annu. Rev. Food Sci. Technol.* **4**, 79–99 (2013).
93. King, D. A. *et al.* Contribution of genetic influences to animal-to-animal variation in myoglobin content and beef lean color stability¹. *Journal of Animal Science* **88**, 1160–1167 (2010).
94. Brooks, M. A. *et al.* CASE STUDY: Carcass and meat characteristics and M. longissimus thoracis histology of beef from calf-fed and yearling-fed Angus steers¹. *The Professional Animal Scientist* **27**, 385–393 (2011).
95. Giller, K. *et al.* Meat and carcass quality of Dexter cattle compared with that of suckler, Charolais-cross calves: a preliminary study. *Anim. Prod. Sci.* **59**, 986 (2019).

96. Rusman, Soeparno, Setiyono & Suzuki, A. Characteristics of Biceps femoris and Longissimus thoracis muscles of five cattle breeds grown in a feedlot system. *Animal Science Journal* **74**, 59–65 (2003).
97. Greenwood, P. L. *et al.* Postweaning substitution of grazed forage with a high-energy concentrate has variable long-term effects on subcutaneous fat and marbling in *Bos taurus* genotypes. *J Anim Sci* **93**, 4132–4143 (2015).
98. Gotoh, T. Histochemical properties of skeletal muscles in Japanese cattle and their meat production ability. *Animal Science Journal* **74**, 339–354 (2003).
99. Choi, C. B. *et al.* Administration of zilpaterol hydrochloride alters feedlot performance, carcass characteristics, muscle, and fat profiling in finishing Hanwoo steers. *Livestock Science* **157**, 435–441 (2013).
100. Gotoh, T. & Joo, S.-T. Characteristics and Health Benefit of Highly Marbled Wagyu and Hanwoo Beef. *Korean J Food Sci Anim Resour* **36**, 709–718 (2016).
101. Smith, S. B. & Johnson, B. J. Marbling: Management of cattle to maximize the deposition of intramuscular adipose tissue. *Journal of Animal Science* **94**, 382–382 (2016).
102. Cho, S. H. *et al.* Fatty Acid Profiles and Sensory Properties of Longissimus dorsi, Triceps brachii, and Semimembranosus Muscles from Korean Hanwoo and Australian Angus Beef. *Asian Australas. J. Anim. Sci* **18**, 1786–1793 (2005).
103. Hausman, G. J. *et al.* BOARD-INVITED REVIEW: The biology and regulation of preadipocytes and adipocytes in meat animals^{1,2}. *Journal of Animal Science* **87**, 1218–1246 (2009).
104. Mezgebo, G. B. *et al.* Fatty acid, volatile and sensory characteristics of beef as affected by grass silage or pasture in the bovine diet. *Food Chemistry* **235**, 86–97 (2017).
105. Mitchell, G. E., Reed, A. W. & Rogers, S. A. Influence of Feeding Regimen on the Sensory Qualities and Fatty Acid Contents of Beef Steaks. *J Food Science* **56**, 1102–1103 (1991).
106. Wanders, A. J., Brouwer, I. A., Siebelink, E. & Katan, M. B. Effect of a High Intake of Conjugated Linoleic Acid on Lipoprotein Levels in Healthy Human Subjects. *PLoS ONE* **5**, e9000 (2010).

107. Gilmore, L. A. *et al.* Consumption of High-Oleic Acid Ground Beef Increases HDL-Cholesterol Concentration but Both High- and Low-Oleic Acid Ground Beef Decrease HDL Particle Diameter in Normocholesterolemic Men. *The Journal of Nutrition* **141**, 1188–1194 (2011).
108. Siqin, Q. *et al.* Relationships among muscle fiber type composition, fiber diameter and *MRF* gene expression in different skeletal muscles of naturally grazing Wuzhumuqin sheep during postnatal development. *Anim Sci J* **88**, 2033–2043 (2017).
109. Wang, B. *et al.* Neonatal vitamin A injection promotes cattle muscle growth and increases oxidative muscle fibers. *J Animal Sci Biotechnol* **9**, 82 (2018).
110. Zierath, J. R. & Hawley, J. A. Skeletal Muscle Fiber Type: Influence on Contractile and Metabolic Properties. *PLoS Biol* **2**, e348 (2004).
111. Gotoh, T. & *et al.* Relationship between myofiber type and fatty acid composition in skeletal muscles of Wagyu (Japanese Black) and Holstein cattle. in 1–4 (2011).
112. Du, M. *et al.* Fetal programming of skeletal muscle development in ruminant animals¹. *Journal of Animal Science* **88**, E51–E60 (2010).
113. Asakura, A., Rudnicki, M. A. & Komaki, M. Muscle satellite cells are multipotential stem cells that exhibit myogenic, osteogenic, and adipogenic differentiation. *Differentiation* **68**, 245–253 (2001).
114. Singh, N. K. Conversion of C2C12 Myoblast into Adipoblast with Thiazolidinediones - A Possible Basis for Intramuscular Fat Generation in Meat Animals. *Asian Australas. J. Anim. Sci* **20**, 432–439 (2007).
115. Nishimura, T., Hattori, A. & Takahashi, K. Structural changes in intramuscular connective tissue during the fattening of Japanese black cattle: effect of marbling on beef tenderization. *Journal of Animal Science* **77**, 93 (1999).
116. Li, X. Z. *et al.* Oleic acid in the absence of a PPAR γ agonist increases adipogenic gene expression in bovine muscle satellite cells¹. *Journal of Animal Science* **97**, 4114–4123 (2019).
117. Chung, K. Y., Smith, S. B., Choi, S. H. & Johnson, B. J. Oleic acid enhances G protein coupled receptor 43 expression in bovine intramuscular adipocytes but not in subcutaneous adipocytes¹. *Journal of Animal Science* **94**, 1875–1883 (2016).

118. Choi, S. H. *et al.* AMPK α , C/EBP β , CPT1 β , GPR43, PPAR γ , and SCD Gene Expression in Single- and Co-cultured Bovine Satellite Cells and Intramuscular Preadipocytes Treated with Palmitic, Stearic, Oleic, and Linoleic Acid. *Asian-Australas J Anim Sci* **28**, 411–419 (2015).
119. Gstraunthaler, G. Alternatives to the use of fetal bovine serum: serum-free cell culture. *ALTEX* **20**, 275–281 (2003).
120. Saclier, M., Theret, M., Mounier, R. & Chazaud, B. Effects of Macrophage Conditioned-Medium on Murine and Human Muscle Cells: Analysis of Proliferation, Differentiation, and Fusion. *Methods Mol Biol* **1556**, 317–327 (2017).
121. Saclier, M. *et al.* Differentially activated macrophages orchestrate myogenic precursor cell fate during human skeletal muscle regeneration. *Stem Cells* **31**, 384–396 (2013).
122. Khodabukus, A. *et al.* Electrical stimulation increases hypertrophy and metabolic flux in tissue-engineered human skeletal muscle. *Biomaterials* **198**, 259–269 (2019).
123. Yu, Q. P. *et al.* Studies on meat color, myoglobin content, enzyme activities, and genes associated with oxidative potential of pigs slaughtered at different growth stages. *Asian-Australas J Anim Sci* **30**, 1739–1750 (2017).
124. Schiaffino, S. & Reggiani, C. Fiber types in mammalian skeletal muscles. *Physiol Rev* **91**, 1447–1531 (2011).
125. Karamucki, T., Jakubowska, M., Rybarczyk, A. & Gardzielewska, J. The influence of myoglobin on the colour of minced pork loin. *Meat Science* **94**, 234–238 (2013).
126. Kim, G.-D. *et al.* The influence of fiber size distribution of type IIB on carcass traits and meat quality in pigs. *Meat Science* **94**, 267–273 (2013).
127. Lee, S. H. *et al.* The influence of pork quality traits and muscle fiber characteristics on the eating quality of pork from various breeds. *Meat Science* **90**, 284–291 (2012).
128. Wittenberg, B. A. Both hypoxia and work are required to enhance expression of myoglobin in skeletal muscle. Focus on 'Hypoxia reprograms calcium signaling and regulates myoglobin expression'. *Am J Physiol Cell Physiol* **296**, C390-392 (2009).

129. Jerkovic, R., Argentini, C., Serrano-Sanchez, A., Cordonnier, C. & Schiaffino, S. Early myosin switching induced by nerve activity in regenerating slow skeletal muscle. *Cell Struct Funct* **22**, 147–153 (1997).
130. Ito, A. *et al.* Induction of functional tissue-engineered skeletal muscle constructs by defined electrical stimulation. *Sci Rep* **4**, 4781 (2014).
131. Arnold, L. *et al.* Inflammatory monocytes recruited after skeletal muscle injury switch into antiinflammatory macrophages to support myogenesis. *J Exp Med* **204**, 1057–1069 (2007).
132. D'Angelo, F. *et al.* Macrophages promote epithelial repair through hepatocyte growth factor secretion. *Clin Exp Immunol* **174**, 60–72 (2013).
133. Kuwabara, K. *et al.* Hypoxia-mediated induction of acidic/basic fibroblast growth factor and platelet-derived growth factor in mononuclear phagocytes stimulates growth of hypoxic endothelial cells. *Proceedings of the National Academy of Sciences* **92**, 4606–4610 (1995).
134. Jasper, M. J. *et al.* Macrophage-derived LIF and IL1B regulate alpha(1,2)fucosyltransferase 2 (Fut2) expression in mouse uterine epithelial cells during early pregnancy. *Biol Reprod* **84**, 179–188 (2011).
135. Lolmede, K. *et al.* Inflammatory and alternatively activated human macrophages attract vessel-associated stem cells, relying on separate HMGB1- and MMP-9-dependent pathways. *J Leukoc Biol* **85**, 779–787 (2009).
136. Hsieh, P.-L., Rybalko, V., Baker, A. B., Suggs, L. J. & Farrar, R. P. Recruitment and therapeutic application of macrophages in skeletal muscles after hind limb ischemia. *J Vasc Surg* **67**, 1908-1920.e1 (2018).
137. Zheng, M. H. *et al.* Porcine small intestine submucosa (SIS) is not an acellular collagenous matrix and contains porcine DNA: possible implications in human implantation. *J Biomed Mater Res B Appl Biomater* **73**, 61–67 (2005).
138. Takezawa, T., Mori, Y. & Yoshizato, K. Cell culture on a thermo-responsive polymer surface. *Biotechnology (N Y)* **8**, 854–856 (1990).
139. Chan, B. P. & Leong, K. W. Scaffolding in tissue engineering: general approaches and tissue-specific considerations. *Eur Spine J* **17 Suppl 4**, 467–479 (2008).

140. Ruoslahti, E. RGD and other recognition sequences for integrins. *Annu Rev Cell Dev Biol* **12**, 697–715 (1996).
141. Gröhn, P., Klöck, G. & Zimmermann, U. Collagen-Coated Ba²⁺-Alginate Microcarriers for the Culture of Anchorage-Dependent Mammalian Cells. *BioTechniques* **22**, 970–975 (1997).
142. Batorsky, A., Liao, J., Lund, A. W., Plopper, G. E. & Stegemann, J. P. Encapsulation of adult human mesenchymal stem cells within collagen-agarose microenvironments. *Biotechnol Bioeng* **92**, 492–500 (2005).
143. Modulevsky, D. J., Lefebvre, C., Haase, K., Al-Rekabi, Z. & Pelling, A. E. Apple Derived Cellulose Scaffolds for 3D Mammalian Cell Culture. *PLoS ONE* **9**, e97835 (2014).
144. Gilbert, P. M. *et al.* Substrate Elasticity Regulates Skeletal Muscle Stem Cell Self-Renewal in Culture. *Science* **329**, 1078–1081 (2010).
145. Claflin, D. R. & Faulkner, J. A. Shortening velocity extrapolated to zero load and unloaded shortening velocity of whole rat skeletal muscle. *The Journal of Physiology* **359**, 357–363 (1985).
146. Josephson, R. K. & Edman, K. A. P. Changes in the maximum speed of shortening of frog muscle fibres early in a tetanic contraction and during relaxation. *The Journal of Physiology* **507**, 511–525 (1998).
147. Reggiani, C. When fibres go slack and cross bridges are free to run: a brilliant method to study kinetic properties of acto-myosin interaction: Classical Perspectives. *The Journal of Physiology* **583**, 5–7 (2007).
148. Sanger, J. W., Wang, J., Fan, Y., White, J. & Sanger, J. M. Assembly and Dynamics of Myofibrils. *Journal of Biomedicine and Biotechnology* **2010**, 1–8 (2010).
149. Weist, M. R. *et al.* TGF- β 1 enhances contractility in engineered skeletal muscle: Effect of TGF- β 1 on Engineered Skeletal Muscle. *J Tissue Eng Regen Med* **7**, 562–571 (2013).
150. Filvaroff, E. H., Ebner, R. & Derynck, R. Inhibition of myogenic differentiation in myoblasts expressing a truncated type II TGF-beta receptor. *Development* **120**, 1085–1095 (1994).
151. Turrina, A., Martínez-González, M. A. & Stecco, C. The muscular force transmission system: Role of the intramuscular connective tissue. *Journal of Bodywork and Movement Therapies* **17**, 95–102 (2013).

152. Dahl, K. N., Ribeiro, A. J. S. & Lammerding, J. Nuclear Shape, Mechanics, and Mechanotransduction. *Circulation Research* **102**, 1307–1318 (2008).
153. Costa, M. L. Cytoskeleton and Adhesion in Myogenesis. *ISRN Developmental Biology* **2014**, 1–15 (2014).
154. Meyer, G. A. & Lieber, R. L. Elucidation of extracellular matrix mechanics from muscle fibers and fiber bundles. *Journal of Biomechanics* **44**, 771–773 (2011).
155. Fontana, G. *et al.* Biofunctionalized Plants as Diverse Biomaterials for Human Cell Culture. *Adv Healthc Mater* **6**, (2017).
156. Hickey, R. J., Modulevsky, D. J., Cuerrier, C. M. & Pelling, A. E. Customizing the Shape and Microenvironment Biochemistry of Biocompatible Macroscopic Plant-Derived Cellulose Scaffolds. *ACS Biomater. Sci. Eng.* **4**, 3726–3736 (2018).
157. Gershlak, J. R. *et al.* Crossing kingdoms: Using decellularized plants as perfusable tissue engineering scaffolds. *Biomaterials* **125**, 13–22 (2017).
158. Contessi Negrini, N., Toffoletto, N., Farè, S. & Altomare, L. Plant Tissues as 3D Natural Scaffolds for Adipose, Bone and Tendon Tissue Regeneration. *Front. Bioeng. Biotechnol.* **8**, 723 (2020).
159. Al-Rekabi, Z. & Pelling, A. E. Cross talk between matrix elasticity and mechanical force regulates myoblast traction dynamics. *Phys. Biol.* **10**, 066003 (2013).
160. Kang, S.-M., Lee, J.-H., Huh, Y. S. & Takayama, S. Alginate Microencapsulation for Three-Dimensional In Vitro Cell Culture. *ACS Biomater. Sci. Eng.* acsbiomaterials.0c00457 (2020) doi:10.1021/acsbiomaterials.0c00457.
161. Kinney, M. A., Sargent, C. Y. & McDevitt, T. C. The multiparametric effects of hydrodynamic environments on stem cell culture. *Tissue Eng Part B Rev* **17**, 249–262 (2011).
162. Van Winkle, A. P., Gates, I. D. & Kallos, M. S. Mass transfer limitations in embryoid bodies during human embryonic stem cell differentiation. *Cells Tissues Organs* **196**, 34–47 (2012).
163. Hay, I. D., Rehman, Z. U., Moradali, M. F., Wang, Y. & Rehm, B. H. A. Microbial alginate production, modification and its applications: Bacterial alginates. *Microbial Biotechnology* n/a-n/a (2013) doi:10.1111/1751-7915.12076.

164. Donati, I. & Paoletti, S. Material Properties of Alginates. in *Alginates: Biology and Applications* (ed. Rehm, B. H. A.) vol. 13 1–53 (Springer Berlin Heidelberg, 2009).
165. Hausman, G. J., Wright, J. T. & Richardson, R. L. The influence of extracellular matrix substrata on preadipocyte development in serum-free cultures of stromal-vascular cells. *J Anim Sci* **74**, 2117–2128 (1996).
166. Duffy, R. M., Sun, Y. & Feinberg, A. W. Understanding the Role of ECM Protein Composition and Geometric Micropatterning for Engineering Human Skeletal Muscle. *Ann Biomed Eng* **44**, 2076–2089 (2016).
167. Bellis, S. L. Advantages of RGD peptides for directing cell association with biomaterials. *Biomaterials* **32**, 4205–4210 (2011).
168. Jahanbakhsh, A., Nourbakhsh, M. S., Bonakdar, S., Shokrgozar, M. A. & Haghighipour, N. Evaluation of alginate modification effect on cell-matrix interaction, mechanotransduction and chondrogenesis of encapsulated MSCs. *Cell Tissue Res* **381**, 255–272 (2020).
169. Frith, J. E., Mills, R. J., Hudson, J. E. & Cooper-White, J. J. Tailored Integrin–Extracellular Matrix Interactions to Direct Human Mesenchymal Stem Cell Differentiation. *Stem Cells and Development* **21**, 2442–2456 (2012).
170. Yasa, I. C., Gunduz, N., Kilinc, M., Guler, M. O. & Tekinay, A. B. Basal Lamina Mimetic Nanofibrous Peptide Networks for Skeletal Myogenesis. *Sci Rep* **5**, 16460 (2015).
171. Silva Garcia, J. M., Panitch, A. & Calve, S. Functionalization of hyaluronic acid hydrogels with ECM-derived peptides to control myoblast behavior. *Acta Biomaterialia* **84**, 169–179 (2019).
172. Mortera-Blanco, T., Mantalaris, A., Bismarck, A., Aqel, N. & Panoskaltsis, N. Long-term cytokine-free expansion of cord blood mononuclear cells in three-dimensional scaffolds. *Biomaterials* **32**, 9263–9270 (2011).
173. Daoud, J. T. *et al.* Long-term in vitro human pancreatic islet culture using three-dimensional microfabricated scaffolds. *Biomaterials* **32**, 1536–1542 (2011).
174. Utech, S. *et al.* Microfluidic Generation of Monodisperse, Structurally Homogeneous Alginate Microgels for Cell Encapsulation and 3D Cell Culture. *Adv Healthc Mater* **4**, 1628–1633 (2015).

175. Wang, X. *et al.* Proliferation and Differentiation of Mouse Embryonic Stem Cells in APA Microcapsule: A Model for Studying the Interaction between Stem Cells and Their Niche. *Biotechnol. Prog.* **22**, 791–800 (2006).
176. Zeeb, B., Saberi, A. H., Weiss, J. & McClements, D. J. Formation and characterization of filled hydrogel beads based on calcium alginate: Factors influencing nanoemulsion retention and release. *Food Hydrocolloids* **50**, 27–36 (2015).
177. Thu, B. *et al.* Alginate polycation microcapsules. *Biomaterials* **17**, 1069–1079 (1996).
178. Mierisch, C. M. *et al.* Transforming growth factor-beta in calcium alginate beads for the treatment of articular cartilage defects in the rabbit. *Arthroscopy* **18**, 892–900 (2002).
179. Lee, B. *et al.* Challenges and Solutions for Commercial Scale Manufacturing of Allogeneic Pluripotent Stem Cell Products. *Bioengineering (Basel)* **7**, (2020).
180. Beef Grading Shields. *USDA.gov* <https://www.ams.usda.gov/grades-standards/beef/shields-and-marbling-pictures>.
181. Japan Meat Grading Association (JMGA) Beef Carcass Trading Standards. (2014).
182. Factors influencing, and selection for, eating quality in Wagyu beef. *wagyuinternational.com* http://www.wagyuinternational.com/eating_quality.php (2019).
183. Gotoh, T., Takahashi, H., Nishimura, T., Kuchida, K. & Mannen, H. Meat produced by Japanese Black cattle and Wagyu. *Animal Frontiers* **4**, 46–54 (2014).
184. Lonergan, S. M., Topel, D. G. & Marple, D. N. Fat and fat cells in domestic animals. in *The Science of Animal Growth and Meat Technology* 51–69 (Elsevier, 2019). doi:10.1016/B978-0-12-815277-5.00005-6.
185. Gotoh, T., Nishimura, T., Kuchida, K. & Mannen, H. The Japanese Wagyu beef industry: current situation and future prospects — A review. *Asian-Australas J Anim Sci* **31**, 933–950 (2018).